# MAREES TERRESTRES

# BULLETIN D'INFORMATIONS

## 1 1 7

## 30 SEPTEMBRE 1993

**Association Internationale de Géodésie**

**Commission Permanente des Marées Terrestres**

*Editeur Prof. Paul MELCHIOR*
*Observatoire Royal de Belgique*
*Avenue Circulaire 3*
*1180 Bruxelles*

BIM 117

30 septembre 1993

Special issue

# Meeting of the three Working Groups of the Permanent Commission on Earth Tides

Bonn, October 1992

Part III

## Table des matières



*

* *

Paper not presented at the Bonn Workshop - Received august 17, 1993.

# Core Modes and Slichter Modes: Fact and Fancy.

David J. Crossley
Department of Earth and Planetary Sciences
McGill University
3450 University Street
Montreal H3A2A7
Canada

**Abstract**

The situation regarding the possible detectibility of gravity core modes and the Slichter triplet is briefly reviewed as it exists in the current literature. Using as a source the standard seismic earthquake excitation, this being the only calculation which has been quantitatively estimated to date, the tentative result is that both types of motion are at or slightly below current detectability levels. Therefore it is not surprising that these signals are not yet seen (certainly not clearly, at least), and the stacking of global superconducting gravimeter records will be necessary to observe these elusive messengers from the Earth's core.

## Introduction

The scientific goal of this work is to ascertain the density profile in the Earth's outer core and the density jump at the inner core boundary (ICB). For the first problem the mechanism is the detection of internal gravity/inertial modes (core undertones) in the rotating fluid and for the second problem it is the detection of the Slichter triplet (the components of the translational motion of the inner core). From a seismic point of view the density profile in the outer core is close to being adiabatic within the resolving power of the data (Masters, 1979). A purely adiabatic core is dynamically inert, i.e. radially displaced material simply remains at the new radius, there is neither convection nor oscillation of the fluid. Exact adiabaticity is unlikely everywhere in the core since this implies the core is chemically homogeneous and it is now accepted that some form of chemical buoyancy, which implies gravitational settling, contributes energy to power the geodynamo.

On the other hand, large departures from adiabaticity are unlikely on the superadiabatic side, since an excess thermal gradient stimulates convection that redistributes the temperature towards the adiabatic gradient (e.g. Higgins and Kennedy, 1971). Similarly a large departure towards subadiabaticity would completely inhibit radial convection everywhere in the core and this poses almost (but not quite, see Singer & Olson (1984)) insurmountable problems

for the geodynamo generation mechanism. The most likely possibilty is that the actual thermal gradient in the core hovers around the adiabat, but on which side and where in the core is too delicate a question for current seismology.

The possibility that another branch of geophysics, namely gravity variations (or geodesy, if you like) may be able to shed light on this problem is sufficiently interesting to have stimulated a dedicated band of theorists to solve the mathematical and numerical problems associated with gravity waves in the core. In the last few years, this theory has run into the distinct possibility of being tested by surface-based measurements from the highly stable superconducting gravimeters (SGs). So what was once mathematical fancy has run into experimental fact. I shall briefly review the essentials and the current situation.

## Internal Gravity and Inertial Waves

The branch of rotating fluids that deals with internal gravity waves and inertial waves tells us that the stability structure of the fluid (desribed through its Brünt-Väisälä frequency $N^2$, e.g. Crossley & Rochester, 1980) plays a very important role in determining the spectrum of such wave motions. Internal gravity waves are the natural wave motion of a non-rotating fluid with a stable density stratification. For the case of uniformly stable stratification the possible (internal) gravity (G) waves are confined to the frequency regime $N^2 < \omega^2 < \infty$. For a fluid with variable stability, one replaces $N^2$ by $N^2_{max}$, where the latter is the maximum radial value in the fluid, in our case between the ICB and the CMB. This result is well known in atmospheric and oceanic dynamics since these fluids are generally stably stratified. The restoring force for G waves is of course gravity supplied by the stable density stratification.

One important fact about G waves in the core is that they do not require the fluid to be compressible and self-gravitating. These properties are not important for oceanic gravity waves where the assumption of incompressibility is quite sound. Crossley & Rochester (1980) showed that small departures from the adiabatic condition $N^2 = 0$ of a compressible, self gravitating fluid can be faithfully mimicked by an incompressible, non-self gravitating fluid (the so-called near-adiabatic approximation, which is a close cousin to the well-known Boussinesq approximation), a situation that is certainly satisfied in the core. The seismic limits give a lower bound to the buoyancy period $2\pi/N$ of about 6 hrs for the core, near the CMB. Thus G waves would exist in the period range 6 $hr$ to $\infty$ for a non-rotating Earth model.

On the other hand the natural wave motion in a rotating fluid is an inertial wave (I wave); here we restrict the definition to global inertial waves, not the local inertial waves seen for example in the world's oceans. I waves exist in their purest form for a neutrally stratified (rotating) fluid, in which case they fill the frequency range $4\Omega^2 < \omega^2 < \infty$, where the rotation period of the system is $2\pi/\Omega$. The restoring force for the I waves is the Coriolis force (which of course does no real work in a cycle of oscillation), i.e. the rotation itself. A purely inertial wave does not perturb the gravity potential and therefore can be only be detected by a surface gravimeter through deformation of the core boundaries. The spectrum of I waves for an inviscid rotating shell of fluid is infinitely dense but discrete (Aldridge &

Toomre, 1969), as is the spectrum of G waves (Pekeris & Accad, 1972).

An alternative detection mechanism is to observe changes in the mantle's rotation rate through degree 1 I waves which exchange angular momentum between the mantle and core. This possibility has been considered by Lumb et al. (1992) in the context of high rate VLBI measurements.

The combination of non-zero $N^2$ with non-zero $\Omega^2$ leads to a mixing of the above wave types. If $0 < 4\Omega^2 < N^2$, we say the fluid is strongly stably stratified and refer to the waves as gravity-inertial (GI) waves, i.e. gravity waves modified by rotation. Otherwise ($0 < N^2 < 4\Omega^2$), the fluid is weakly stable and we have inertial-gravity (IG) waves, or inertial waves modified by gravity. The combination of wave types in a rotating shell can readily be evaluated using analytic techniques on the basic equations (Friedlander & Siegmann, 1982; Crossley, 1984; Smylie & Rochester, 1986).

The results are somewhat complicated as the admissibility of wavelike domains depends on latitude. This implies that some wave type are global, and others may be trapped either at the pole (of rotation) or, more likely, at the equator. For the present purpose, the most likely possibility for the core is that it is weakly stably stratified near the CMB and weakly unstably stratified elsewhere. Thus we would expect to find equatorially trapped high freqency (HF)waves in the range $(N^2 + 4\Omega^2) < \omega^2 < 4\Omega^2$, global IG waves in the range $4\Omega^2 < \omega^2 < N^2$ and equatorially trapped Rossby-Kelvin (RK) waves in the range $N^2 < \omega^2 < \infty$ (Crossley, 1984). As an example, if $2\pi/N = 17\ hr$, then RK waves exist at periods longer than 17 $hr$, IG waves between 17 and 12 $hr$ and HF waves between 12 and 9.8 $hr$. Again $N^2$ in these expressions is replaced by its maximum value if it is non-uniform.

The elucidation of these frequency limits has been derived independently by Crossley & Rochester (1980), Smylie & Rochester (1981) and the extension to non-constant $N^2$ developed by Friedlander (1985a). However, it is one step to derive existence regimes, and quite another to actually calculate the eigensolutions for a particular Earth model.

## The Free Mode Spectrum

Initial attempts to take into account the Coriolis force in the seismic equations of motion first omitted the toroidal (or torsional) components of the motion (Smylie, 1974) and then ran into the problem of truncating the infinite chain of spheroidal/toroidal spherical harmonic (SH) components of the motion (Crossley, 1975). The complexities of the full problem (Johnson & Smylie, 1977) led Crossleÿ & Rochester (1980) and Smylie & Rochester (1981) to propose the Boussinesq and subseismic approximations (SSA) to the equations of motions respectively. These simplifications do not change substantially the structure of the differential equation (Friedlander, 1985b) and therefore not the previously derived frequency limits. Although both approximations reduce the governing equations from 4th to 2nd order, the SSA continues to require solution of the Poisson equation (for the perturbed gravity potential) which the Boussinesq approximation ignores altogether.

At one point it appeared as though the SH approach was doomed to failure through the

severe truncation problem (Crossley, 1984) and the SSA, as developed by Smylie et al. (1984), seemed more promising. In the last few years the situation has changed somewhat as difficulties with the SSA became apparent (Crossley & Rochester, 1982) and the truncation problem for SHs is somewhat alleviated both by the behaviour of the mantle Love numbers and by the addition of viscous damping in the fluid.

For the original problem of the rotating spherical shell, the internal gravity waves for a stably stratified 6 *hr* core (Crossley, 1993; Wu & Rochester, 1993) demonstrate the anticipated convergence with higher truncation levels to the frequency limits previously quoted. To date only the strongly stratified core has been used as the basis model. For a weakly stratified core, the spectrum contains singularities which pose some numerical problems.

However from the observational point of view, the eigensolutions of a core with rigid boundaries is not interesting since the boundaries prevent any external source of excitation. Also, rigid boundaries limit the surface gravity response to only one component of the detection problem, i.e. the perturbation in gravitational potential in the core, while preventing any transmission of stress through the CMB into the mantle. The next step in the problem is therefore to treat the case of elastic boundaries. This is achieved through the use of Love numbers to represent the passive resonse of the inner core and mantle to the core dynamics. Approaches to the Love number problem were independently derived by Smylie et al. (1990) and Crossley et al. (1991) through suggestions from our colleagues Dehant and Hinderer (personal communications). For the core undertones, numerical experiments confirm that one can use static Love numbers (independent of frequency) for the passive response of the inner and outer cores, thus considerable speeding up the numerical calculations.

One of the remarkable properties of the Love numbers for deformations at the ICB and CMB is that they are highly dependent on SH degree. At degrees two and higher, the Love numbers fall rapidly in amplitude until they become asymptotically small at degrees beyond 10-15. This is an important factor for the gravity detection problem, as it implies that high degree harmonics in the core will be preferentially lost in their transmission through the mantle. Thus the mantle deformation field will be composed mainly of low degree SH components, i.e. large wavenumber surface perturbations (Crossley, 1993), even though in the fluid core a large number of harmonics might be needed to get convergent eigenfrequencies.

Smylie et al. (1990) used the Love number formulation for elastic boundaries and the subseismic approximation to the flow both in the body of the fluid core and at the core boundaries. The SSA is indeed a good approximation to use in the body of the fluid core (we will call this the weak form, SSA-1) , as confirmed by Crossley et al., (1991) and Wu & Rochester (1993) and the eigenfrequencies match to better than 1% the full solutions (at least in a non-rotating Earth). However the use of the SSA at the core boundaries (we call the strong form, SSA-2) has been challenged by Crossley & Rochester (1992) on the basis that the almost rigid boundaries of the actual core prevent the SSA condition being filled. This is a rather subtle dynamical point that nonetheless is crucial to the whole approach of Smylie et al, (1992) as adopting the SSA at the core boundaries allows the construction of a variational principle for a single variable in the liquid core, on which their numerical algorithms are based.

These issues aside, the theoretical calculations of eigenperiods are finally producing testable suites of eigenperiods and two independent sets of eigenfrequencies for a 6 *hr* core by Wu & and Rochester (1993) and Crossley (unpublished results) are in excellent agreement. The final results for elastic boundaries with various approximations should be available in the near future. Naturally other more likely Earth models will also have to be considered, as discussed above.

I will not discuss in any detail the intrinsic nature of the core spectrum, except to point out that there has been some unresolved debate on the discreteness vs the continuity of the spectrum both with and without viscosity (Valette, 1989). In practise, finite physical damping will always render the spectrum as continuous, moreover the finite length of the data records cannot in any case resolve an infinitely dense spectrum. One hopes that the dominance of perhaps low-degree harmonics, together with a selective excitation process, could lead to an interesting (quasi-discrete) spectrum rather than one that is broadband and difficult to interpret.

## Excitation and Detection

The basic theory behind the earthquake excitation of the core undertones was given by Crossley (1989), following a standard seismic method given originally by Gilbert (1970). In short, there is absolutely no difference for a non-rotating Earth model between a seismic normal mode and a GI mode as far as the theory is concerned; one simply substitutes the appropriate eigenfunction into the expressions. The results of Crossley et al. (1991) suggest that the core modes are only very weakly excited, even by a large Chilean-type earthquake. By weak, we mean below the current detection threshold of 1 *ngal*. The physical reason is fairly clear, for the whole mantle is virtually a node for the core oscillations, and elementary considerations dictate that a physical system cannot efficiently be excited at a node.

The excitation for core modes in a rotating model has not yet been published. It will be very interesting to see whether the surface gravity is increased or decreased in comparion with the non-rotating solutions. In principle the rotation, by coupling together all SHs of the same azimuthal order, should enhance the surface gravity. However the enhancement may be quite insignificant due to the rapid weakening of the mantle solutions with higher degrees (the Love number behaviour mentioned earlier).

In order to be detectable, surface gravity variations connected to core motions must be persistent to allow the signal to be enhanced in the presence of a relatively high background noise (caused for example by residual atmospheric and site effects). This means the core modes should have high Q's as anticipated in the computations of Crossley et al. (1991) who found damping times well exceeding a year for most modes in a non-rotating model. The damping mechanism in this computation assumes anelasticity (i.e. imperfections in shear modulus and bulk incompressibility) throughout the Earth, though the dominant loss of energy is through the slight bulk inelasticity in the fluid core rather than shear dissipation (as for the seismic normal modes).

The role of viscosity is more difficult to model as it changes the order of the differential sys-

tem, but Rieutord (1991) has shown that even the low solid state (laboratory extrapolation) value of viscosity is sufficient to damp out the contribution of the short wavelength (high degree) harmonics in the coupling chain. This is a major encouragement to the use of SH for the core eigenfunctions. Friedlander & Siegmann (1983) estimated the damping time of the core modes to be greater than a year, about the same as the anelastic dissipation. Using a value for viscosity in the high range, i.e. the 'geophysical' measurement of viscosity (Lumb & Aldridge, 1991), would lead to a much quicker convergence of the coupling chain but also much greater damping. The magnetic field has little effect on core ocillations (Crossley & Smylie, 1975).

Thus our current picture of core undertones is a wavefield that is both weakly excited (by earthquakes) and very persistent. This situation is best exploited at the surface by a network of long-running detectors such as the SG. To be realistic, we must allow for other mechanisms to excite wavelike motions in the core. It would appear that tidal forcing has not yet been identified as present (Lumb et al., 1992). Although references to anomalous semi-diurnal gravimetric factors have occasionally been made, to date no connections have made between these and core processes as in the case of some diurnal waves associated with the NDFW. Of course tidal gravimetric factors are notoriously dependent on ocean load models, so there is still room for a small effect. Finally, intermittent, chemically driven radial disturbances are possible that may originate for example at the ICB, and these might be quite efficient at exciting the wavefield.

## The Slichter Triplet

After some years of being neglected, the topic of the translational motions of the inner core has reappeared in the literature with a vengence (Smylie, 1992; Crossley et al., 1992; Rochester & Peng, 1990, 1993). Whether or not a particular harmonic peak (or peaks) can be seen in noisy data is clearly a subject of long standing interest in many fields of science. The subject is muddied by a number of issues concerning detection algorithms, the use of various spectral power density measures and often a healthy dose of subjectivity. What is most relevent to the current controversy over the Slichter triplet is the admission, stated clearly in Smylie (1992), that the three weak peaks in a stack of four SG records can be recognised only through the support of an appropriate theory. There is nothing untoward about this, as many major discoveries in science have been based on speculations only weakly supported by existing data. After all, if the Slichter triplet had been clearly excited by earthquakes, it would already have been seen in seismic studies (e.g. Rydelek & Knopoff, 1984) !

The current limitation of SG data seems to be at about the 1 *ngal* level (Hinderer et al., 1993) and it requires careful data processing to achieve this. Various methods are currently being investigated to perform the global stacking of SG records for the very weak signals involved (e.g. Hinderer et al., 1992; Jensen et al., 1992). Again, the GGP (Global Geodynamics Project) seems to be an appropriate tool for acquiring the necessary data.

Theoretically, the calculation of the eigenfrequencies of the Slichter triplet is quite straightforward. Until recently (Smylie & Qin, 1992) all calculations ignored viscosity in the outer

core. Of these inviscid computations, Smylie (1992) used the strong form of the SSA (in the body of the fluid and at the boundaries), Rochester & Peng (1993) used the weak form of the SSA (only in the body of the fluid) and Crossley et al. (1992) checked all approximations including both forms of the SSA, the Boussinesq approximation and the full equations. It turns out that all of these forms of the equations of motion yield approximately the same eigenperiods of the Slichter triplet, though the eigenfunctions in the mantle are significantly different.

The next question is one of rotation. The traditional estimation of the eigenperiods of seismic oscillations uses first or second order perturbation theory (Dahlen & Sailor, 1979) because the periods are generally much shorter than 1 day. However the periods obtained by a truncation of the full coupling chain to two terms $S_1^1 + T_2^1$ (Crossley, 1975; Smith 1976) are almost almost equivalent to those obtained by perturbation theory. Smylie (1992) uses a truncation of the SH expansion of his core eigenfunctions but does not state the truncation level; one presumes his eigenperiods have converged so that he has fully taken into account the rotation. Both Crossley et al. (1992), Crossley (1992) and Rochester & Peng (1993) used SH expansions $S_1^1 + \ldots + S_5^1$ and found convergence for models such as CORE11 (Widmer et al., 1988) and PREM (Dziewonski & Anderson, 1981). Thus all recent authors have full rotation in the eigensolutions.

The final question is the one of static vs. dynamic Love numbers. Smylie (1992) ignores the inertial and Coriolis terms in his computation of the IC and mantle Love numbers, following his use of the same technique for the core modes (Smylie et al., 1990). Crossley et al. (1992) and Rochester & Peng (1993) have demonstrated that the inertial and Coriolis terms generate a Love number resonance not far from the Slichter solutions. This resonance substantially changes the Love numbers, particularly those of degree 1, from their static values and confirms that the Slichter eigenperiods are almost identical to the seismic values and some 40% longer than those obtained using static values.

Thus the Love number issue is the key to understanding the theoretical problem in the literature; it is certainly not the use of the SSA, neither the issue of rotation nor viscosity. According to the simple theory of an underdamped harmonic oscillator, a resistance to motion such as viscosity will not shift the location of the undamped Fourier spectral peak, but will lower the amplitude of the peak and broaden it. Smylie \& Qin (1992) however claim that a viscous boundary layer affects not only the dissipation but also the splitting (i.e. frequencies) of the Slichter triplet; this implies a loss of agreement between Smylie's (1992) inviscid theoretical periods and the experimental SG peaks. It would appear that only a large ICB density jump could reconcile the Slichter periods of Crossley (1992) and Rochester \& Peng (1990, 1993) to the SG peaks claimed by Smylie (1992). Table 1 summarises the situation just described for CORE11.

## References

Aldridge, K.D. & Toomre, A., 1969. Axisymmetric inertial oscillations of a fluid in a rotating spherical container, J. Fluid Mech., **37**, 307-323.

Crossley, D.J., 1975. Core undertones with rotation, Geophys. J. Roy. astr. Soc., **42**, 477-488.

Crossley, D.J. & Smylie, D.E., 1975. Electromagnetic and viscous damping of core oscillations, Geophys. J. Roy. astr. Soc., **42**, 1101-1033.

Crossley, D.J., & Rochester, M.G., 1980. Simple core undertones, Geophys. J. Roy. astr. Soc., **60**, 129-161.

Crossley, D.J., 1984. Oscillatory flow in the liquid core, Phys. Earth Planet. Int., **36**, 1-16.

Crossley, D.J., 1989. The excitation of core modes by earthquakes, in *Structure and Dynamics of Earth's Deep Interior, Geophysical Monograph 46, IUGG*, Volume 1, 41-50, D.E. Smylie and R. Hide, AGU.

Crossley, D.J., Hinderer, J. & Legros, H., 1991. On the excitation, detection and damping of core modes, Phys. Earth Planet. Int., **68**, 97-116.

Crossley, D.J. & Rochester, M.G., 1992. The subseismic approximation in core dynamics, Geophys. J. Int., **108**, 502-506.

Crossley, D.J., Rochester, M.G. & Peng, Z.R., 1992. Slichter modes and Love numbers, Geophys. Res. Lett., **19**, 1679-1682.

Crossley, D.J., 1992. Eigensolutions and seismic excitation of the Slichter mode triplet for a fully rotating Earth model, EOS, Trans. Am. Geophys. Un., **73**, 60-.

Crossley, D.J., 1993. The gravity effect of core modes for a rotating Earth, submitted to J. Geomag. Geoelec..

Dahlen, F. A., & Sailor, R.V., 1979. Rotation and elliptical splitting of the free oscillations of the Earth, Geophys. J. Roy. astr. Soc., **58**, 609-623.

Dziewonski, A.M., & Anderson, D.L., 1981. Preliminary reference Earth model, Phys. Earth Planet. Int., **25**, 297-356.

Friedlander, S. & Siegmann, W.L., 1982. Internal waves in a rotating stratified fluid in an arbitrary gravitational field, Geophys. Astr. Fluid Dyn., **19**, 267-291.

Friedlander, S. & Siegmann, W.L., 1983. Effects of dissipation on internal waves in a contained rotating stratified fluid, Geophys. Astr. Fluid Dyn., **27**, 183-216.

Friedlander, S., 1985a. Internal oscillations in the Earth's fluid core, Geophys. J. Roy. astr. Soc., **80**, 345-361.

Friedlander, S., 1985b. Stability of the subseismic wave equation for the Earth's fluid core, Geophys. Astr. Fluid Dyn., **31**, 151-167.

Gilbert, F., 1970. Excitation of the normal modes of the Earth by earthquake sources, Geophys. J. Roy. astr. Soc., **22**, 223-236.

Higgins, G. & Kennedy, G.C., 1971. The adiabatic gradient and the melting point gradient in the core of the Earth, J. Geophys. Res., **76**, 1870-1878.

Hinderer, J., Crossley, D.J., Jensen, O.G. & Xu, H., 1992. Gravity noise levels and periodic signals observed from a common 2 year analysis of the French and Canadian superconducting gravimeters, EOS, Trans. Am. Geophys. Un., **73**, 60-.

Hinderer, J., Crossley, D.J. & Xu, H., 1993. A 2 year comparison between the French and Canadian superconducting gravimeter data, Geophys. J. Int., (in press).

Jensen, O.G., Crossley, D.J. & Hinderer, J., 1992. Simple data decomposition reveals a surprisingly rich harmonic spectrum in superconducting gravimeter data, EOS, Trans. Am. Geophys. Un., **73**, 60-.

Johnson, I. & Smylie, D.E., 1977. A variational approach to whole-Earth dynamics, Geophys. J. Roy. astr. Soc., **50**, 35-54.

Lumb, L.I., Aldridge, K.A. & Henderson, G.A., 1992. Towards a generalised 'core resonance' phenomenon : inferences from a Poincaré core model, AGU/IUGG Geophysical Monographs, (in press).

Masters, G., 1979. Observational constraints on the chemical and thermal structure of the Earth's deep interior, Geophys. J. Roy. astr. Soc., **57**, 507-534.

Pekeris, C.L., & Accad, Y., 1972. Dynamics of the liquid core of the Earth, Phil. Trans. Roy. Soc. London, Ser. A, **273**, 237-260.

Rieutord, M., 1991. Linear theory of rotating fluids using spherical harmonics Part II, time-periodic flows, Geophys. Astr. Fluid Dyn., **59**, 185-208.

Rochester, M.G. & Peng, Z.R., 1990. The Slichter mode revisited : a test of the subseismic approximation, EOS, Trans. Am. Geophys. Un., **71**, 1479-.

Rochester, M.G. & Peng, Z.R., 1993. The Slichter modes of the rotating Earth : a test of the subseismic approximation, Geophys. J. Roy. astr. Soc., **113** (in press).

Rydelek, P.A., & Knopoff, L., 1984. Spectral analysis of gapped data: search for mode ${}_1S_1$ at the South Pole, J. Geophys. Res., **89**, 1899-1902.

Singer, H.A. & Olson, P.L., 1984. Dynamo action in a stably stratified core, Geophys. J. Roy. astr. Soc., **78**, 371-.

Smith, M.L., 1976. Translational inner core oscillations of a rotating, slightly elliptical Earth, J. Geophys. Res., **81**, 3055-3065.

Smylie, D.E., 1974. Dynamics of the outer core, Veroff. Zentralinst. Phys. Erde. Akad. Wiss. DDR., **30**, 91-104.

Smylie, D.E. & Rochester, M.G., 1981. Compressibility, core dynamics and the subseismic wave equation, Phys. Earth Planet. Int., **24**, 308-319.

Smylie, D.E., Szeto, A.M.K. & Rochester, M.G., 1984. The dynamics of the Earth's inner and outer cores, Rep. Prog. Phys., **47**, 855-906.

Smylie, D.E. & Rochester, M.G., 1986. Long period core dynamics, in *Earth Rotation : Solved and Unsolved Problems; Proc. NATO Advanced Study Workshop*, 297-324, A. Cazanave, D. Reidel.

Smylie, D.E., Szeto, A.M.K., & Sato, K., 1990. Elastic boundary conditions in long-period core oscillations, Geophys. J. Int., **100**, 183-192.

Smylie, D.E., 1992. The inner core translational triplet and the density near Earth's center, Science, **255**, 1678-1682.

Smylie, D.E., Jiang, X., Brennan, B.J. & Sato, K., 1992. Numerical calculation of modes of oscillation of the Earth's core, Geophys. J. Int., **108**, 465-490.

Valette, B., 1989. Étude d'une classe de problèmes spectraux, C.R. Acad. Sci. Paris, **309**, 785-788.

Smylie, D.E. & Qin, Y., 1992. The effects of viscosity and rotation on the translational oscillations of the inner core, EOS, Trans. Am. Geophys. Un., **73**, 60-.

Widmer, R., Masters, G. & Gilbert, F., 1988. The spherical Earth revisited, EOS, Trans. Am. Geophys. Un., **69**, 1310-.

Wu, W.-J. & Rochester, M.G., 1993. Computing core oscillations eigenperiods for the rotating Earth: a test of the subseismic approximation, Phys. Earth Planet. Int., (in press).

TABLE 1. Periods[1] of the Slichter triplet for CORE 11

| Truncation Level | $m = +1$ retrograde | $m = 0$ central | $m = -1$ prograde | Comments |
|---|---|---|---|---|
| ? | 3.7195 | 3.5056 | 3.3432 | computed[2] |
| - | 4.0150 | 3.7677 | 3.5820 | 'observed'[2] |
| $\Omega = 0$ | 5.9469 | 5.9469 | 5.9469 | 5.9520[3] |
| $S_1$ | 5.2523 | 5.9469 | 6.7336 | Self coupling |
| $T_2$ | 5.1638 | 5.8068 | 6.6100 | |
| $T_2$ | 5.1663 | 5.8044 | 6.5980 | Perturbation theory |
| $S_3$ | 5.1605 | 5.7999 | 6.6035 | |
| $T_4$ | 5.1603 | 5.7994 | 6.6029 | |
| $S_5$ | 5.1603 | 5.7993 | 6.6029 | Converged periods |

[1]Periods in *hr* include rotation as noted, but no viscosity. From Crossley (1992), using dynamic Love numbers and no SSA.

[2] Smylie (1992), using static Love numbers and SSA-2.

[3] Masters & Dahlen, personal communications (1992).

# Three Years of Experiences with a Movable Superconducting Gravimeter at the Underground Installation Site in the Salt Mine ASSE in Northern Germany.

D. Flach, G. Gommlich
Institut für Tieflagerung der GSF
Theodor-Heuss-Str. 4
D-3300 Braunschweig
Germany

G. Jentzsch
Institut für Geophysik der TU Clausthal
Postfach 1253
D-3392 Clausthal-Zellerfeld
Germany

## 1. Introduction

According to the reference concept for direct disposal of spent fuel, large and heavy disposal casks will be employed onto the floor of repository drifts. Licensing of this concept requires demonstration of a suitable backfilling technique, investigation of the behaviour of the rock salt and the backfill material, and comparison of results of these in-situ measurements with predictive model calculations. The investigations are taken out in the Asse salt mine in Northern Germany. Participating companies in the demonstration experiment are DBE, GSF, BGR and KfK*).

Measurements of rock salt deformation and temperature distributions will be performed by GSF. Additionally GSF performs measurements of the settling behaviour and the density of the backfill material. In the geotechnical program stresses in the rock salt and permeabilities in the backfill will be determined. There are important interests to describe the compaction of the backfill under compaction pressure as a function of time and temperature.

All conventional methods used to determine the density and porosity of formations need a borehole directly into the body investigated. The probes represented the petrophysical parameters only for a small locality. More values of slow variations of parameters by integral methods such as gravity measurements are needed. To get information about the behaviour of the rock salt under thermal conditions like flew of masses and changes of rock density due to convergence should be investigated with a mobile gravimeter system with sensitivity and resolution of about one magnitude better than available by normal field gravimeters.

A known gravimeter type with expected characteristic is the superconducting gravimeter of GWR, but this instrument was constructed for stationary observations. First contacts with the

*) DBE: Deutsche Gesellschaft zum Bau und Betrieb von Endlagern für Abfallstoffe mbH,
GSF: Forschungszentrum für Umwelt und Gesundheit,GmbH,
BGR: Bundesanstalt für Geowissenschaften und Rohstoffe,
KfK: Kernforschungszentrum Karlsruhe

producer lead to a new movable system based on the gravimetric reference station TT70 modified to costomers specifications installed in a movable frame (GWR, 1989).

## 2. Description of the movable superconducting gravimeter

The given boundary conditions for the application of a movable superconducting gravimeter system under the special conditions of a mine (relative high but constant temperature and the restriction that one cannot control the system all the time) required lots of extra construction work by the staff of GWR. The most obvious design changes of the new system are the triangular frame construction which supports the electric drive and the levelling platform for the gravimeter resting on the rails. There are two levelling systems: The fast system controls the vertical adjustment by electromechanical micrometer screws during the mobile phase while the other electro-hydraulic levellers aligne the gravimeter during the measurement.

The external additional cooling supply is dismounted when the gravimeter is moving outside the permanent station. The Helium consumption under cool head is 0.4 litre/day. It amounts to 2.9 litre/day when the instrument is driven without external cooling. These values are best and worst. When a leakage occurs in the Helium compressor unit, the Helium consumption under cool head is increased by factor two.

The whole electronics are mounted to the movable platform. The recording of tide and mode channels as well as air pressure at the station and other diagnostic data was done by a multichannel digital paper chart recorder with a paper speed of 20 mm/h. A high resolution data acquisition system was installed later and was not in use for the long time period discussed here. Now we are able to ask all parameters via telephone modem and personal computer under DOS. Even the time problem is solved by OMEGA time base. Air pressure was recorded on the surface of the mine by a meteorological station.

## 3. Some experimental results

The profile for the superconducting gravimeter was installed on the 750 m level of the mine. Fig. 1 shows a 3-dimensional view with the gravimeter gallery on the upper level (light grey) and the other drifts on the same and deeper level which must be taken into account for reductions. For better orientation there is the projection of the gravimeter gallery down to the 800 m level.

The backfill experiment is situated 50 m below the gravimeter position. The profile consists of a 70 m long rail road track section with 15 stations separated from each other by 5 meters. These rails are accurately levelled in both horizontal directions in order to minimise horizontal accelerations during a run from one station to another with a speed of 0.05 m/s. There is a positioning system in combination with a program controlled acceleration and retardation drive mode. The positioning accuracy is better than 1 mm for all distances.

During the first time of operation many steps were observed in the records of the tide and mode channels. But in course of

time they became more seldom and perhaps smaller so that they can not be seen in the records any more. These steps did occur also when the gravimeter was touched. This problem is not solved until now and it happened some times that a step occurred just before the start for the motion to the next station. Therefore it is not sure whether or not during the motion one or more steps had appeared and had effected the whole measurement program.

Fig. 2a shows the original data (differences in gravity) recorded when the SCG had been positioned at different stations. The letter A denotes measurements at the reference station A, whereas the other values mark the station numbers which are in accordance to the distance from the basic station A. A fairly strong drift can be observed over the whole period. For comparison fig. 2b gives the theoretical tides taking into account the local tidal parameters.

The normal drift of the instrument under stationary conditions is substantially less (see special section on data analysis). The differences between observed and theoretical gravity are the anomaly along the profile seen in fig. 3.

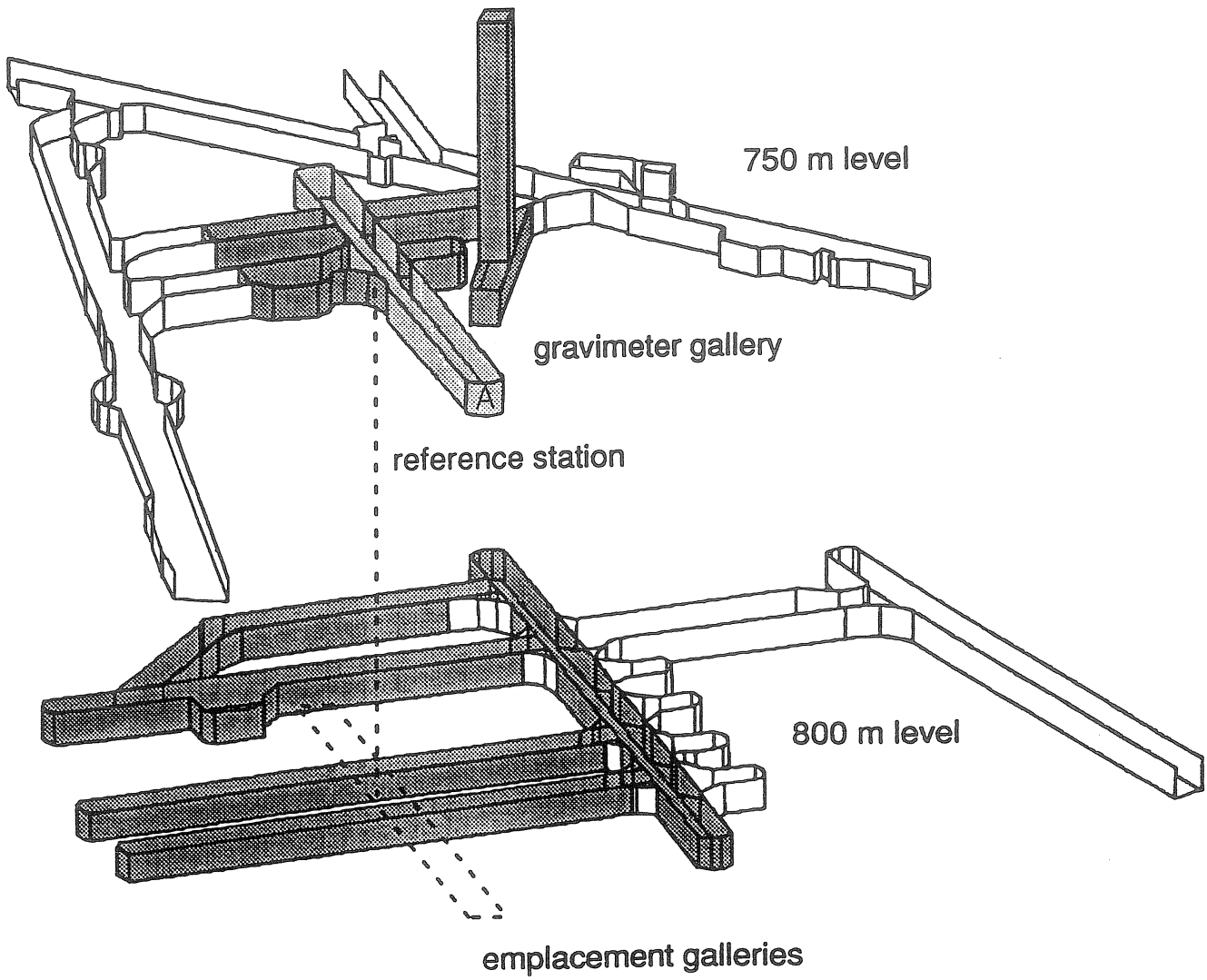


Fig. 1: 3-d view of a part of the mine drifts for the 750 m and 800 m levels: The gravimeter is installed with reference station A (750 m level, light grey). Galleries which have to be taken into account for reduction computation are in dark grey.

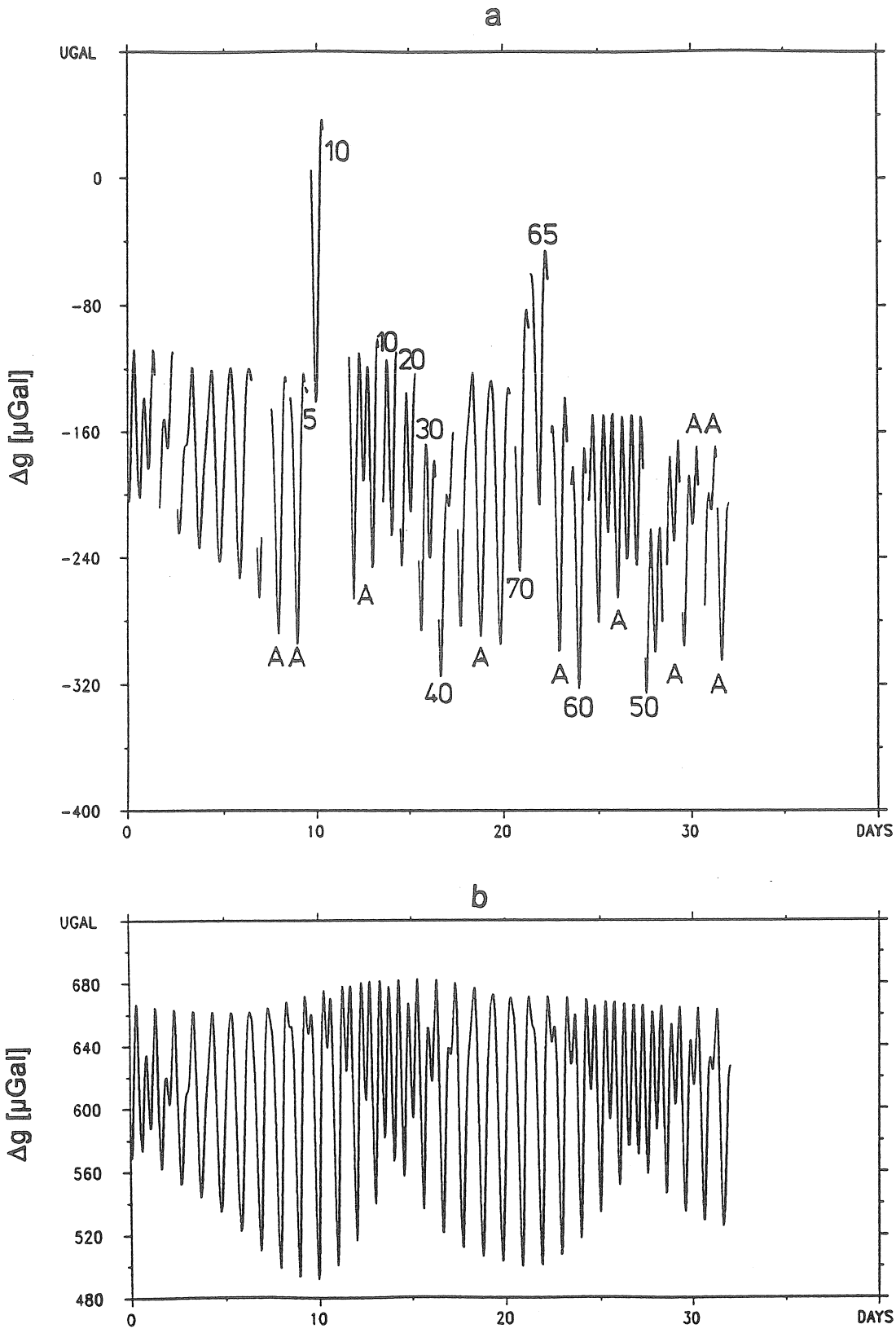


Fig. 2: (a) Record from the roving phase (13.02.90, 0:00 UTM to 16.03.90, 23:00 UTM): 'A' indicates the position at the reference station; numbers denote the other stations; (b) theoretical tides including local tidal parameters for the same period.

Fig. 3a gives the observations in chronological order which is not identical with local order provided in fig. 3b (grid space is 100 h, tic mark space is 1 day). The squares denote the values for the location A (reference station). These points are to be found on a straight line which shows the enormous drift when the instrument was moved. The linearity indicates constant rates. This phase could continue over long times, longer than some days.

Fig. 3b is the tidally corrected anomaly of gravity differences versus distances. The profile direction is south to north. For this case the gravity increases about 3.5 $\mu$Gal per 5 m (station spacing) to the north. This effect and the regional effect of the Asse run in the same direction for the gravity anomaly. On the other hand complicated modelling is necessary for the compensation of local effects of cavities in the vicinity of the gravimeter gallery. These computations were done by the program G3D (Casten, 1992).

## 4. Data analysis and calibration

The first part of the data set recorded anlogously (one hour samples) was analysed by Jentzsch (1992) according to standard methods (Wenzel, 1976). Fig. 4 shows the plot of the data before corrections were applied. For the same period the air pressure data from the surface was available.

All the steps and disturbances (esp. around 7000 to 7500 hours) are due to instrumental tests and the discussed movements, respectively. Obviously the drift of the gravimeter is very small. But, due to the resolution of the digitization the dynamic range of the data is less than 10 bit (equivalent to 60 dB).

The calibration of the record was carried out comparing the calculated tidal vector with the theoretically expected one. This theoretical vector consists of the vector for the earth tidal model (Dehant et al., 1991) equivalent to the amplitude of the theoretical tides multiplied by the appropriate $\delta$-factor and the vector of ocean loading calculated according to Farrell (1972). Here, the results for M2 and O1 were used: The ocean loading vector for M2 is 1.072 $\mu$Gal / 68.8°, and for O1 we find 0.169 $\mu$Gal / 173.0°.

The calculations were carried out for a hundred days interval of the record to find the smallest rest vector. The application to the whole data set revealed that the calibration factor of 0.172 $\mu$Gal per scale unit provided the best fit.

Several analyses were performed: The whole data set was analysed applying 21 different wave groups as well as 22 wave groups including Mf (comp. tab. 1). The resulting mean square error of little more than 0.5 $\mu$Gal corresponds well to the resolution of the digitization. Further, analyses were carried out covering 100 days periods shifted by 50 days. Here, the least squares errors varied between 0.4 $\mu$Gal and 1.1 $\mu$Gal. The parameters for M2 and O1 showed significant variations of ± 0.2% and ± 0.5% in amplitude and ± 0.3° and ± 0.2° in phase, respectively.

The correction of air pressure resulted in a regression coefficient of 0.220 $\mu$Gal/HPa. Applying this correction reduced the noise levels in the tidal bands not considerably; only in case of the diurnal constituents a reduction by nearly 20% appeared.

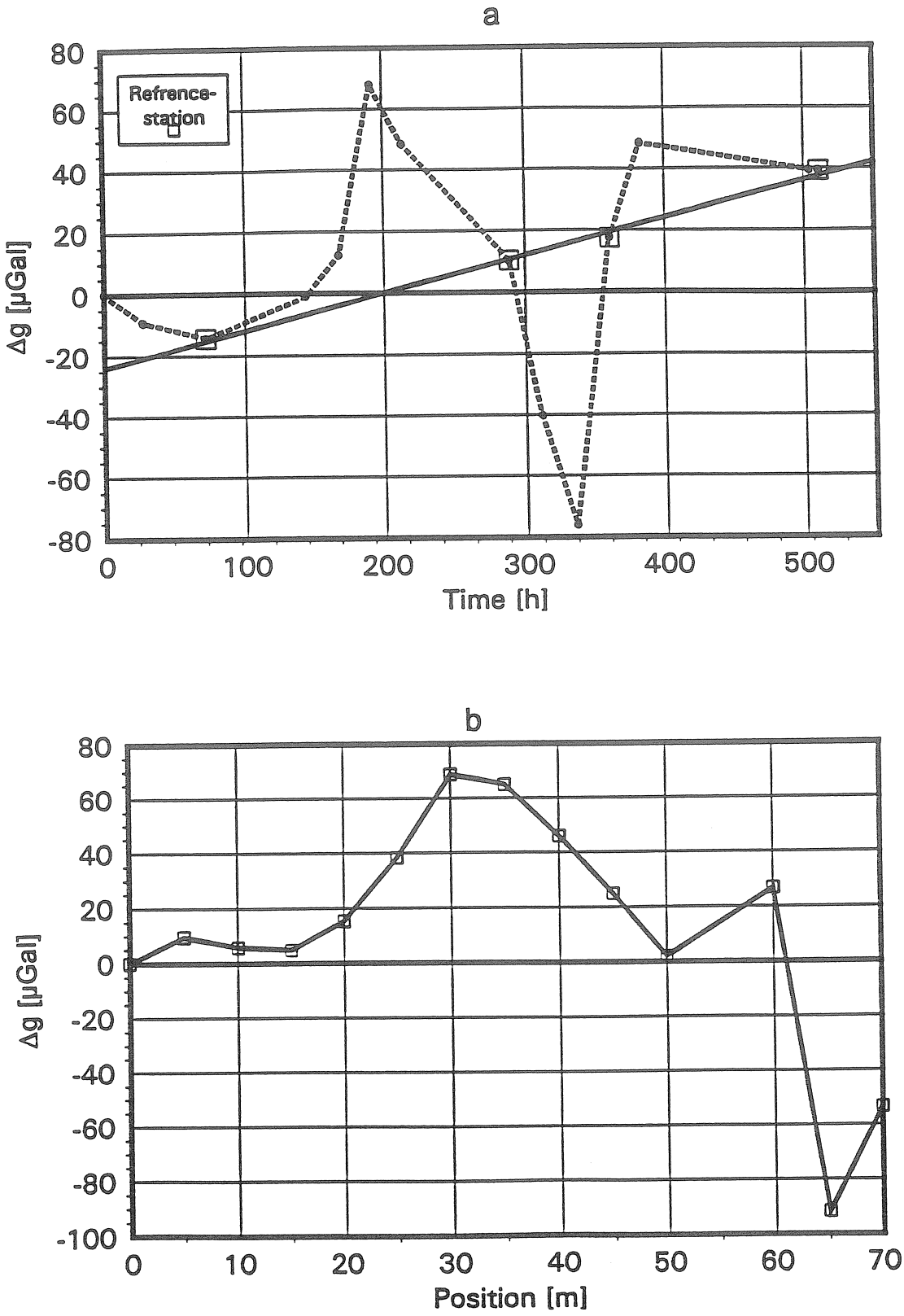


Fig. 3: (a) Chronological sequence of the gravity record corrected for tides showing the strong instrumental drift; (b) The anomaly measured along the gallery (drift reduced).

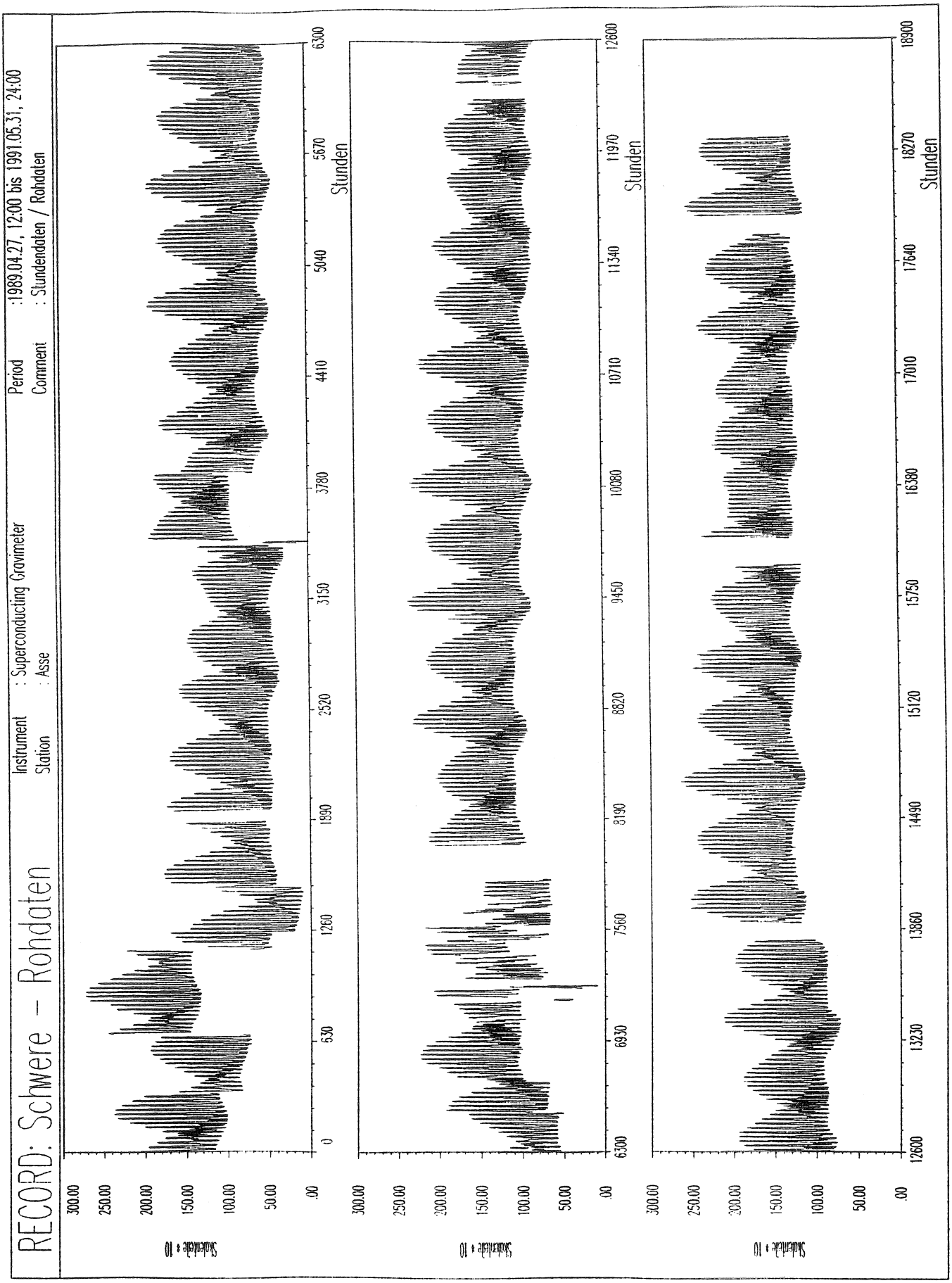


Fig. 4: Hourly samples of the gravimeter data covering the period of more than three years (April 27, 1989 to May 31, 1991). One scale unit corresponds to 0.172 $\mu$Gal; times are given in hours and amplitudes in scale units.

Tab. 1: Results for the main tidal waves (671.8 days equiv. degree of freedom 16078); error bars from noise levels of the residuals; msq error for fit of diurnal and semi-diurnal waves is 0.671 μGal.

| NR. | FROM | TO | WAVE | AMPL. MYGAL | SIGNAL/ NOISE | AMPLI.FAC. | PHASE LAG DEG |
|---|---|---|---|---|---|---|---|
| 1 | 60 | 74 | MF | 4.6779 | 78. | .8399 | -7.3263 |
| | | | | ± .0598 | | .0107 | .7329 |
| 3 | 164 | 178 | Q1 | 6.7117 | 112. | 1.1641 | -1.1047 |
| | | | | ± .0598 | | .0104 | .5108 |
| 5 | 194 | 219 | O1 | 34.9780 | 585. | 1.1615 | -.3383 |
| | | | | ± .0598 | | .0020 | .0980 |
| 6 | 220 | 241 | M1 | 2.7473 | 46. | 1.1601 | -1.1786 |
| | | | | ± .0598 | | .0253 | 1.2480 |
| 7 | 242 | 251 | P1 | 16.0991 | 269. | 1.1487 | -.3663 |
| | | | | ± .0598 | | .0043 | .2130 |
| 9 | 255 | 265 | K1 | 48.4929 | 810. | 1.1449 | -.2515 |
| | | | | ± .0598 | | .0014 | .0707 |
| 11 | 268 | 304 | J1 | 2.8020 | 47. | 1.1835 | -.9820 |
| | | | | ± .0598 | | .0253 | 1.2236 |
| 15 | 375 | 398 | N2 | 6.4145 | 148. | 1.1831 | .5902 |
| | | | | ± .0432 | | .0080 | .3859 |
| 16 | 399 | 424 | M2 | 33.7342 | 781. | 1.1913 | .8368 |
| | | | | ± .0432 | | .0015 | .0734 |
| 19 | 444 | 450 | S2 | 15.5982 | 361. | 1.1840 | -.5626 |
| | | | | ± .0432 | | .0033 | .1587 |
| 20 | 451 | 459 | K2 | 4.2952 | 99. | 1.1991 | .1187 |
| | | | | ± .0432 | | .0121 | .5763 |
| 22 | 489 | 505 | M3 | .3282 | 17. | .9602 | -6.9907 |
| | | | | ± .0189 | | .0552 | 3.2937 |

Fig. 5 containes the long-term drift after separation of the tides including the long period wave Mf. The drift over the two years covers a range of about 180 μGal where the first running-in period of nearly 100 days comprises already about one half of this magnitude. To resolve signals like man made gravity changes in the mine or even the height changes due to the salt tectonics a careful analysis of the air pressure effect in that particular period range is cruxial.

## 5. Discussion and conclusions

Up to now the movable SCG does not provide the expected resolution for field measurements because of strong drifts and after effects. An increase of drift ( < 3 μGal/day) is correlated with the start of the roving phase of the instrument. During the tests by the company GWR in San Diego this behaviour was not observed. A possible reason could be the relatively high temperature of 38°C in the gallery. Further, it takes several hours for the sphere to stabilize after these movements which also effects the accuracy of the measured differences.

All data shown here were taken from a paper recorder with an resolution of about 0.16 μGal; the sampling rate was 1 hour. Thus, according to the resolution we cannot expect that the evaluated

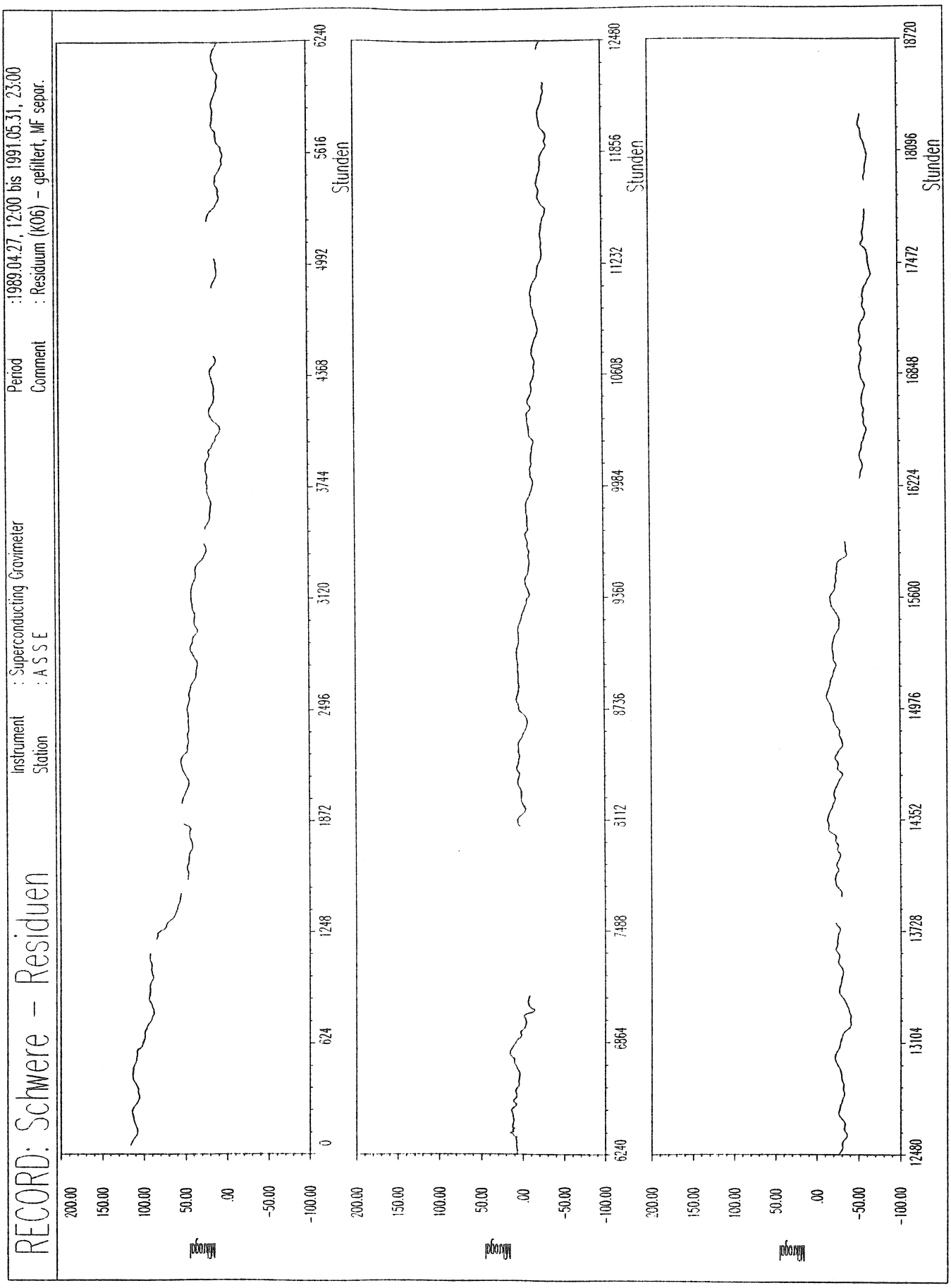


Fig. 5: Long-term drift of the gravimeter covering the same period as fig. 4; amplitudes are given in micorgal and time in hours. The oscillations are not due to tides (Mf separated).

tidal parameters and the errors derived from the spectrum of the residuals are able to compete with the results published by Richter (1987) for the station Bad Homburg, Germany. But the results are comparable to those obtained from the station Wuhan, China, where at the beginning the chart stepped analog record hat to be used, too. Later, also there a high resolution data acquisition system was applied, but due to the noisy surroundings for the tides not much improvement could be achieved (Hsu et al., 1991; 1993). On the other hand, the Chinese data as well as the stationary underground observations at Asse show very small drifts nearly without any linear term. Compared to the air pressure it looks like that most of the effect is due to this source.

Thus, it seems obvious to us that the movable TT70 is not applicable to its originally intended purpose, but according to the stable long-term properties it is worth using it in the usual stationary way to record gravity changes induced by the activities in the mine. But for this purpose esp. the long-term part of the record has to be calibrated against air pressure very carefully.

For the continuation of the recording a digital data acquisition system provided by GWR is now attached (starting at the beginning of 1993). This includes a diagnostic system and a 22 bit ADC for the tidal channel. For most channels different sample rates can be selected. For the tidal channel the sample rate is 0.05 Hz equivalent to a sampling intervall of 20 seconds.

## 5. References

Casten, U., 1992. Gravimetrische Messungen im PAE-Feld zur Bestimmung der Schwereanomalie mit einem Feldgravimeter. Unpublished report.

Dehant, V., B. Ducarme, G. Jentzsch, J. Kääriäinen, G.Y. Li, S.M. Molodensky, S. Okubo, J. Wahr, Q.W. Xi, and J. Zschau, 1991. Report of the working group on Theoretical Tidal Model. Proc. 11th Int. Symp. Earth Tides, Helsinki, 1989, Schweitzerbart, Stuttgart.

Farrell, W.E., 1972. Deformation of the earth by surface loads. Rev. Geophys. Space Phys., 10, 761-797.

GWR Instruments, 1989. Superconducting Gravity Meter Model TT70 Cryogenic Refrigeration, Operating Manual.

Hsu, H.T., Jahr, G. Jentzsch, and G.X. Tao, 1989. Some results from SCG in Wuhan/China. BIM., 110, 7973-7979.

Hsu, H.T., G. Jentzsch, C. Kroner, G.X. Tao, and A. Weise, 1993. The 6-years record of the SCG at Wuhan/China. In prep.

Jentzsch, G., 1992. Analyse der Daten des Supraleitenden Gravimeters im Salzbergwrk Asse. Unpublished report.

Richter, B., 1987. Das supraleitende Gravimeter. Deutsche Geodätische Kommission, Reihe C, Nr. 329.

Wenzel, H.G., 1976. Zur Geneuigkeit gravimetrischer Erdgezeiten-beobachtungen. Wiss. Arb. Lehrst. Geodäsie, Photogrammetrie und Kartographie, TU Hannover, Nr. 67.

# First Results of the Registration with the Superconducting Gravimeter installed at Gravimetric Observatory Potsdam.

J. Neumeyer, H-J. Dittfeld
GeoForschungsZentrum Potsdam
Telegrafenberg
O-1561 Potsdam
Germany

To prolongate the long term tidal registration with Askania spring gravimeters on a higher level a new Superconducting Gravimeter (SCG) TT70 No.18 of company GWR San Diego California has been installed at the Gravimetric Observatory Potsdam Telegrafenberg. It is in operation since June 1992.

The location of the SCG is the north-east-cellar of building A17 site S12, very near to the absolute measurement point S14 (Elstner 1991).

The environmental parameters of the observation are as follows:
Geological structure: sedimentary
Room temperature: 22±3 degrees in Celcius
Relative humidity: 50±10%.

Fig. 1 shows the components of the Superconducting Gravimeter.

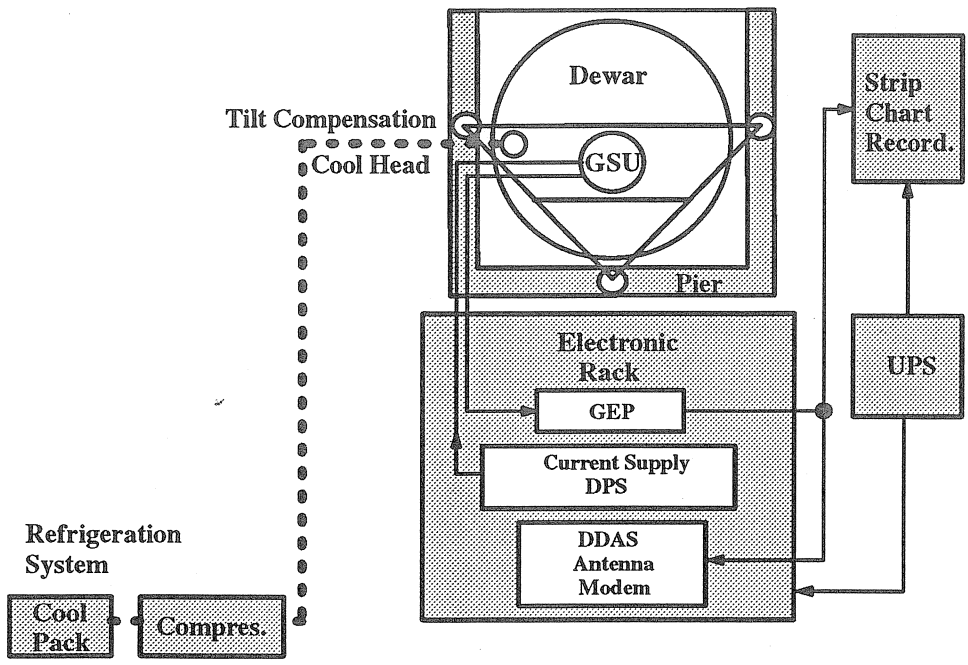


Fig.1. Complete SCG in operation

The Pier made of blocks of porphyrry carriers the Dewar with the Gravity Sensing Unit (GSU).

The Dewar filled with liquid Helium has a lost rate of about 0.4 liters a day. This means the system can work about 400 days without refilling. The refrigeration system Cool-Pack and Compressor support the cooling process.

The Gravity Sensing Unit inside the Dewar works at a temperature of 4.2 K under superconducting conditons. The measurement princip is the levitation of a sphere in a constant magnetic field and the detection of it's displacements by a capacitive tranducer. The system has an automatically working tilt compensation.

The temperature controlled Electronic Rack contains the measurement electronics (GEP), the current supply for the magnetic coils (DPS) and the data acquisition and communication system (DDAS).

The DDAS has 33 input channels. One of the channels has a resolution of 22 bits. It is used as gravity channel. The other 32 channels have a resolution of 16 bits. They are used as tide and mode channels, for recording of air pressure, special supervising parameters of the SCG and the room temperature. The online working digital filter produces two additional channels filtered gravity and filtered air pressure. The data are stored in a ring buffer on a hard disk with a capacity of 30Mb. Depending on sampling rate data of several month can be stored.

Access to the data is possible via floppy disk or modem. The time synchronization is done by a Omega clock. An uninterruptable power supply (UPS) supplies the whole system.

The calibration factor of the SCG was determined by comparison with a local tidal model based on results of former registrations with well calibrated LaCoste Romberg Gravimeters. The time lag of the SCG was measured according to the step response method (Richter, Wenzel 1991) by means of the built in electrostatic force. It changes the position of the sphere by leaps. The recorded data were evaluated with the program ETSTEP (Wenzel 1991)

The processing of the data is shown in Fig. 2.

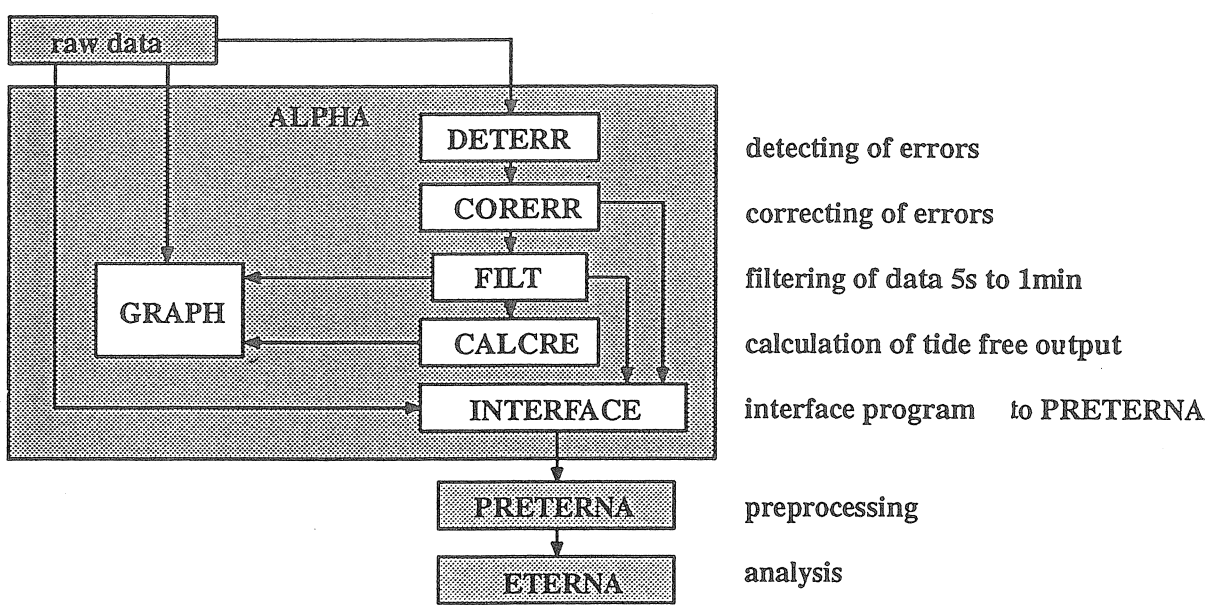


Fig.2. Processing of SCG data

The processing of data starts with the program ALPHA. The input data of ALPHA are the raw data gravity-file and pressure-file of the data acquisition system (DDAS) sampled in 5

seconds intervals. These data must be prepared for preprocessing and analysing. The program ALPHA has been developed to solve this task. The preprocessing is done by PRETERNA (Wenzel 1992) and the tidal analysis is done by ETERNA (Wenzel 1991).

The following steps are carried out by ALPHA:
- detecting and correcting of sequence errors
- detecting of data gaps
- closing of data gaps by a gap value
- calculation of tide free signal
- filtering of gravity-file and pressure-file (5 seconds to 1 minute)
- online plotting of theoretical tide, tide free signal, filtered gravity file, gravity-file and filtered pressure file
- print a listing of sequence errors and data gaps
- generate a sequence corrected gravity file
- generate a sequence corrected pressure file
- generate the inputfile for PRETERNA

The functions of PRETERNA and ETERNA are discribed in the corresponding read me files.

Fig. 3. Air Pressure and Tide free output of SCG

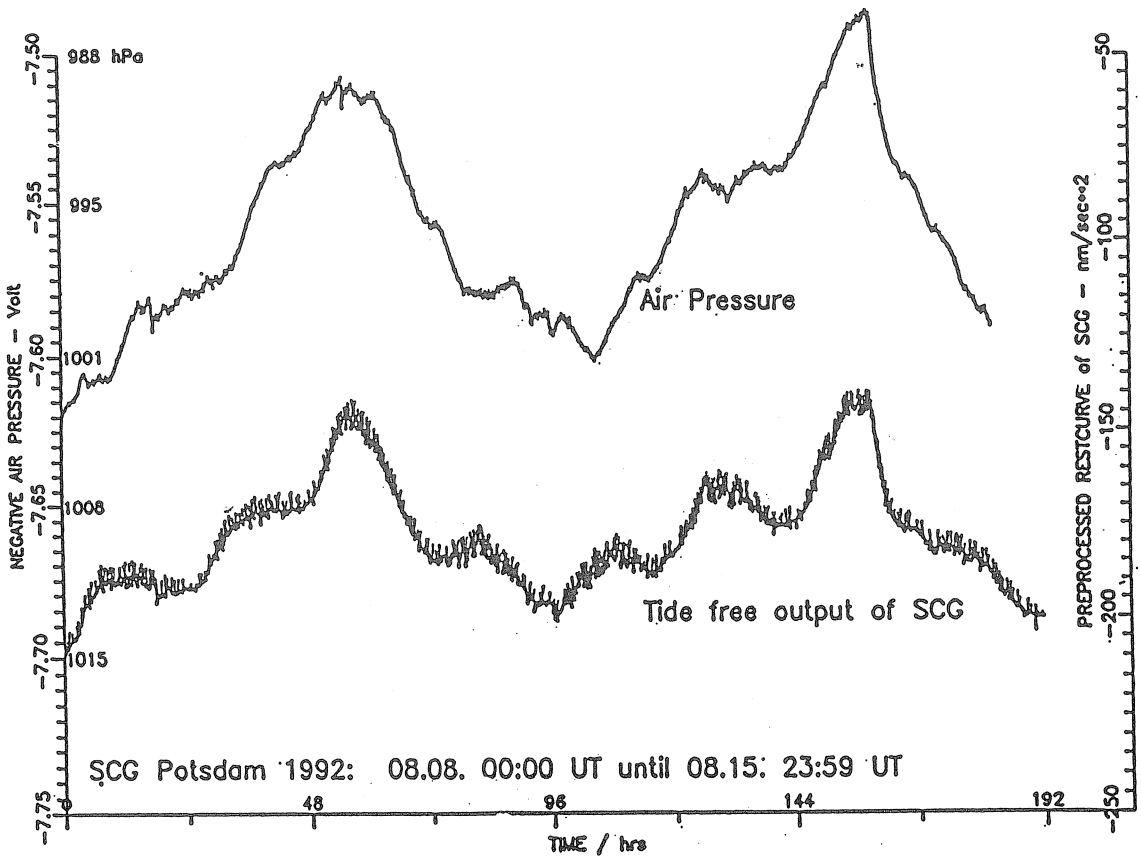


The tide free output reveals a high correlation with the non tidal effect due to air pressure (s. Fig. 3)

Appendix 1 shows the analysis result of the first measurements of the SCG of a period of 231 days from the end of June to the end of February 1992. The analysis result is air pressure corrected and yields a standard deviation of 1.06 nm/s$^2$.

In Appendix 2 a first attempt to get parameters for longperiodic tidal waves is reported. The standard deviation is about ten times higher than those of the analysis of short periodic tidal waves. Nevertheless and in spite of the short measuring interval the MF amplitude factor is estimated with a comparatively good accuracy and differs after the ocean correction 0.01 % against the model only (Dehant 1987).

The analysis of this registration period already demonstrates the high quality and stability of the Superconducting Gravimeter. The inner accuracy in the short periodic range is about 30 % higher than those obtained with the best classical instrument (LaCoste Romberg) at the Potsdam station.

The drift reveals a nearly linear behaviour during the observation period. The best fitted line of the tide free output shows a drift of 15.2 nm/s$^2$ per month although long periodic effects like polar motion are not yet regarded. These small drift offers to research long periodic non tidal and tidal effects.

## REFERENCES

Elstner, C. (1991); On the results of absolute gravity measurements at Potsdam in the period 1976 - 1990, Cahiers du Centre de Geodynamique et de Seismologie Volume 3 - 1991.

Wenzel, H.-G. (1992); Program PRETERNA, University of Karlsruhe.

Wenzel, H.-G. (1991); Program ETERNA20, University of Karlsruhe.

Wenzel, H -G. (1991); Program KSPRUNG, University of Karlsruhe.

Richter B.; Wenzel H. -G. (1991); Precise Instrumental Phase Lag Determination by the Step Response Method, Bulletin d´Informations Marees Terrestres, 111, 8033-8052 Bruxelles.

Richter B. (1987); Das supraleitende Gravimeter, Dt. Geod. Komm., Reihe C, Nr.329 Frankfurt 1987

Dehant, V. (1987); Tidal Parameters for an Inelastic Earth, Physics of the Earth and Planetary Interiors, 49, 97-116, 1987

## Appendix 1 Analysis Result of SCG Potsdam

EARTH TIDE STATION NR. 765
GRAVIMETRIC OBSERVATORY, GEOFORSCHUNGSZENTRUM POTSDAM,
52.3806N 13.0682E H 81M P 1M VERTICALCOMPONENT
GRAVIMETER TT70 NO. 018
1992 UNIFIED VERSION - CORRECTED BY DEC-FILE
INSTALLATION R. REINEMANN - GWR, SAN DIEGO
MAINTENANCE H.-J. DITTFELD; J. NEUMEYER - POTSDAM
PRETERNA PREPROCESSING; ETERNA ANALYSIS OF GRAVFLT CHANNEL
INSTRUMENTAL LAG CORRECTED FOR 0.065 DEG O1 AND 0.136 DEG M2

SUMMARY OF OBSERVATION DATA :
1992. 6.30: 0...1993. 2.15:23

INITIAL EPOCH FOR TIDAL FORCE : 1992.10. 1. 0
NUMBER OF RECORDED DAYS IN TOTAL : 231.0
TAMURA 1987 TIDAL POTENTIAL USED.
WAHR-DEHANT-ZSCHAU INELASTIC EARTH MODEL USED FOR A PRIORI AMPLITUDES.
UNITY WINDOW USED FOR LEAST SQUARES ADJUSTMENT.
NUMERICAL FILTER IS PERTZEV 1959 WITH 51 COEFFICIENTS.

ESTIMATION OF NOISE BY FOURIER-SPECTRUM OF RESIDUALS

| | | | |
|---|---|---|---|
| 0.1 CPD BAND | 9999.9999 NM/S**2 | 1.0 CPD BAND | .0852 NM/S**2 |
| 2.0 CPD BAND | .0367 NM/S**2 | 3.0 CPD BAND | .0346 NM/S**2 |
| 4.0 CPD BAND | .0274 NM/S**2 | | |

ADJUSTED TIDAL PARAMETERS :

| NO. | FROM | TO | WAVE | OBS.AMPL. NM/S**2 | SIGNAL/ NOISE | AMPL.FAC. | STDV. | PHASE LAG DEGREE | STDV. DEGREE |
|---|---|---|---|---|---|---|---|---|---|
| 1 | 282 | 424 | Q1 | 65.972 | 774.6 | 1.14662 | .00148 | -.0889 | .0740 |
| 2 | 425 | 482 | O1 | 345.572 | 4057.5 | 1.14996 | .00028 | .1742 | .0141 |
| 3 | 483 | 530 | M1 | 27.178 | 319.1 | 1.14998 | .00360 | .5030 | .1795 |
| 4 | 531 | 547 | P1 | 160.760 | 1887.6 | 1.14971 | .00061 | .0360 | .0304 |
| 5 | 548 | 551 | S1 | 6.362 | 74.7 | 1.92393 | .02576 | .4947 | .7670 |
| 6 | 552 | 586 | K1 | 480.670 | 5643.8 | 1.13733 | .00020 | .2456 | .0102 |
| 7 | 587 | 626 | J1 | 27.278 | 320.3 | 1.15425 | .00360 | .3078 | .1789 |
| 8 | 627 | 731 | OO1 | 14.910 | 175.1 | 1.15300 | .00659 | .1948 | .3273 |
| 9 | 732 | 830 | 2N2 | 9.944 | 270.8 | 1.16129 | .00429 | 2.2886 | .2116 |
| 10 | 831 | 880 | N2 | 62.934 | 1713.9 | 1.17374 | .00068 | 2.0599 | .0334 |
| 11 | 881 | 936 | M2 | 332.127 | 9045.1 | 1.18596 | .00013 | 1.4421 | .0063 |
| 12 | 937 | 975 | L2 | 9.165 | 249.6 | 1.15784 | .00464 | 2.0501 | .2296 |
| 13 | 976 | 996 | S2 | 154.338 | 4203.2 | 1.18454 | .00028 | .1892 | .0136 |
| 14 | 997 | 1108 | K2 | 42.030 | 1144.6 | 1.18656 | .00104 | .6468 | .0501 |
| 15 | 1109 | 1190 | M3 | 3.596 | 103.9 | 1.06863 | .01028 | .6035 | .5513 |
| 16 | 1191 | 1200 | M4 | .003 | .1 | .06808 | .73065 | 116.2093 | 614.8893 |

STANDARD DEVIATION : 1.060 NM/S**2 DEGREE OF FREEDOM : 5461

ADJUSTED METEOROLOGICAL OR HYDROLOGICAL PARAMETERS :

| NO. | REGR.COEFF. | STDV. | PARAMETER |
|---|---|---|---|
| 1 | -.03175 | .00013 | AIRPRES.PASCAL |

## Appendix 2 Analysis Result according longperiodic Tidal Waves

EARTH TIDE STATION NR. 765
GRAVIMETRIC OBSERVATORY, GEOFORSCHUNGSZENTRUM POTSDAM,
52.3806N 13.0682E H 81M P 1M VERTICALCOMPONENT
GRAVIMETER TT70 NO. 018
1992 UNIFIED VERSION - CORRECTED BY DEC-FILE
INSTALLATION R. REINEMANN - GWR, SAN DIEGO
MAINTENANCE H.-J. DITTFELD; J. NEUMEYER - POTSDAM
PRETERNA PREPROCESSING; ETERNA ANALYSIS OF GRAVFLT CHANNEL
INSTRUMENTAL LAG CORRECTED FOR 0.065 DEG O1 AND 0.136 DEG M2

SUMMARY OF OBSERVATION DATA :
1992. 6.30: 0...1993. 2.15:23
INITIAL EPOCH FOR TIDAL FORCE : 1992.10. 1. 0
NUMBER OF RECORDED DAYS IN TOTAL : 231.0
TAMURA 1987 TIDAL POTENTIAL USED.
WAHR-DEHANT-ZSCHAU INELASTIC EARTH MODEL USED FOR A PRIORI AMPLITUDES.
UNITY WINDOW USED FOR LEAST SQUARES ADJUSTMENT.
NO FILTER, DRIFT APPROXIMATION BY TSCHEBYSCHEFF POLYNOM

ESTIMATION OF NOISE BY FOURIER-SPECTRUM OF RESIDUALS
0.1 CPD BAND 1.2440 NM/S**2 1.0 CPD BAND .1009 NM/S**2
2.0 CPD BAND .0402 NM/S**2 3.0 CPD BAND .0338 NM/S**2
4.0 CPD BAND .0280 NM/S**2

ADJUSTED TIDAL PARAMETERS :

| NO. | FROM | TO | WAVE | OBS.AMPL. NM/S**2 | SIGNAL/ NOISE | AMPL.FAC. | STDV. | PHASE LAG DEGREE | STDV. DEGREE |
|---|---|---|---|---|---|---|---|---|---|
| 1 | 35 | 90 | MM | 35.145 | 28.3 | 1.17731 | .04167 | -1.8802 | 2.0281 |
| 2 | 91 | 152 | MF | 64.553 | 51.9 | 1.14223 | .02201 | .0592 | 1.1041 |
| 3 | 153 | 281 | MTM | 12.112 | 9.7 | 1.11940 | .11497 | 1.1869 | 5.8845 |
| 4 | 282 | 424 | Q1 | 65.927 | 653.3 | 1.14583 | .00175 | -.1192 | .0877 |
| 5 | 425 | 482 | O1 | 345.559 | 3424.4 | 1.14991 | .00034 | .1703 | .0167 |
| 6 | 483 | 530 | M1 | 27.139 | 268.9 | 1.14832 | .00427 | .5424 | .2130 |
| 7 | 531 | 547 | P1 | 160.740 | 1592.9 | 1.14958 | .00072 | .0457 | .0360 |
| 8 | 548 | 551 | S1 | 6.399 | 63.4 | 1.93501 | .03052 | .1982 | .9036 |
| 9 | 552 | 586 | K1 | 480.646 | 4763.1 | 1.13727 | .00024 | .2487 | .0120 |
| 10 | 587 | 626 | J1 | 27.291 | 270.4 | 1.15478 | .00427 | .2423 | .2119 |
| 11 | 627 | 731 | OO1 | 14.913 | 147.8 | 1.15317 | .00780 | .2512 | .3877 |
| 12 | 732 | 830 | 2N2 | 9.966 | 247.8 | 1.16389 | .00470 | 2.2876 | .2312 |
| 13 | 831 | 880 | N2 | 62.952 | 1565.6 | 1.17408 | .00075 | 2.0714 | .0366 |
| 14 | 881 | 936 | M2 | 332.147 | 8260.3 | 1.18603 | .00014 | 1.4445 | .0069 |
| 15 | 937 | 975 | L2 | 9.154 | 227.6 | 1.15639 | .00508 | 1.9356 | .2517 |
| 16 | 976 | 996 | S2 | 154.398 | 3839.8 | 1.18501 | .00031 | .2186 | .0149 |
| 17 | 997 | 1108 | K2 | 42.027 | 1045.2 | 1.18650 | .00114 | .6355 | .0548 |
| 18 | 1109 | 1190 | M3 | 3.589 | 106.2 | 1.06654 | .01005 | .5180 | .5397 |
| 19 | 1191 | 1200 | M4 | .011 | .4 | .30465 | .74599 | 68.4823 | 140.2998 |

STANDARD DEVIATION : 10.047 NM/S**2 DEGREE OF FREEDOM : 5501

ADJUSTED METEOROLOGICAL OR HYDROLOGICAL PARAMETERS :

| NO. | REGR.COEFF. | STDV. | PARAMETER |
|---|---|---|---|
| 1 | -.02853 | .00014 | AIRPRES.PASCAL |

ADJUSTED TSCHEBYSCHEFF POLYNOMIAL BIAS PARAMETERS :

| BLOCK NO. | DEGREE | BIAS | STDV |
|---|---|---|---|
| 1 | 0 | 198.1776209874162 | .1589187847430 |
| 1 | 1 | 67.1689840040630 | .2904695629419 |
| 1 | 2 | -17.4943821502211 | .2467077964711 |
| 1 | 3 | 22.0138916839068 | .2291341701746 |

# Drift Representation and Recent Crustal Movements.

T. Chojnicki
Space Research Centre
Warsaw

P.A. Blum
Institute of Earth Physics
Paris
France

*SUMMARY.* The results of analysis of the clinometric measurements, performed from 1974 to 1988 at the Książ station in Poland using a pair of Blum pendulums, are presented. The analysis has been made as a side-product of tidal observations in order to obtain the variations of ground tilting. Comparison of obtained results with the map of recent vertical crustal movement is presented.

Horizontal components of Earth tides have been continuously observed in Poland at the station Książ since the end of 1973. Quartz horizontal pendulums of Blum were used for measurement [Blum, 1963]. The main objective of these studies was to examine short term (diurnal and semidiurnal) variations of ground tilting due to tidal forces. The horizontal pendulum records also long term variation, however, these are not normally analysed and prior to tidal analysis are eliminated as the so-called instrumental drift.

The drift, a side-product of tidal observations, may provide important information on ground movement in the vicinity of the station and contribute to the current studies of vertical movements of the Earth crust. Of substantial value are the data collected at the stations, such as Książ, conducting observations over many years.

Let it be assumed that "purely instrumental" pendulum drift corresponds to the linear trends of full observed drift. After elimination of the instrumental drift we obtain the diagrams of ground tilt on the Książ station for components NS (H-74) and EW (H-75) in the years 1974-1988 - s. Fig. 1. Another words we can say Fig. 1. presents the variation of normal to the ground surface.

Based on these diagrams, Fig. 2 shows a simplified version (by showing only two points per one year) of the movement of the normal line at the station Książ for the period in question..

In order to define the extent of the periodicity of the normal's lppmovement, the data were subjected to Fourier analysis. Fig. 3 shows spectra of individual NS and EW components, with clear yearly oscillations as well as their two-yearly and four-yearly subharmonics. The very shape of the component curves indicates that 16-years' and 8-years' oscillations are also possible, the latter evident only for the NS component.

Yearly oscillations and their subharmonics were expected since they are a natural consequence of seasonable variations on the Earth during the year. Of some interest were oscillations showing frequency of about 0.65 cycles per year (i.e. periodicity of 1.54 years) for the NS component and frequency of about 0.75 cycles per year (periodicity of 1.33 years) for the EW component, considering both their non-seasonable nature and different values for individual components. The oscillations are marked by arrows in Fig. 3. More detailed analysis of these oscillations will be presented below.

The periods given above were used for determination of the parameters of oscillations. The parameters: amplitudes $A_i$, phases $\Phi_i$, linear trend $K$ and difference of reference levels $C$ were calculated by the least square method. The formula used for the minimalised correction $v_t$ was:

$$v_t = F(A_1, \Phi_1, A_2, \Phi_2, \ldots A_n, \Phi_n, K, C) - P_t \qquad (1)$$

where $F$ is a model and $P_t$ is an observed value in the moment $t$. The results are given in Table 1. Fig. 1 presents NS and EW components regularized on the basis of the determined oscilations, shown against the real components. Fig. 4 shows in a simplified manner (half-year values only) the movement of the normal, regularized from the

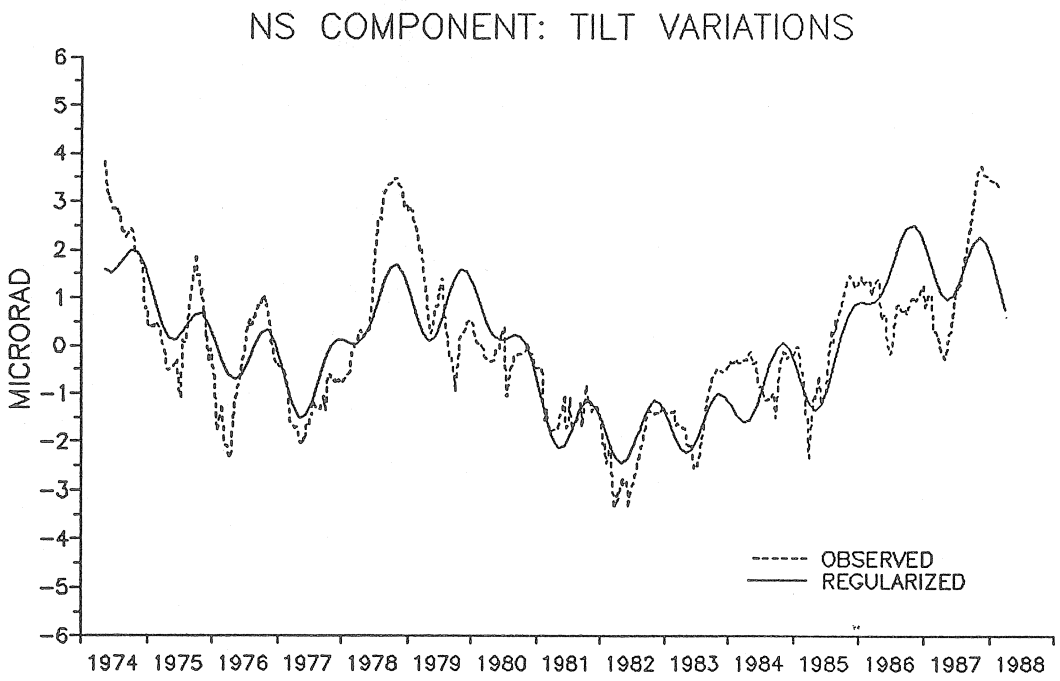


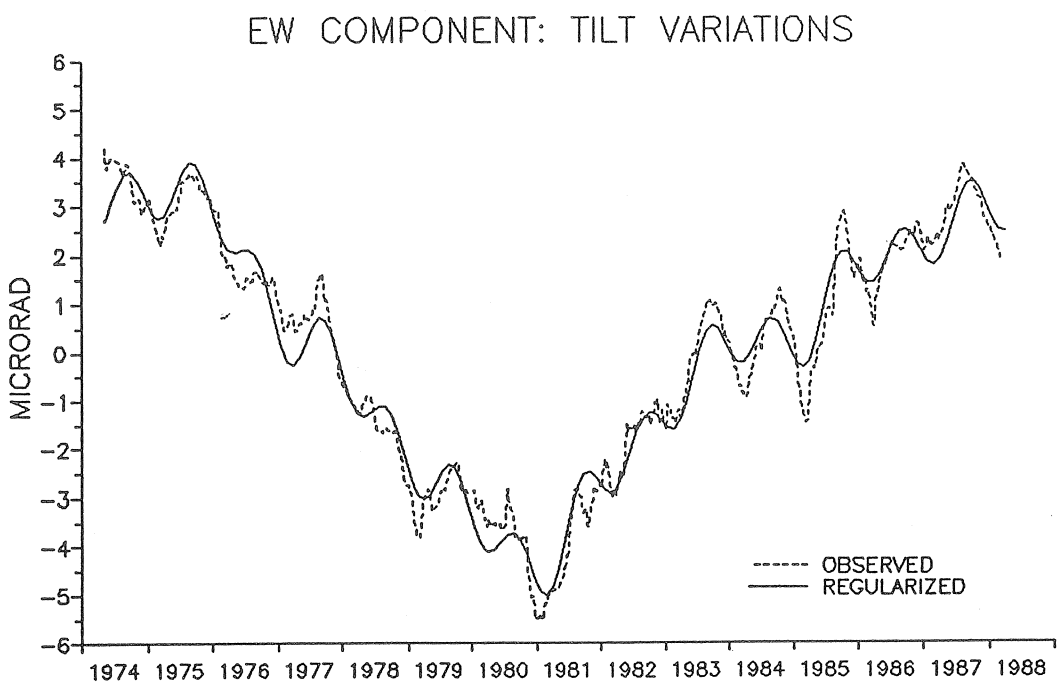


Fig. 1.

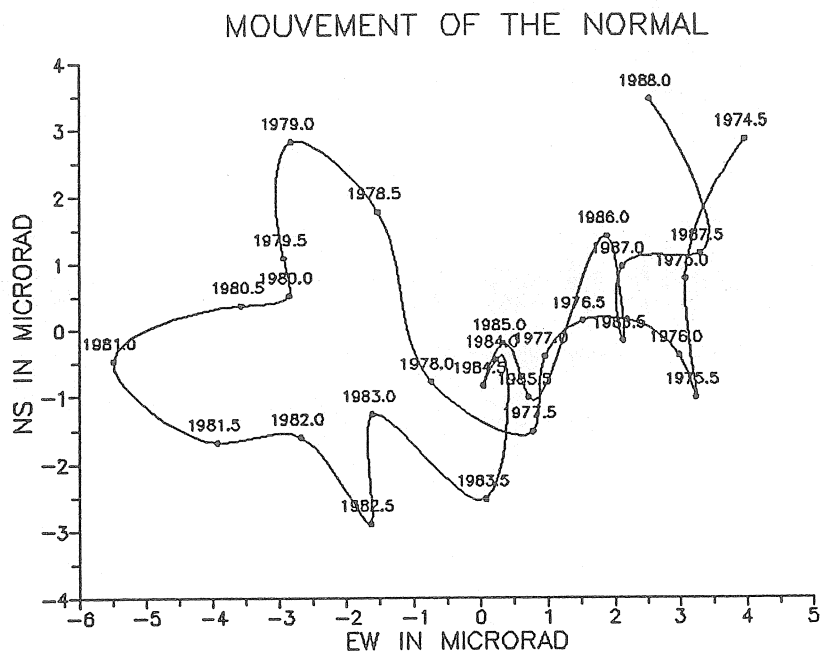
MOUVEMENT OF THE NORMAL
NS IN MICRORAD
EW IN MICRORAD
1988.0
1974.5
1979.0
1978.5
1986.0
1987.5
1979.5
1987.0
1975.0
1980.5
1980.0
1976.5
1985.0
1984.0
1977.0
1978.0
1984.5
1985.5
1976.0
1975.5
1983.0
1977.5
1981.0
1981.5
1982.0
1983.5
1982.5

Fig. 2.

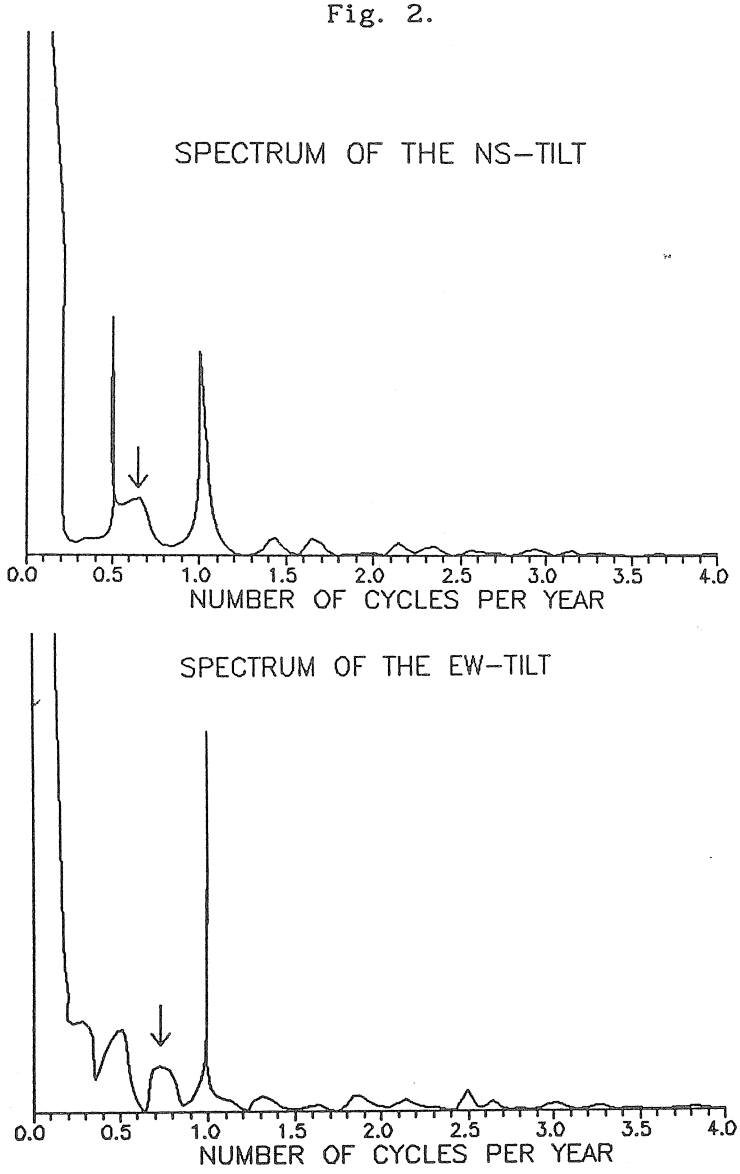
SPECTRUM OF THE NS-TILT
NUMBER OF CYCLES PER YEAR
SPECTRUM OF THE EW-TILT
NUMBER OF CYCLES PER YEAR

Fig. 3.

determined oscillations. It is seen in Figures 1 and 4 that the determined oscillations satisfactorily characterize the real movement of the normal measured at the Książ station.

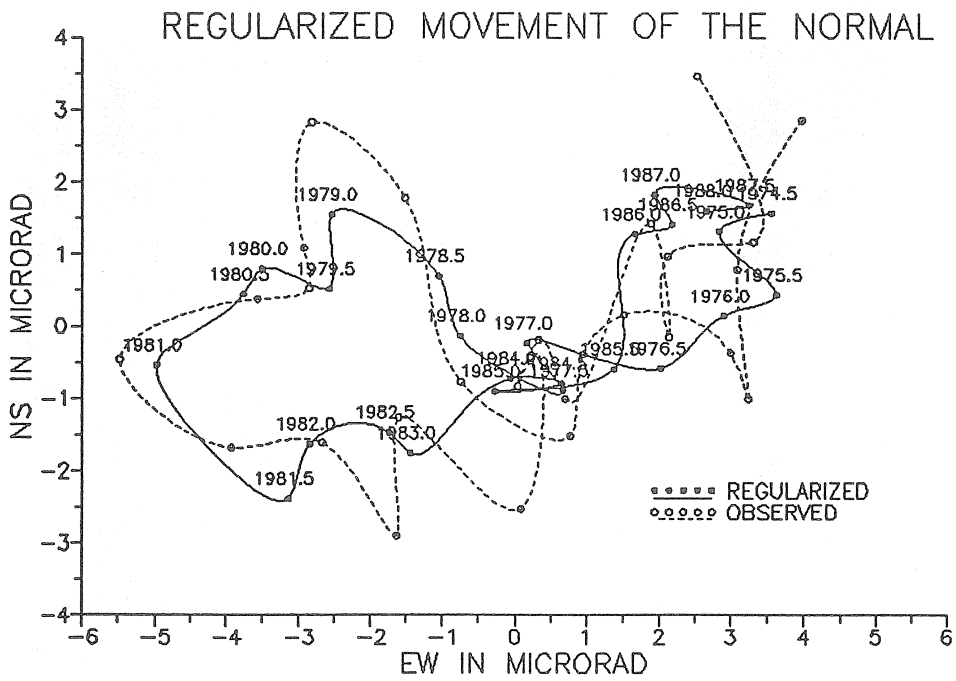


Fig. 4.

Table 1.

| Compos. | Index $i$ | $T_i$ years | $A_i$ μrad | $mA_i$ μrad | $\Phi_i$ rad | $m\Phi_i$ rad |
|---|---|---|---|---|---|---|
| NS | 1 | 1.00 | 0.59851 | 0.17866 | 4.67837 | 0.29806 |
| | 2 | 1.54 | 0.33865 | 0.17874 | 2.90776 | 0.52742 |
| | 3 | 2.00 | 0.32401 | 0.17871 | 1.10560 | 0.55203 |
| | 4 | 4.00 | 0.50020 | 0.17921 | 5.97849 | 0.35936 |
| | 5 | 8.00 | 1.81409 | 0.17789 | 3.83092 | 0.10454 |
| | 6 | 16.00 | 2.08312 | 0.22017 | 2.96100 | 0.15041 |
| | $K$ | | -0.40745 | 0.03148 | | |
| | $C$ | | 2.9938 | 0.2197 | | |
| EW | 1 | 1.00 | 0.56676 | 0.09301 | 5.63078 | 0.16298 |
| | 2 | 1.33 | 0.08589 | 0.09304 | 2.58489 | 1.07947 |
| | 3 | 2.00 | 0.35087 | 0.09302 | 2.75907 | 0.26501 |
| | 4 | 4.00 | 0.44447 | 0.09286 | 0.38901 | 0.21000 |
| | 5 | 8.00 | 1.11883 | 0.09443 | 0.19078 | 0.08627 |
| | 6 | 16.00 | 3.26363 | 0.06518 | 1.87859 | 0.05747 |
| | $K$ | | 0.11795 | 0.01612 | | |
| | $C$ | | -0.4608 | 0.1125 | | |

We may assume that the ground shifts with period of one or a multiple of a year, measured by the pendulums, are due to seasonable local ground movements and are unrelated to recent vertical crust movements. At the Książ station such local movements may be substantial, since two probably active fault zones are located in the region close to the station (see Fig. 8).

Of particular interest is the analysis of the movement of the normal dependent on two above-mentioned non-seasonable oscillations. Their frequencies, about 0.65 cycles per year for the NS component and about 0.75 cycles per year for the EW component, can be read from Fig. 3 with but limited accuracy. Since the accuracy is rather essential for characterisation of the movement of the normal dependent on these oscillations, this subject will be treated in more detail later on.

Due to the non-seasonable oscillations the direction of the normal will perform a fairly complex movement. It is not difficult to notice that if the relation between the periods for the NS- and EW-components $T_{ns}$ and $T_{ew}$ fits the formula:

$$n_{ns} . T_{ns} = n_{ew} . T_{ew} = T \qquad (2)$$

where $n_{ns}$ and $n_{ew}$ are the closest integers having no common denominator greater then 1, $T$ will represent the repetion period of the normal's movement. In other words, after this period the normal will return to the starting point, moving at the same time along the line $A$-$B$ in agreement with linear trend, what can be termed a tilt trend.

Table 2.

| $T_{ns}$ | $T_{ew}$ | $f_{ns}$ | $f_{ew}$ | $n_{ns}$ | $n_{ew}$ | $T$ |
|---|---|---|---|---|---|---|
| years | | cycles/year | | | | years |
| 1.750 | 1.400 | 0.571 | 0.714 | 4 | 5 | 7 |
| 1.800 | 1.500 | 0.556 | 0.667 | 5 | 6 | 9 |
| 1.667 | 1.429 | 0.600 | 0.700 | 6 | 7 | 10 |
| 1.571 | 1.375 | 0.637 | 0.727 | 7 | 8 | 11 |
| 1.500 | 1.333 | 0.667 | 0.750 | 8 | 9 | 12 |
| 1.625 | 1.444 | 0.615 | 0.692 | 8 | 9 | 13 |

$T_{ns}$ and $T_{ew}$ periods (and frequencies $f$) forming $T$ periods (integers) for the range 7-13 years were calculated from formula (2) (Table 2). The 8-years' period was omitted since it represented the subharmonic of the yearly period earlier accounted for. In Fig. 5 these periods are shown against the spectra fragments of Fig. 3 for non-seasonable oscillation bands. Fig. 5 shows that the 11-years' period best fitted the spectral curve. It is known that this period is, due to the sun spot cycle, critical for variations on the Earth. For this cycle the appriopriate $T_{ns}$ and $T_{ew}$ periods equal 1.571 and 1.375 years (i.e. 0.637 and 0.727 cycles per year), respectively. The pattern of the normal in this case is shown in Fig. 7 and oscillation parameters are given in Table 3.

Fig. 6 shows the direction and tilt trends for the discussed 7-13years' periods. Segment $A$-$B$ represent tilt changes from $A$ to $B$ during 200 years. The data of Fig. 6 and Table 3 indicate that for the 11-years' period the normal will decline systematically in the direction $A$-$B$ at about 0.003 μrad per year.

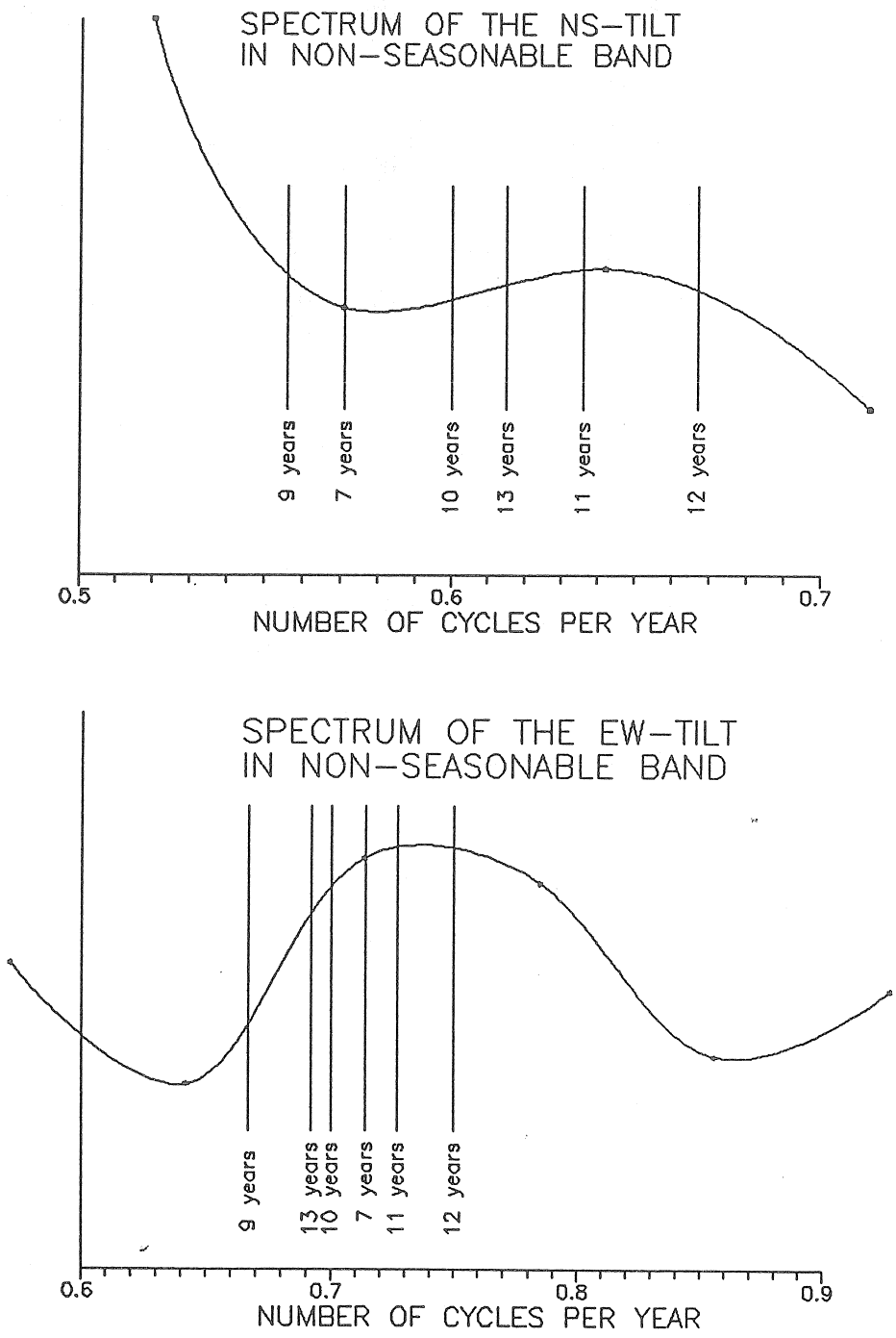


Fig. 5.

Fig. 8 shows a map of recent vertical movements of the Earth crust for Poland [Wyrzykowski, 1985]. A 100-km segment with Książ in the middle, with direction A-B for the periodicity of 11 years from Fig. 6, has been drawn on the map. It can be calculated from the difference in vertical movement of the Earth crust readed at the ends of the segment that it tilts 0.005 μrad per year, with the southern end declining. This value is of similar order of magnitude and direction as the secular tendency of the Earth crust movement included in the movement recorded by the pendulums.

Table 3.

| $T$ | $T_{ns}$ years | $T_{ew}$ | $A_{ns}$ | $A_{ew}$ | $K_{ns}$ μrad | $K_{ew}$ |
|---|---|---|---|---|---|---|
| 7 | 1.75 | 1.40 | 0.32704 | 0.21411 | -0.00482 | 0.00215 |
| 9 | 1.80 | 1.50 | 0.55257 | 0.29831 | -0.00371 | -0.00174 |
| 10 | 1.67 | 1.43 | 0.20325 | 0.34725 | -0.00062 | 0.00178 |
| 11 | 1.57 | 1.38 | 0.21988 | 0.08145 | -0.00289 | 0.00109 |
| 12 | 1.50 | 1.33 | 0.38812 | 0.19279 | -0.00329 | -0.00038 |
| 13 | 1.63 | 1.44 | 0.21797 | 0.38363 | -0.00010 | 0.00096 |

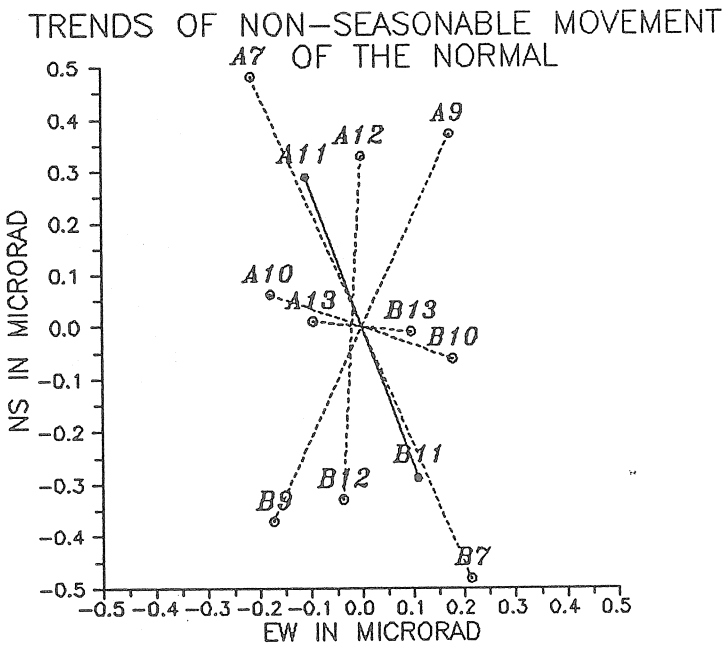


Fig. 6.

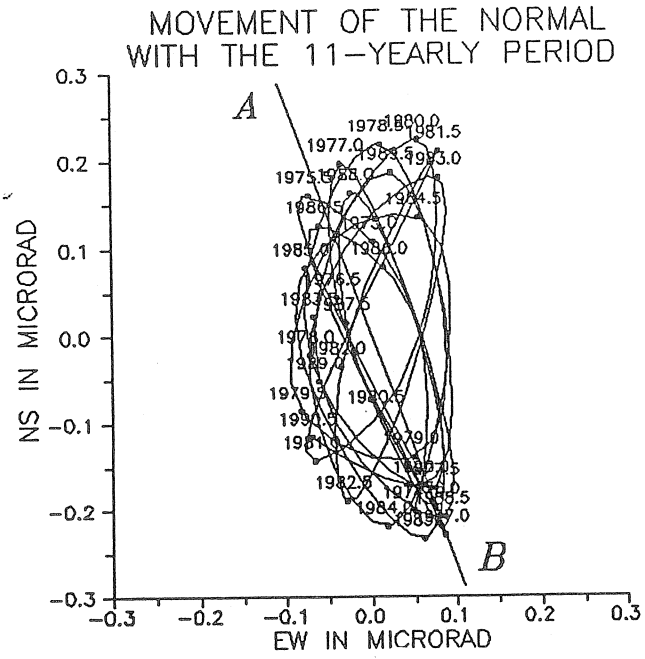


Fig. 7.

# MAP OF THE RECENT VERTICAL MOVEMENTS OF THE EARTH CRUST IN POLAND

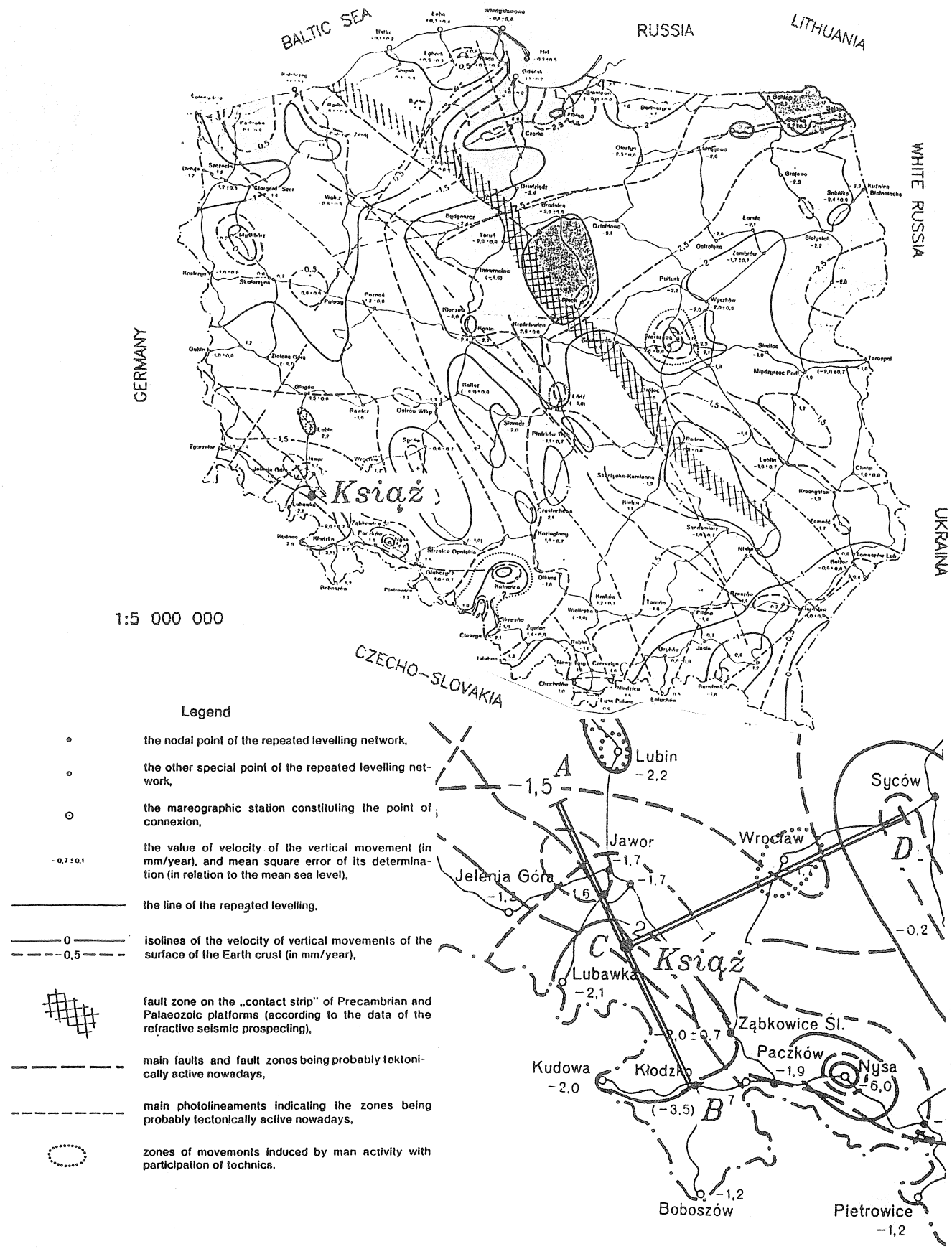


Fig. 8.

The present data of clinometric measurements and the strictly associated movements of the Earth crust justify certain conclusions that may be important for development of levelling methods of determination of recent vertical Earth crust movement applied in geodesy.

Vertical Earth crust movements are mostly oscillatory in nature [Kowalski, 1984]. With the exception of seismically active and some special areas (such as, e.q., Fennoskandia), oscillations may be more pronounced than possible linear movements in the area.

In the studies of recent vertical Earth crust movements using repeated precision levelling, the existence of oscillatory movement must necessarily be considered during development of measuring methods and evaluation of the data. When this is neglected, the precision with which the magnitude of the movement is determined is seriously affected. This is probably the reason why the order of magnitude of the so determined movements is often equal to the order of accuracy with which they were determined - a situation thet need not necessarily be dependent on poor precision of levelling.

While determining the vertical movements of the Earth crust, the duration of the consecutive series of repeated levelling should be kept as short as possible - an appropriate selection of the epoch for such measurements is also important.

Some associations between the data on ground movements at Książ and geological or geophysical characteristics of the surrounding area are worth consideration. As expected, the segment *A-B* which shows linear changes is directed toward Fennoskandia with its ascending end. It is also parallel to the Teisseyre-Tornquist zone. On the other hand, the oscilatory movements are perpendicular to this direction, as if originating from this zone. The association of periods for the non-seasonable movements of normal to the ground surface and for the sun spot variations is also of interest.

We may also ask a question if perhaps the 1 mm (or a little less) is accuracy limit of precision levelling technique because of the even waving Earth crust.

## References

Blum P. A., 1963, Contribution à l'étude des variations de la verticale en un lieu, Annales de Géophysique, t. 19, no 3.

Kowalski W. C., 1984, Współczesne ruchy skorupy ziemskiej w świetle nowej tektoniki globowej. Przegląd geologiczny, nr 10 (378), Warszawa.

Wyrzykowski T., 1985, Map of the recent vertical movements of the surface of the Earth crust on the territory of Poland, Instytut Geodezji i Kartografii, Warszawa.

# Annual and Semiannual Modulations of Planetary Waves in the Spectra of Air Pressure and some Consequences on Gravity Variations.

Cl. Elstner (Potsdam), M. Harnisch (Potsdam)
W. Schwahn (Frankfurt)
Institut für Angewandte Geoddäsie
Frankfurt/Main
Germany

**Summary**

Air pressure variations caused by solar radiation changes due to the rotation of the Earth and the inclination of its spin axis against the ecliptic are characterized by diurnal and annual variations showing a high temporal and spatial stability. The amplitudes of these S-type air pressure waves reach about 100 Pa in the equatorial regions and seldom exceed 40 Pa in middle latitudes corresponding to maximum gravity variations of 100 nanogal or $10^{-9}$ m $s^{-2}$. Due to the modulation in the S1-band the air pressure influences the weak gravity tides like PSI1 situated near to the resonance frequency of the free nutations of the outer core of the Earth.

Fourier presentations of local air pressure at Potsdam (52 N, 13 E) from three years intervals inside the period 1974-1990 show a noise level of five to ten Pa and some significant peaks up to eighteen Pa at P1, S1, K1 and PSI1 frequencies in single intervals.

For the elimination of the air pressure as usual the regression coefficient between air pressure and gravity variations is assumed to -3.0 nGal/Pa for the whole air pressure spectrum, while inside the diurnal band only -1.25 nGal/Pa should be valid (Spratt 1982). The difference generates in the PSI1 tide a disturbation in the order of the effect of the free core nutations.

## Introduction

The gravitational and loading effects of the atmospheric masses on gravity at a certain place mostly are estimated by the regression between the time series of gravity and of the local air pressure. The application of global air pressure distributions instead of local data results in slight changes of about ten to twenty percent in the regression coefficients. The air pressure corrections mainly diminish the noise in the tidal bands of the gravity time series especially in the diurnal one. This effect is demonstrated also by the well-known power spectra of the local air pressure for a multi-annual period (Warburton and Goodkind 1977, Spratt 1982, Florsch et al. 1991). Here the pressure variations produced by weather processes with amplitudes in the order of tens of hPa completely are canceled, while the very small solar or S-type air pressure waves with amplitudes in the order of a few tens of Pa, two orders of magnitude below the other ones, clearly are to be seen. The power spectrum of the local air pressure at Potsdam is shown in Fig.1.

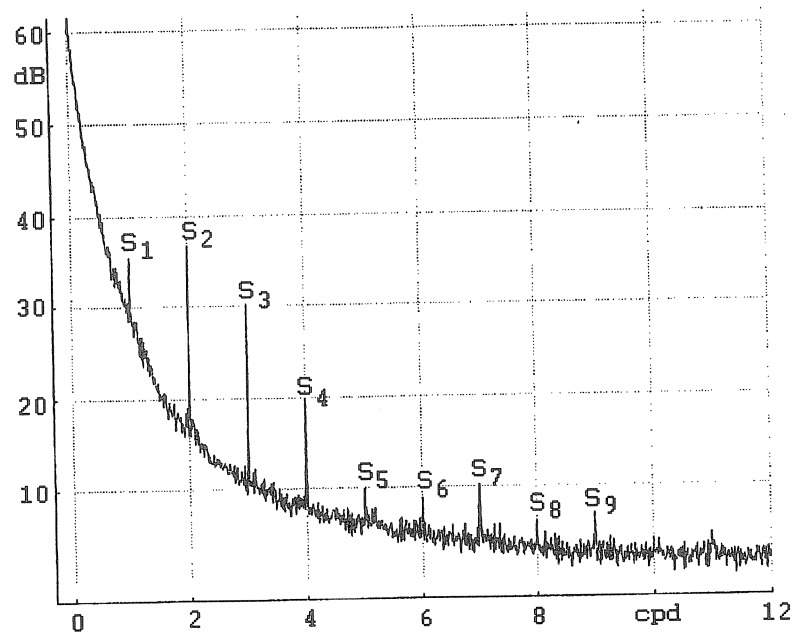


Fig.1: Power spectrum of the air pressure time series at Potsdam 1974 - 1986 (after Savin and Schwahn)

The global character of these waves widely is known. They are generated by the variations of the solar radiation with its daily and yearly rhythms which are also existent in the parameters of the atmospheric state like temperature, pressure

and density. Inspite of the fact that the solar waves of the air pressure are not caused by tidal forces they appear in the tidal frequencies of pure solar origin, i.e. PI1, P1, S1, K1, PSI1 or 2T2, T2, S2, R2, K2. Inside these solar frequency bands the energy of the S-waves will be distributed in dependence on the temporal changes of the state of the atmosphere. The driving forces of these waves are governed by laws containing the reciprocal squares of the distances while the tidal forces depend on the reciprocal cubes. Besides their annual and semiannual modulations the temporal changes of the S-waves may be understood as indications of large scale variations in the mean state of the atmosphere.

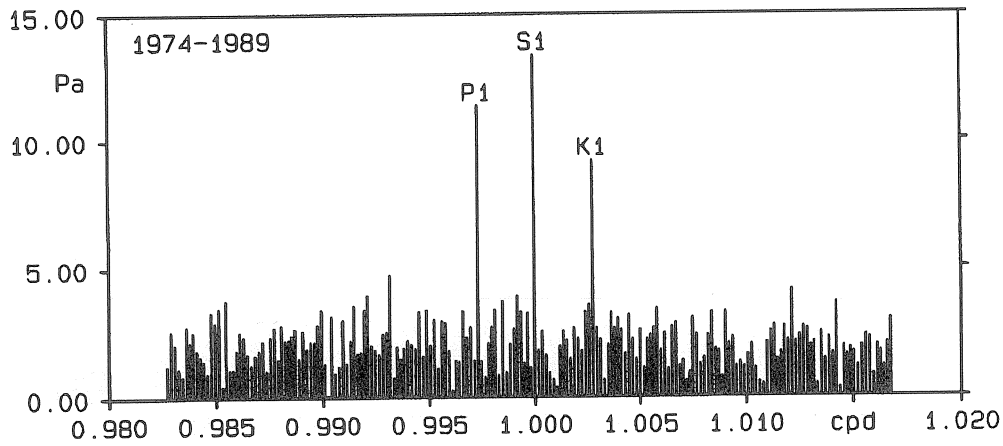


Fig.2: Long-term air pressure spectrum Potsdam 1974 - 1989, diurnal band S1, amplitudes

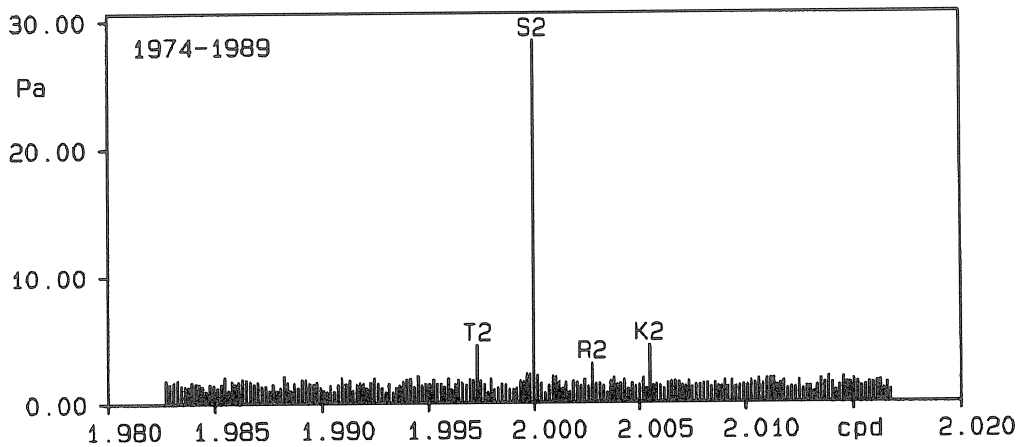


Fig.3: Long-term air pressure spectrum Potsdam 1974 - 1989, semidiurnal band S2, amplitudes

The regression between S-type air pressure waves and the corresponding gravity variations seems to be quite different for n=1,2 and n>2 on the other hand (Warburton and Goodkind 1977, Spratt 1982). Furthermore the modulations inside the S1 and S2 air pressure bands give rise to temporal variations of this regression.

Starting from the modulations found by Bartels (1927) in our paper we shall study the fine structure within these bands with respect to its consequences on the corresponding gravity tidal parameters.

## 1. Solar-Type Air Pressure Waves and Their Local Spectra

The data base for the following calculations consists of hourly air pressure values measured at the Potsdam Meteorological Observatory (52.38 N, 13.07 E) in 99.64 m height above sea level in the period 1974-1989. The accuracy of the data amounts to about 5 Pa. The Fourier representation of the amplitudes of the entire time series shows Fig.2 for the diurnal band and Fig.3 for the semidiurnal one respectively. The differences in the noise levels and the distinct annual and semiannual modulations are clearly expressed. The amplitude spectra of three different periods, 1974-76, 1977-79 and 1987-89 demonstrate significant variations of the S1-type air pressure waves inside the diurnal band (Figs.4, 5 and 6). In the period 1974-76 strong amplitudes appear and the semiannual modulation is connected with a significant amplitude of the PSI1 wave.

The seasonal variability of the diurnal air pressure waves is presented by an adjustment of the air pressure data from 1980 (weak S1 wave) and 1989 (strong S1 wave) with respect to the sum of the five diurnal frequencies (Fig.7).

The modulations of S1 and S2 are shown by their monthly mean values calculated by the adjustment of the stacked monthly pressure data for the entire period 1974-1990. The results are pictured in harmonic dials (Figs.8, 9). For comparison purposes also the S1 wave at Brussels was calculated in the same manner but for a shorter period (Fig.10). At both the places the main features are comparable.

Already in 1927 Bartels analysed the air pressure waves S1, S2, S3 and S4, using data from the beginning of the observations at the Meteorological Observatory Potsdam in 1893 until 1922. His results show no significant differences in the monthly mean amplitudes and the main features of these waves to our outcomes for the period 1974-1990, but in the phase angles a significant difference of 0.75 ± 0.05 hours exists.

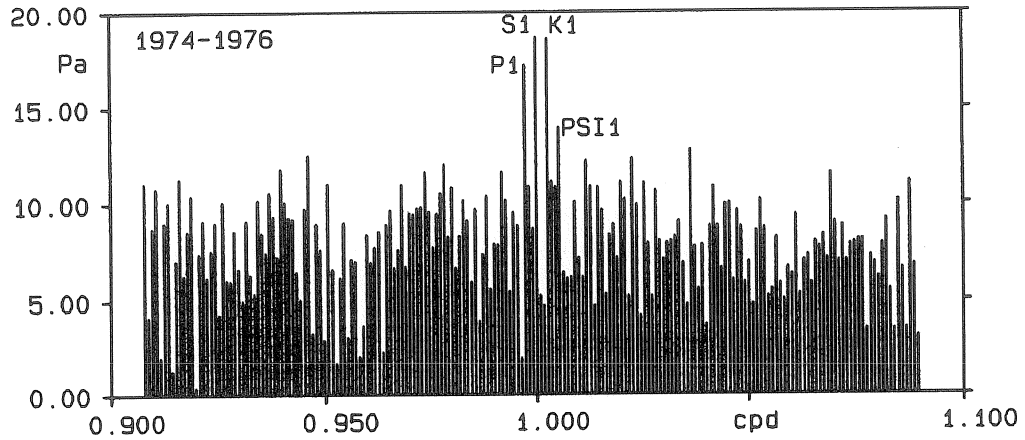


Fig.4: Fourier-spectrum 1974-1976, diurnal band S1, amplitudes

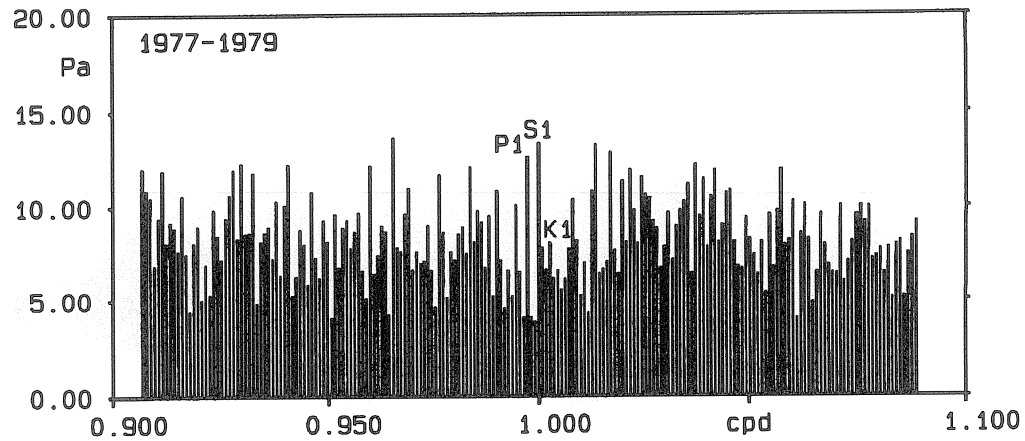


Fig.5: Fourier-spectrum 1977-1979, diurnal band S1, amplitudes

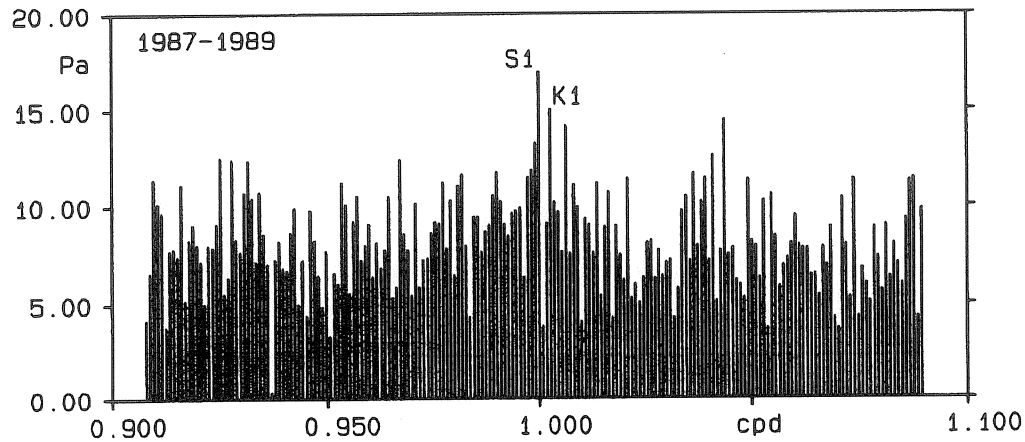


Fig.6: Fourier-spectrum 1987-1989, diurnal band S1, amplitudes

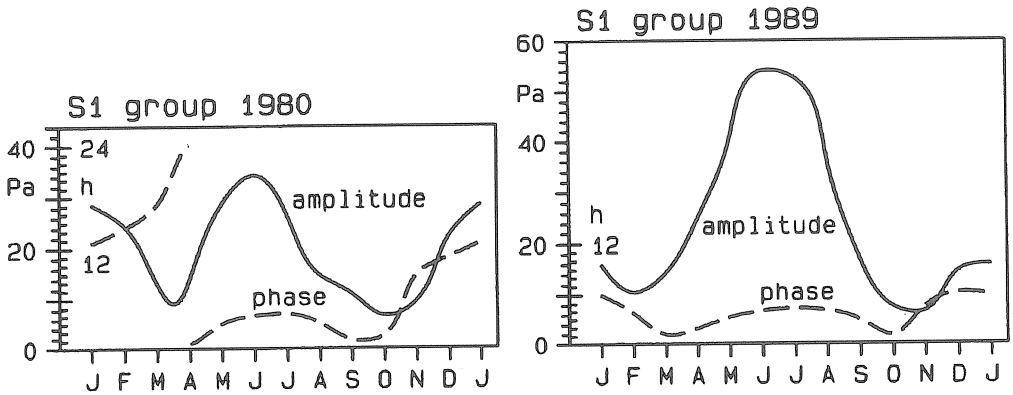


Fig.7: Resultant amplitudes and phases for the air pressure waves of the S1-group (PI1, P1, S1, K1, PSI1) for the years 1980 and 1989

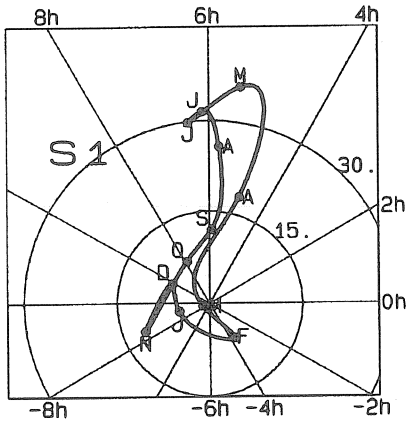


Fig.8: Harmonic dial of air pressure, Potsdam 1974-1990, S1. Maximum amplitude in summer, minimum in winter.

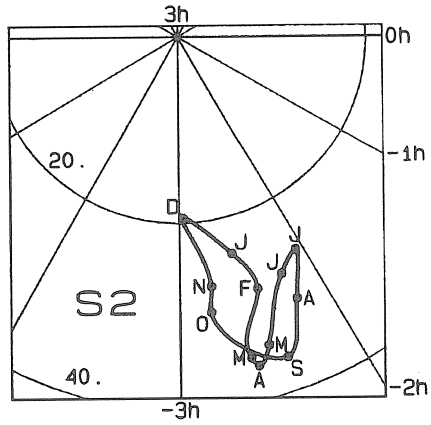


Fig.9: Harmonic dial of air pressure Potsdam 1974-1990, S2. Maxima in spring and autumn, minima in summer and winter.

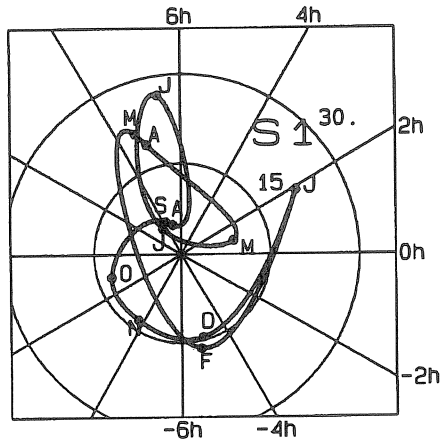


Fig.10: Harmonic dial of air pressure, Brussels 1982-1986, S1

In our calculations the maxima of S2, S3, S4 appear 45 minutes earlier than in Bartels' results. In the S1 band this phase difference is hidden by the general noise.

## 2. Distribution of the Solar-Type Air Pressure Waves at the Surface of the Earth

The air pressure variations of solar type are about two orders of magnitude smaller than those connected with regional weather processes, but in difference to the latter they are more or less regular distributed at the surface of the Earth. A general description of these waves was given by Kertz (1957), other authors carried on the investigations on this topic: Chapman and Lindzen (1970), Haurwitz and Cowley (1973).

The description of the distributions of solar wave parameters at the surface of the Earth is performed by spherical harmonics. The air pressure data are observed by a few hundred of meteorological stations most of them situated on the northern hemisphere.

The S waves may be expressed by

$$S_n = R_n \sin(n t + \sigma_n) \tag{1}$$

where t designates the local time, n = $2\pi$f, and f = 1,2 .. means the frequency in cycles/day.

Amplitude $R_n$ and Phase $\sigma_n$ depend on latitude and longitude and they may be determined for certain latitude circles by the aid of Fourier series.

Following Kertz (1959), the global distribution of $S_n$ is expressed by

$$c_k^s P_k^s(\varphi) \sin(n t_u + s\lambda + \varepsilon_k^s) \tag{2}$$

where $P_k^s$ means associated Legendre functions in the semi-normalized form introduced by A.Schmidt, $t_u = t - \lambda$ designs universal time, t mean local time and $\lambda$ the geographical longitude of the observation point counted positive eastward.

The presentation of S2(p) by Kertz (1956), yielded approximately

$$\begin{aligned} S2(p) = {} & c_2^2 P_2^2 \sin(2 t_u + 2\lambda + \varepsilon_2^2) \\ & + c_4^2 P_4^2 \sin(2 t_u + 2\lambda + \varepsilon_4^2) \\ & + c_2^0 P_2^0 \sin(2 t_u + \varepsilon_2^0) \\ & + c_3^3 P_3^3 \sin(2 t_u + 2\lambda + \varepsilon_3^3) \end{aligned} \tag{3}$$

The first two terms describe the travelling S2-wave synchronous to local mean time $t_u + \lambda$, the third term means a

standing wave synchronous to universal time and the last term gives some further global structure of S2. For numerical calculations the numbers given in table 1 are valid.

Table 1: Parameters of S2 Air Pressure Waves

| $s$ | $k$ | $c_k^s$ /Pa | $\varepsilon_k^s$ /° | $P_k^s(\varphi)$ |
|---|---|---|---|---|
| 2 | 2 | 122 | 158 | $\frac{\sqrt{3}}{2}\cos^2\varphi$ |
| 2 | 4 | 21.6 | 342 | $\frac{7\sqrt{5}}{4}\cos^2\varphi\,(\sin^2\varphi-\frac{1}{7})$ |
| 0 | 2 | 7.2 | 135 | $\frac{3}{2}(\sin^2\varphi-\frac{1}{3})$ |
| 3 | 3 | 10.7 | 88 | $\frac{\sqrt{10}}{4}\cos^3\varphi$ |

The essential global structure of the S2 air pressure waves corresponds to that of the semidiurnal tides given by a spherical harmonic of degree and order two.

The global structure of S1(p) is essentially influenced by the distribution of continents and oceans and was presented by Haurwitz and Cowley (1973) in an analogous form like S2(p). Their calculations based on the air pressure data of about 250 stations situated between ±60° latitude. The five main terms of their development of the data in harmonic functions are given by the following expression:

$$\begin{aligned} S1(p) = {} & 10.8\,P_3^3\sin(t-3\lambda+86°) \\ & + 10.0\,P_2^1\sin(t-\lambda+102°) \\ & + 10.1\,P_2^0\sin(t+152°) \\ & + (57.7\,P_1^1-17.2\,P_3^1)\sin(t+\lambda+12°) \\ & + 10.7\,P_2^2\sin(t+2\lambda+261°) \end{aligned} \qquad (4)$$

The general structure of S1(p) is given approximately by:

$$S_1^1(p) = 62.9\cos^3\varphi\sin(t+\lambda+12^\circ) \quad (5)$$

The diurnal wave S1(p) is much more variable in time and space than the semidiurnal one. Therefore special attention must be paid for the reduction of the air pressure influences inside the diurnal band of the gravity variations (Lambeck 1988).

## 3. Solar Type Air Pressure and Gravity Variations

Extended series of gravity variations with superconducting gravimeters clearly show the effects of solar type air pressure variations (Warburton and Goodkind 1977, Spratt 1982, Elstner and Schwahn 1991). In principle the regression between air pressure and gravity variations is known (Rabbel and Zschau 1985, Richter 1987, Torge 1989).

For these studies mainly local air pressure data were used generating up to 90% of the pressure induced gravity effect. As special tests showed no significant instrumental response on air pressure variations has been observed (Warburton and Goodkind 1977). S1 and S2 air pressure waves may be connected to the corresponding ocean tides and are acting additionally via the ocean loadings on the gravity variations.

The response of gravity to the global atmospheric S-type waves of air pressure differs considerably from that to the weather induced pressure variations. Special investigations on the gravity admittances to S-type pressure variations (Spratt 1982) resulted in a good agreement between the admittances of measurements and models especially for S3 and S4. Spratt found that with increasing order of the air pressure waves the local pressure data were dominating for the generation of the gravity variations.

The admittances with respect to S1 and S2 waves were diminished to about -0.15 $\mu$Gal/hPa or even less. Inside this frequency region the gravity variations are determined by stronger loading influences, the distribution of continents and oceans, the model for the deformations of the surface of the Earth covered with oceans and the temporal variations in the global air pressure distributions.

The observed gravity variations in the S1 and the S2 bands show different regressions to the air pressure. In the case of S1 also instrumental influences may disturb the relations to the pressure variations. On the other hand the temporal energy displacements inside the S1 band give rise to changes of the gravity pressure regression. With respect to the results of Spratt (1982), the admittances for S ($n \geq 3$) are in agreement with model values for an elastic oceanless Earth and the correction of the gravity data easily may be per-

formed. At present no reliable model is available for the diurnal and the semidiurnal regions. To eliminate the influence of regional or global S-type air pressure distributions expended numerical correction procedures are required. As an example the studies of the Free Core Nutations by the aid of gravity data may be mentioned (Legros and Hinderer 1991).

For the evaluation of the resonance phenomenon in the diurnal gravimetric spectrum the small PSI1 tidal wave (amplitude about 0.4 μGal, frequency 1.00547569 c/d) situated nearby the resonance frequency (1.004918 c/d) gets very important. The core resonance affects the amplitude of PSI1 wave with about ten percent of its value, i.e. 0.04 μGal. In the S1 spectrum of the air pressure PSI1 presents the semiannual modulation and reached a maximum amplitude of 15 Pa in the period 1974-76 (Fig.4). Caused by the uncertainties of the gravity-pressure admittances an error may occur in the amplitude of PSI1 up to 0.2 × 0.15 μGal, i.e. 0.03 μGal. This corresponds to the magnitude of the resonance effect in this tidal wave.

## Conclusions

The spatial and temporal structures of the solar type air pressure wave S1 look quite more variable than those of S2. The annual periods and some of its subharmonics, which are clearly expressed in both air pressure waves, require an integer number of years for the analysis to avoid leakage phenomena.

For the precise determination of air pressure corrections on diurnal and semidiurnal gravity variations exact admittances must be derived in dependence on the corresponding global pressure distributions and its temporal variabilities.

Continuous and precise data series of air pressure gravity and ocean level variations extended over many years and observed all around the globe would be very helpful for the understanding and the modelling of the planetary influences of the atmosphere on the gravity variations in diurnal and semidiurnal frequency bands.

References

BARTELS,J., 1927
Über atmosphärische Gezeiten
Abh. Preuss. Meteorol. Inst., 8, H.9, Springer, Berlin

CHAPMAN,S.; LINDZEN,R.S., 1970
Atmospheric Tides
Reidel, Dordrecht

ELSTNER,Cl.; SCHWAHN,W., 1991
Some Remarks on the S3 Gravity and Air Pressure Variations
Proc. 11th Int. Symp. Earth Tides, Helsinki 1989, Schweitzerbarth'sche Verlagsbuchhandlung, Stuttgart

EUBANKS,T.M.; STEPPE,J.A.; SOVERS,O.J., 1986
An analysis and intercomparison of VLBI nutation estimates.
Proc. Int. Conf. Earth rot. and terr. ref. frame,
ed. Mueller,I.I., Ohio, 326-340

FLORSCH,N.; HINDERER,J.; CROSSLEY,D.J.; LEGROS,H.;
VALETTE, B., 1991
Preliminary spectral analysis of the residual signal of a superconducting gravimeter for periods shorter than one day.
Phys. Earth Planet. Int., 68, 85-96

HAURWITZ,B.; COWLEY,A.D., 1973
The Diurnal and Semidiurnal Barometric Oscillations, Global Distribution and Annual Variation
Pageoph., 102, 193-222

LEGROS,H.; HINDERER J., 1991
On some perturbations of diurnal tidal wavës and related nutations
Proc. 11th Int. Symp. Earth Tides, Helsinki 1989, Schweitzerbarth'sche Verlagsbuchhandlung, Stuttgart

LAMBECK,K., 1988
Geophysical Geodesy - The Slow Deformation of the Earth
Oxford, Science Publ.

KERTZ,W., 1966
Components of the semidiurnal pressure oscillation
New York Univ. Dept. Meteor. and Ocean., Sci. Rep. 4

KERTZ,W., 1959
Partialwellen in den halb- und vierteltägigen gezeitenartigen Schwingungen der Erdatmosphäre
Arch. Meteor. Geophys. Bioklim., A 11, 48 - 63

SPRATT,R.S., 1982
Modelling the effect of atmospheric pressure variations on gravity
Geophys. Journ. Roy. astr. Soc., 71, 173 - 186

WARBURTON,R.J.; GOODKIND,J.M., 1977
The influence of barometric pressure variations on gravity
Geophys. Journ. Roy. astr. Soc., 48, 281 - 292

VOLLAND,H., 1988
Atmospheric Tidal and Planetary Waves
Kluwer Acad. Publ., Dordrecht, Boston, London

# A Slew Rate Detection Criterion applied to SG Data Processing.

D. Crossley, O. Jensen, Hui Xu
Department of Earth and Planetary Sciences
McGill University
3450 University Street
Montreal H3A2A7
Canada

J. Hinderer
Institut de Physique du Globe
rue Descartes, 5
67084 Strasbourg
France

**Abstract**

We introduce the concept of slew rate detection as an automatic method of finding anomalous signal changes in a data set. The slew rate between any two samples is simply the gradient of the data, usually in time, and is used to divide the original data into a slew function and a corrected signal. The idea is applied to superconducting gravimeter (SG) data both in a relatively early stage in the processing and then as an analytical tool to investigate the residual gravity following a tidal fitting procedure. We evaluate the advantages and pitfalls of such an approach.

## Introduction

High rate vertical gravity recording systems are becoming more common, particular for the SG. The two main reasons for this are the desire to take full advantage of the dynamic range of the instruments, so the data will be useful in different frequency ranges of study, and also to keep raw data to allow future possible changes in processing methods. For example, the CSGI (Canadian Superconducting Gravimeter Installation) records gravity at 1Hz, pressure at 0.1Hz and ancilliary data every minute. The compressed data for one day takes approximately 0.5MB of disk space.

Modern recording systems can easily cope with this modest amount of data, and the difficulty with producing up-to-date processed data lies in the manpower required to edit and decimate the data. Thus any help from automatic and semi-automatic methods should be welcome, providing the computer algorithms invoked do indeed solve more problems than they might introduce.

# Slew Rate Philosophy

We were led to consider a slew rate procedure in discussions of how to supress non-geophysical offsets and spikes in hourly residual gravity variations (see e.g. Figure 6(a)). This data has already been manually edited for the normal range of disturbances, i.e. gaps, spikes and major offsets prior to a tidal/pressure/drift fitting procedure (in this case HYCON). It seemed reasonable to consider the point-to-point gravity derivative, in electronic terms a slew rate, as a possible diagnostic. After all, bona fide gravity signals should have some upper limit to their slew rate, beyond which the slews might be considered to have an artificial origin (e.g. instrumental or anomalous site effects).

There are three steps to the procedure. The first is to set a critical slew rate which has some physical meaning and which produces 'reasonable looking' results. The second is to use this slew rate to detect anomalies in the time series. The final step is to correct, or replace, the original data wherever it has been deemed to be anomalous. The key concept is that we shall divide the data into two bins, data that is rejected has slews greater than the critical and data that is passed has slews below the critical. Moreover, by retaining and possibly analysing both subsequent data sets, we cannot be accused of disregarding data we 'don't like'.

## The Critical Slew Rate

There are two ways to determine a critical slew rate. The first is statistical. From a histogram of the slews (the time derivatives of the gravity record) one choose a symmetric bound which represent low probabilities in the distribution and thus 'anomalous' values. If the histogram looks Gaussian, one might take the $3\sigma$ level, $\sigma$ being the square root of the 2nd central moment of the slews. In this case, the assumption is that anomalous slews occur about 0.3% of the time. This might seem a dangerous proposition, and indeed we shall see that it can lead to spurious results.

A second, and much preferred, method is to assess all geophysical signals we want to 'pass' for their possible slews and set the critical rate above the largest of these effects. We might include tides, atmospheric pressure fluctuations, and core modes for example as 'passable'. If in doing so, we find that some undesirable effects are passed, then this is the price we pay for compromise (no method is free from problems). It is in any case a much better decision than setting too low a critical slew rate which might reject only part of our geophysical signal. From our data we find that a maximum slew rate for tides is $1.2\mu gal/min$ and for atmospheric pressure effects (in gravity) is $0.015\mu gal/min$.

Hopefully the combination of the above approaches, plus some experience, can lead to an appropriate critical slew rate for the problem at hand. If not, then the slew rate method is inappropriate. This situation is entirely equivalent to declaring that filtering is appropriate only if the frequency ranges of the signal and noise do not overlap, a condition rarely fulfilled in practise !

### Slew Detection

The detection problem is trivial. Take the time derivative of the data and flag all slews that are greater than the critical. Further processing, other than slew correction, could be based on the flagged data values.

### Slew Correction

The final step is also easy. Wherever the slew rate exceeds the critical, we replace it by zero and put the rejected slew rate into a file which contains high slews. Then both derivative files are re-integrated to give two files, the corrected gravity, which is the time integration of the passed and corrected slews, and the slew function, which is the time integration of the rejected (high) slews. As a detail, one notes that this integration requires the initial slew rate of each data set to be specified. For the very first point one assumes the slew is zero, for the first point in a new segment of the data one must have the last slew rate from the previous segment. This consideration preserves the DC levels in the corrected data.

Note that one could use philosophies other than replacing rejected slews by a zero, which effectively keeps the function constant. For example it might be reasonable to maintain the rate (slope in the function) the same as the last acceptable slew rate. We have found that this procedure gives significantly poorer results in the presence of noise than that proposed above.

## Application to Synthetic Data

We now describe four simple experiments that demonstrate the slew rate procedure on synthetic signals. In the first experiment, we take 33 samples of brown noise and add a permanent offset at data point 10 and a spike at point 21 (Figure 1(a)). Examination of the slews suggests a critical slew rate of $5.0 \mu gal/hr$, and de-slewing produces the slew function in Figure 2(b). Notice the slews either side of point 21 are uneven due to the brown noise at this time. Figure 1(c) shows the corrected signal (solid) compared to the original brown noise (dashed). We see that at points 10 and 21 the two signals diverge due to the replacement of the correct slews by zeros.

In the second test, we select four disturbances (a permanent offset, a temporary offset, a spike and a gap) which are added to 1024 samples of small amplitude brown noise (Figure 2(a)). Again a critical slew rate of $5.0 \mu gal/hr$ is applied and the resulting slew function is recovered (Figure 2(b)). The comparison between corrected (solid) and original (dashed) noise functions (Figure 2(c)) shows that the recovered signal is quite reasonable except for the gap, where data is missing completely. There the fluctuation in the signal is ignored in favour of a constant reconstruction, so this would be a situation where the slew correction is inappropriate.

The third test is identical to the previous case but now the noise amplitude is a factor of

10 larger (Figure 3(a)). This time we show the histogram of slews which suggests the same critical slew rate as used before ($5.0 \mu gal/hr$) which produces the slew function shown in Figure 3(c). Now we see that the high amplitude noise corrupts the slews that were added and the correction procedure removes both anomalous slews and local noise indisciminantly. The corrected signal, Figure 3(d), departs significantly from the original noise, although in this case, by chance, the gap does not introduce much of an offset.

Our final synthetic example emphasises the poor behaviour of the slew correction in the presence of high noise. Figure 4(a) is a pure brown noise with a histogram (Figure 4(b)) that suggests a critical slew, on statistical arguments, might be taken between 3.0 and 4.0. Indeed if we take 3.5, we remove about 8 of the largest excursions in the data (Figure 4(c)) and generate a corrected signal (Figure 4(d)) that has *introduced* spurious offsets.

Our conclusions from these experiments are that slew corrections can be appropriate for offsets and spikes, but probably not gaps unless thay are short. Additionally, the critical slew rate must be chosen above the range of slews present in the local noise. One could imagine what would happen if the the critical slew rate was smaller than the largest slew of a large earthquake. Part of the earthquake would be rejected (in the slew function), part would be passed (in the corrected function) with spurious offsets inserted. A real mess !

# Application to Gravity Records

Keeping in mind the problems, we apply the method to two gravity data sets. The first is a record of two years of CSGI data, shown in Figure 5(a): for further details of the record see Hinderer et al. (1993). The original 1 $s$ data has been decimated to a sampling interval of 5 $min$, but otherwise the data is unprocessed, hence the term raw gravity. In Hinderer et al., this 5 $min$ data was edited 'by hand', which means that spikes, offsets and gaps were edited manually and corrected individually.

Visually, Figure 5(a) shows the Earth tides superimposed on a strong instrument drift and interrupted by large offsets and many positive spikes, the latter arising from 99.0 values that replace data lost by the data acquisition system. Before slew correcting, we first subtract a synthetic tidal signal computed by the program GWAVE (Merriam, 1992) modified to use locally determined gravimetric $\delta$ factors.

The difference signal is shown in Figure 5(b). It is evident that the first 70 days of the data are very noisy, after which the number of spikes is small. There are 4 large offsets, two of which are known to be associated with electrical problems on site. A critical slew rate of 0.5 $\mu gal/5$ $min$ was chosen for the slew rate detection and correction.

The slew function shown in Figure 5(c) has two interesting chracteristics. The first is that the four offsets plus all the spikes have been removed. The second is that the first part of the record, with the noisy data, has been somewhat altered by the automatic slew rate correction algorithm. The reason for this is that there were significant gaps in the early part of the data (some many hours long) and we know from the synthetic tests that gaps can be problematical. Not only can a gap *generate* a new offset, but of course there is no tidal

signal in the gap. Therefore subtracting a synthetic tide from a gap will *generate* a tidal signal which then appears in either the slew function or the corrected signal (hopefully the latter). The solution to this problem is to subtract synthetic tides everywhere except where there is a gap.

On the positive side, it has been determined that most of the slew-detected problems coincide well with the anomalies determined previously by manual methods. Considering the slew rate program takes a few seconds to run, this is a major improvement over manual processing.

The corrected gravity, shown in Figure 5(d), shows clearly the initial problems, the steady negative instrument drift and one large remaining offset around day 460. This last event turns out to be a relatively slow offset which took place over many hours. Consequently the slew was below the chosen critical value and therefore not rejected.

The final step of this sequence is the removal of atmospheric pressure, which we did at the step before de-slewing. The result, Figure 5(e), shows that most of the noise in Figure 5(d) has been eliminated. We emphasise here that both Figures 5(c) and 5(d) (or 5(e)) are informative, though we admit that this application of the slew processing has been to creat definite 'pass' and 'reject' signals (corrected gravity and slew function respectively).

The final example shows the slew rate processing applied to 1 $hr$ gravity residuals from the program HYCON. The data (Figure 6(a)) is the same as in Figure 5(a), though at a different stage of processing; note the disturbed initial period and the many offsets in the data. The histogram of the slews obtained from Figure 6(a), and shown in Figure 6(b), suggests that critical slew rate between 0.5 and 1.0 is appropriate. If we de-slew with a critical value of 0.5 $\mu gal/hr$, we obtain the slew function in Figure 6(c) and the corrected gravity in Figure 6(d).

Again both plots are informative. The slew function in the first part of the data has too much 'character' and we are not suprised to find there is in fact a definite tidal tignal in this slew function, which appears on the power spectral density plot (PSD) in Figure 6(e). This is not the most desireable result, as it indicates that the slew function has taken up geophysically interesting signals. In principal, the slew function should have a smooth 'noise-like' PSD and the corrected signal should have the interesting harmonic signals. A second effect of de-slewing is to reduce the signal levels in the corrected gravity, and this aspect has been treated in more detail by Hinderer et al. (1992) and Jensen et al. (1992).

# Discussion

The advantages of the method are in its ease of application and speed of execution. Furthermore, as an analytical tool we can see exactly into which components (slew function, corrected data) the signal has been separated. In conjunction with other techniques to fill gaps, the slew rate proceedure has a useful place.

On the negative side by choosing too small a critical slew rate, we can reject useful signals, or, worse still, split noisy data into two inappropriately-separated components. The slew rate

process is clearly non-linear and can easily change the low-frequency character of signals. Thus where one is looking for long period information in the data, for example polar motion, one would have to be very careful not to introduce spurious offsets by de-slewing.

In summary, we can give a cautious vote of approval to the slew rate method of signal 'processing', provided the major pitfalls are recognised and moderated. At best this is only one of many tools that might be considererd for the rapid processing of gravity data.

### Acknowledgements

We would like to thank Walter Zürn for use of the HYCON programme and for various grants from the Natural Science and Engineering Research Council of Canada.

## References

Hinderer, J., Crossley, D.J., Jensen, O.G. & Xu, H., 1992. Gravity noise levels and periodic signals observed from a common 2 year analysis of the French and Canadian superconducting gravimeters, EOS, Trans. Am. Geophys. Un., **73**, 60-.

Hinderer, J., Crossley, D.J. & Xu, H., 1993. A 2 year comparison between the French and Canadian superconducting gravimeter data, Geophys. J. Int., (in press).

Jensen, O.G., Crossley, D.J. & Hinderer, J., 1992. Simple data decomposition reveals a surprisingly rich harmonic spectrum in superconducting gravimeter data, EOS, Trans. Am. Geophys. Un., **73**, 60-.

Merriam, J.B., 1992b. An ephemeris for gravity tide predictions at the nanogal level, Geophys. J. Int., **108**, 415-422.

Fig 1(a) Offset + spike + brown noise

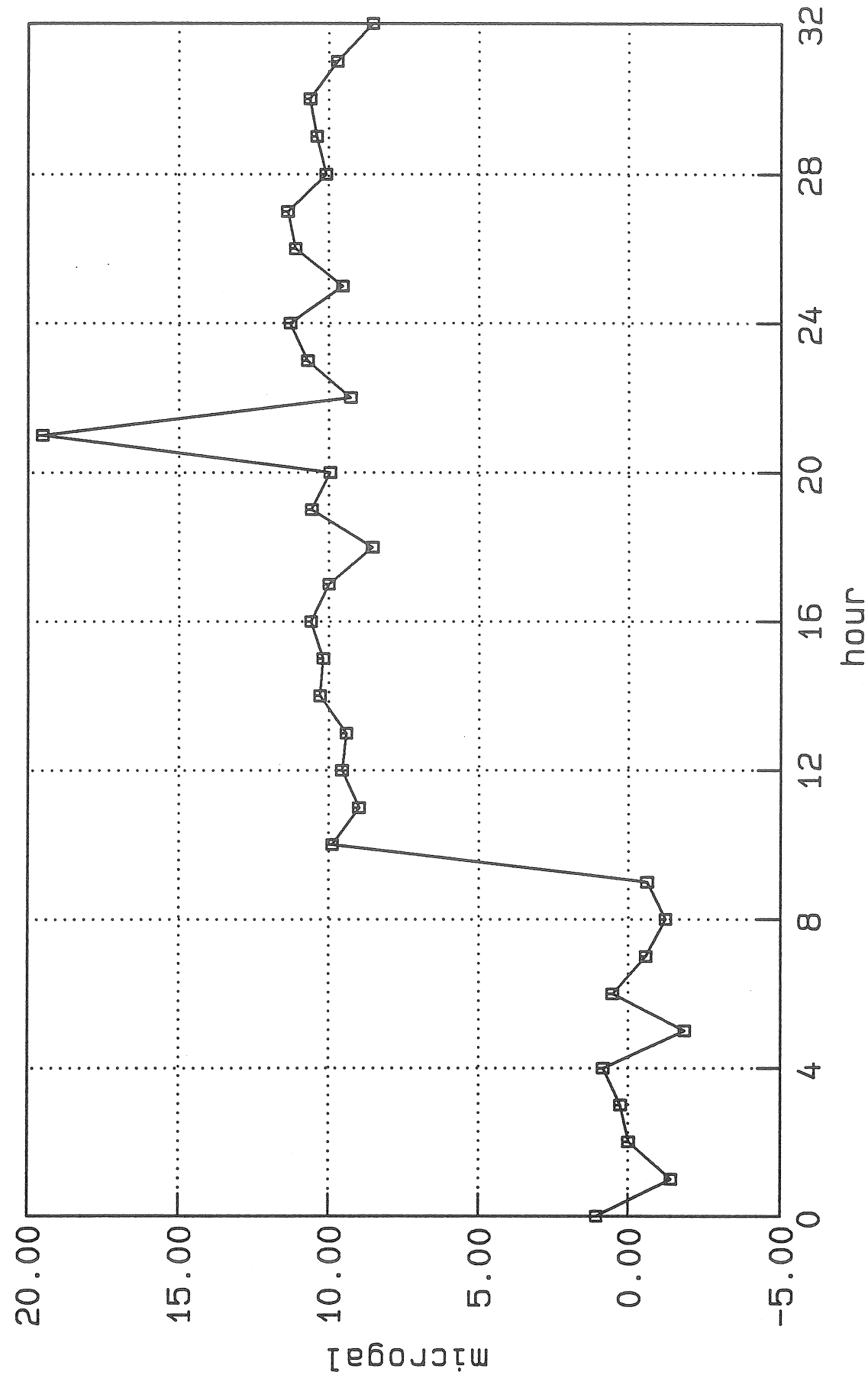

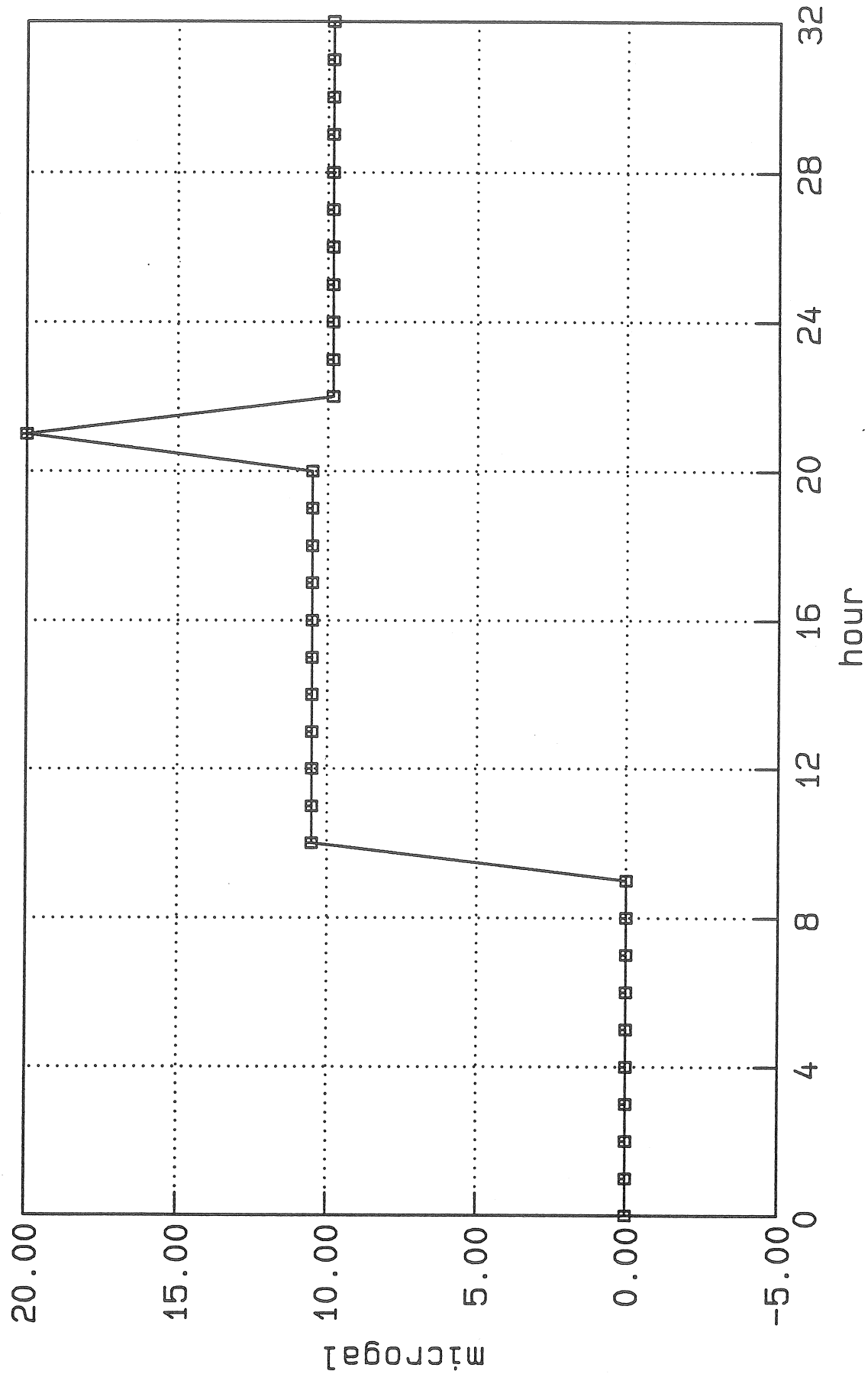


Fig 1(b) Slew function

DATA

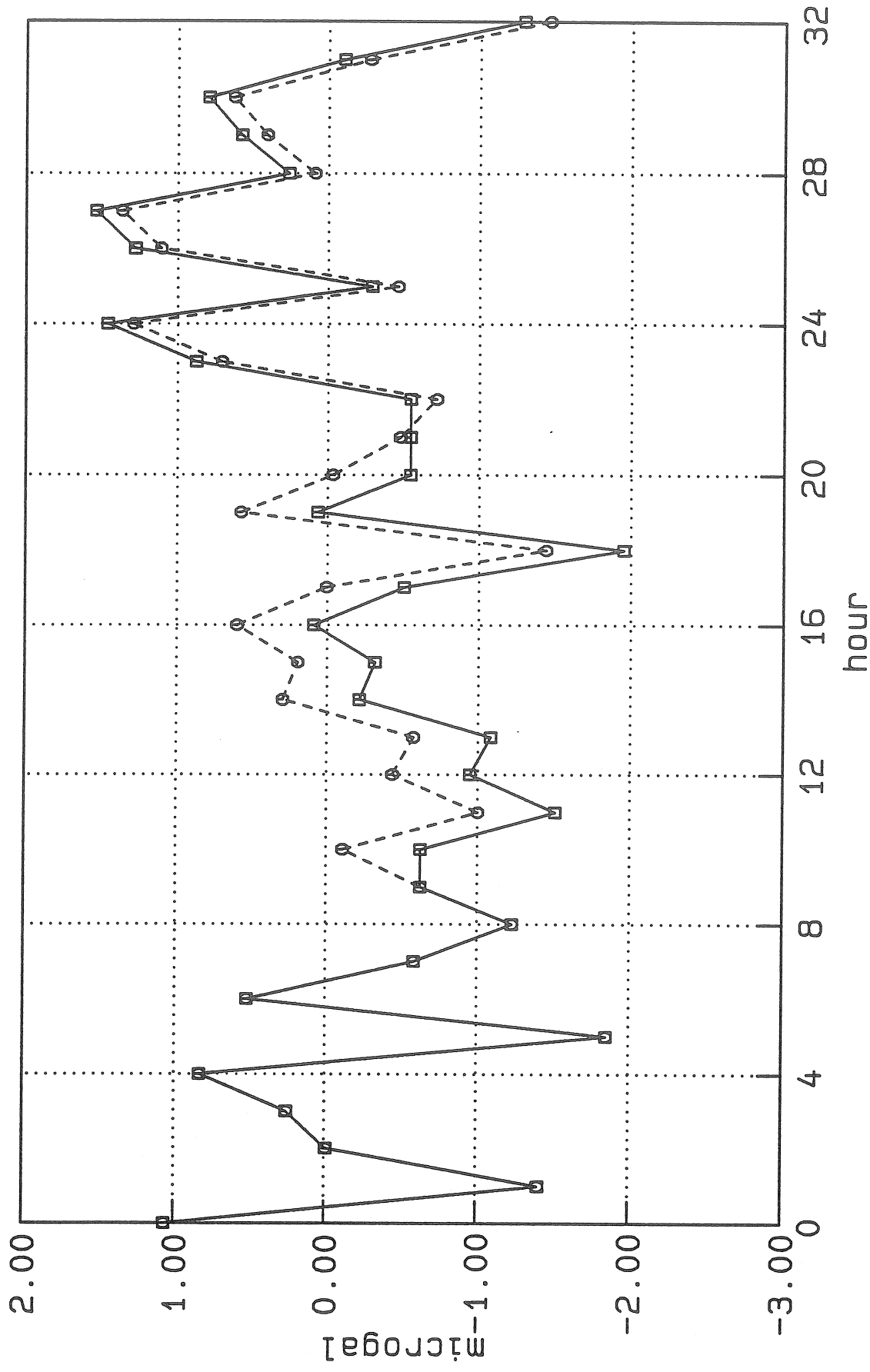


Fig 1(c) Corrected and original noise functions

DATA

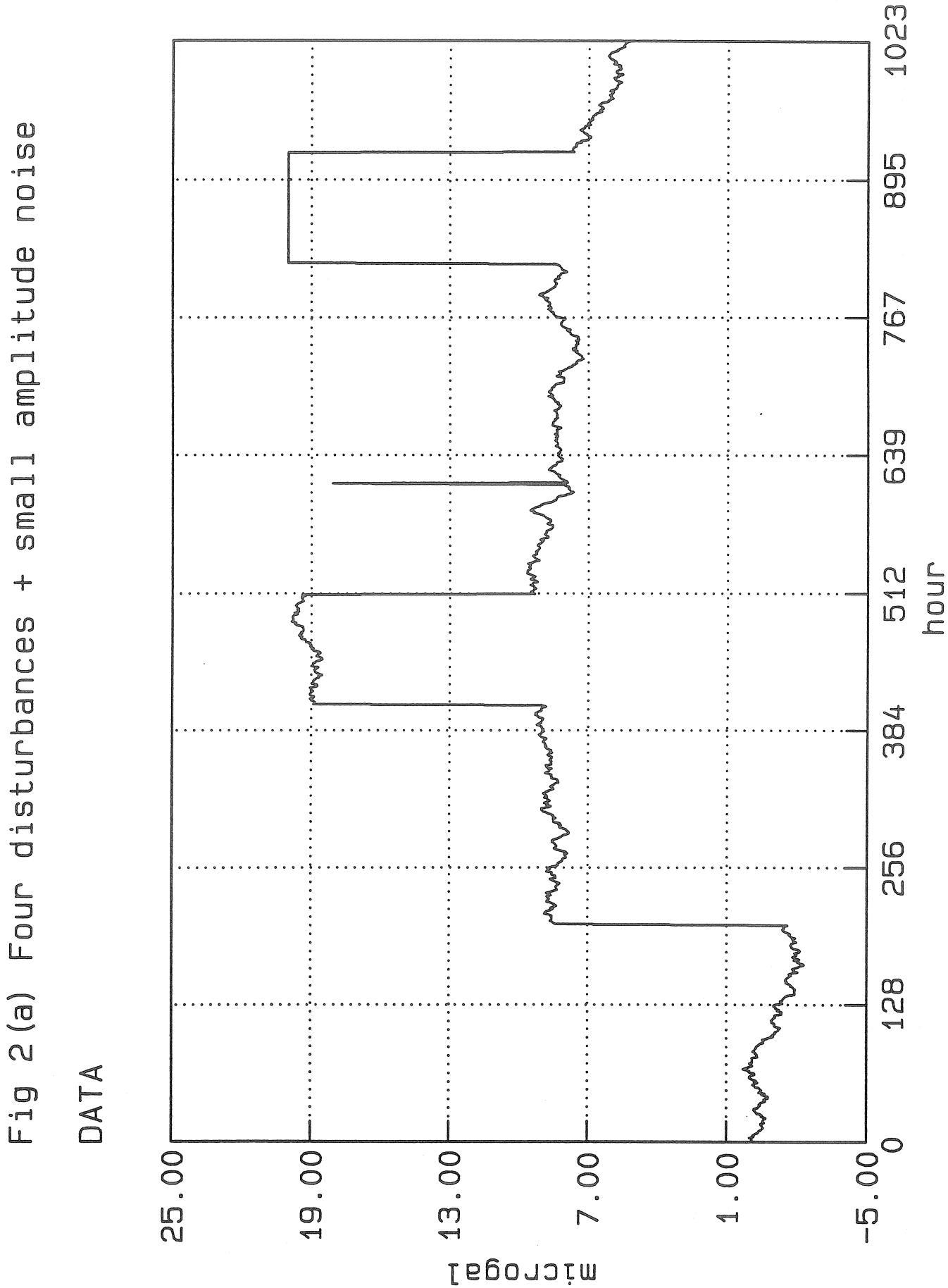


Fig 2(a) Four disturbances + small amplitude noise

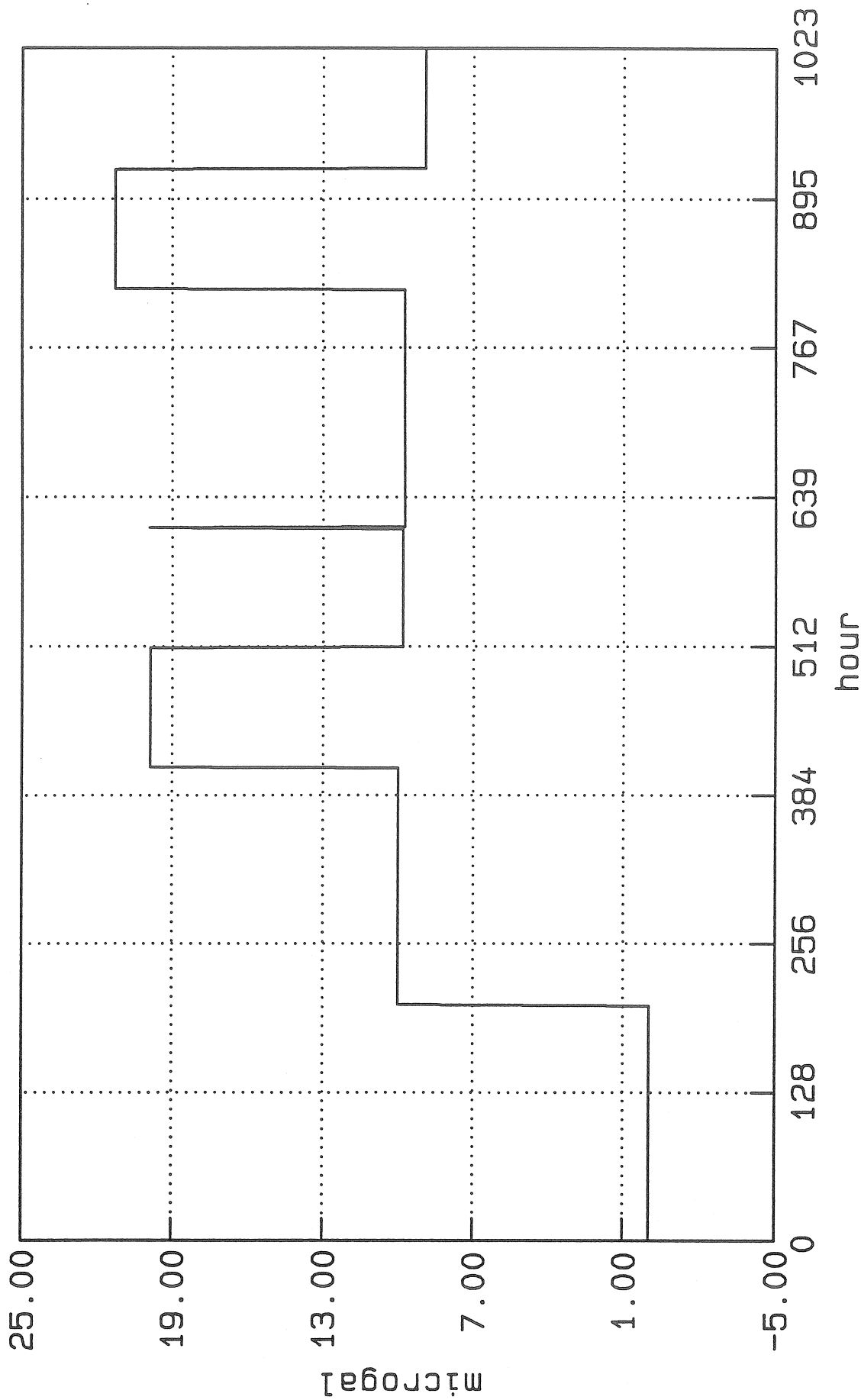


Fig 2(b) Slew function

DATA

Fig 2(c) Corrected and original noise functions

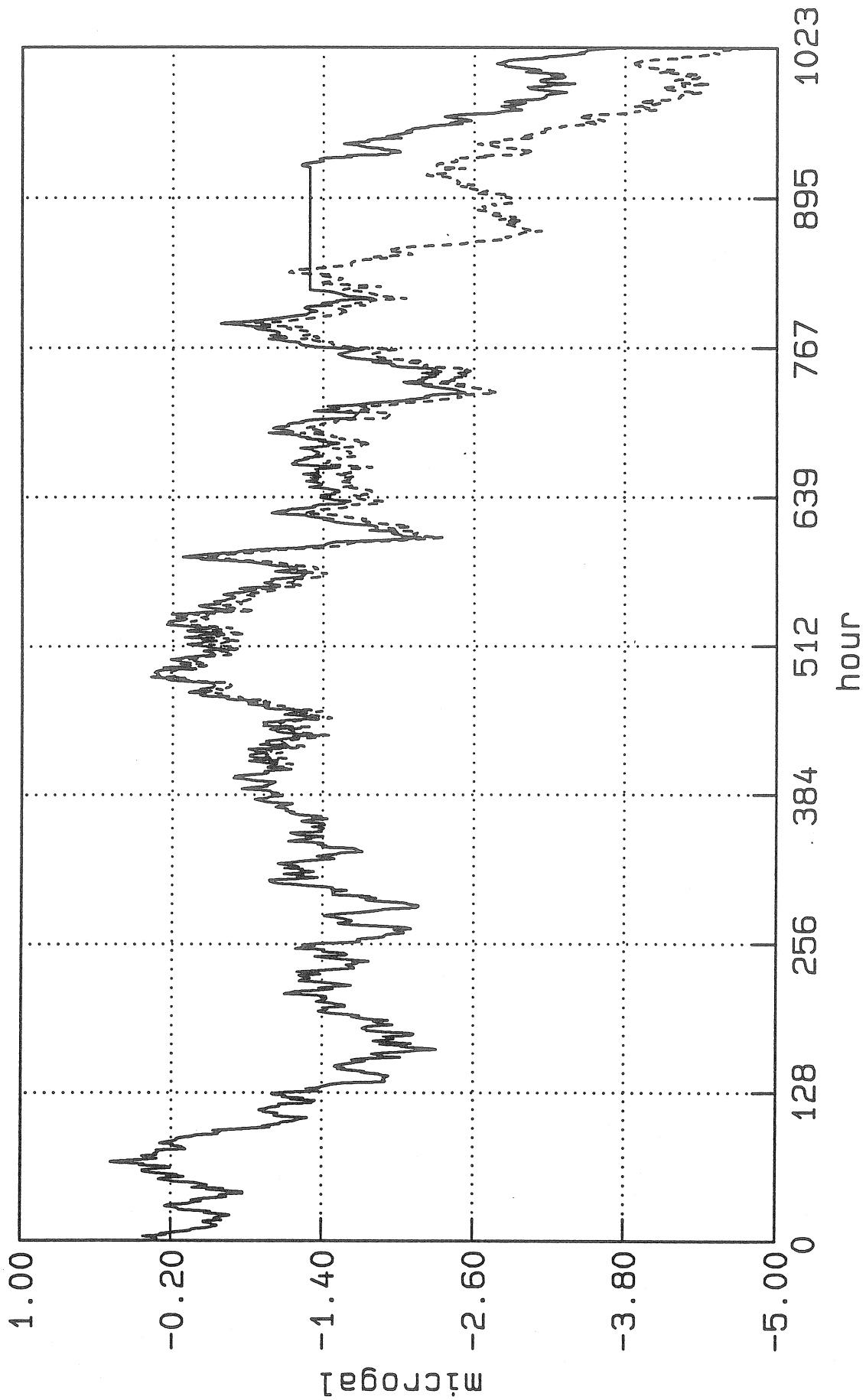

Fig 3(a) Four disturbances + large amplitude noise

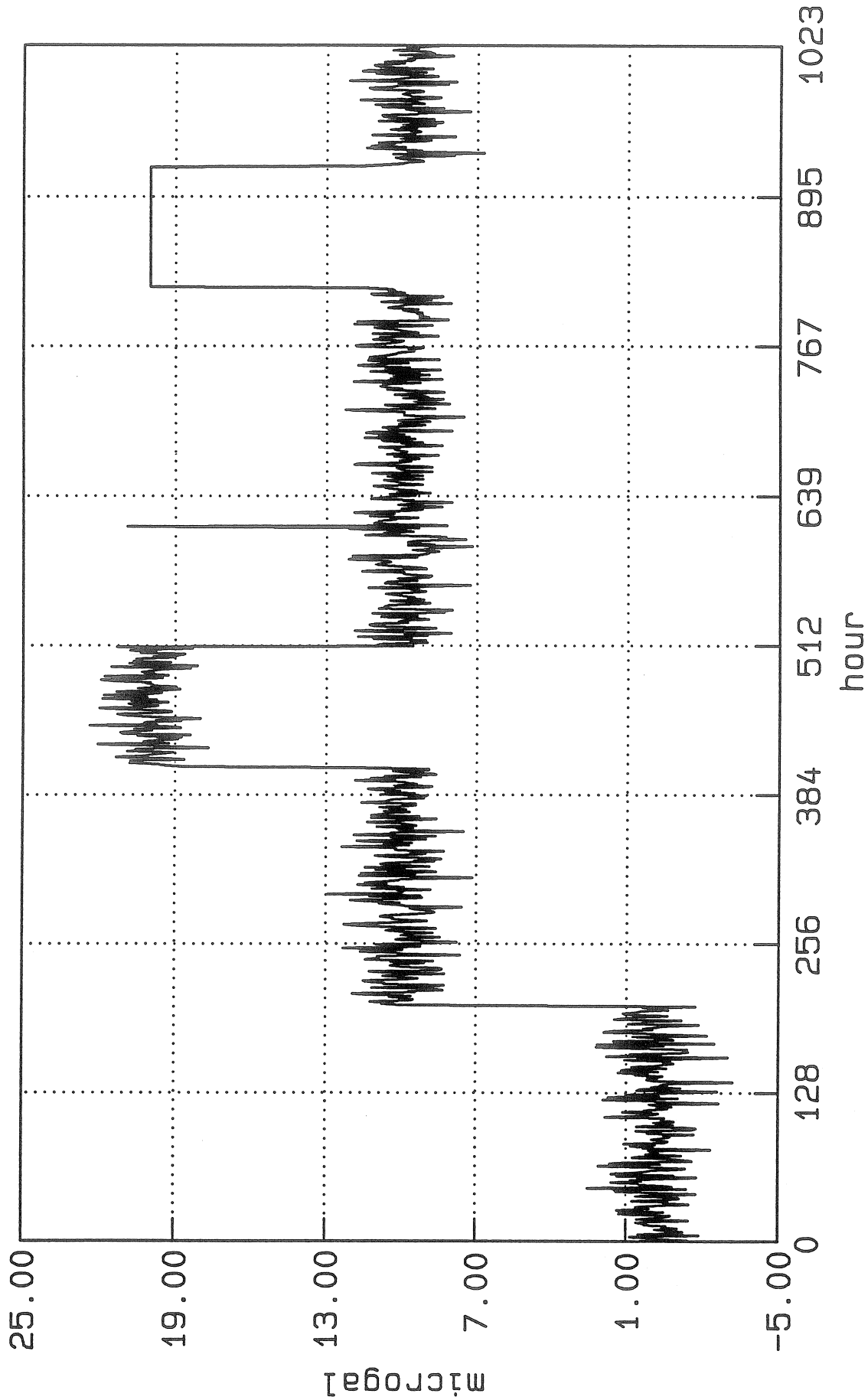

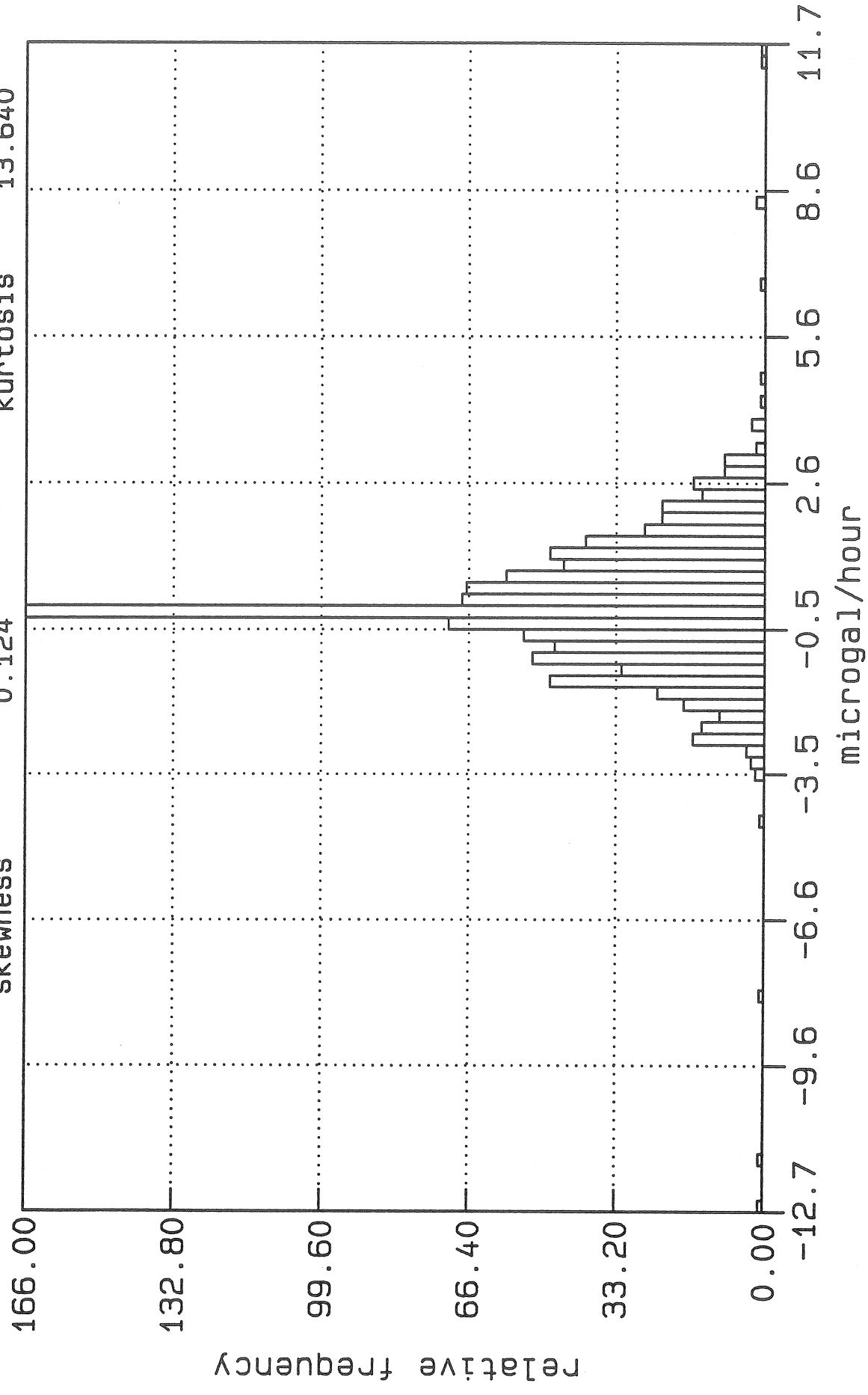


Fig 3(b) Histogram of slews

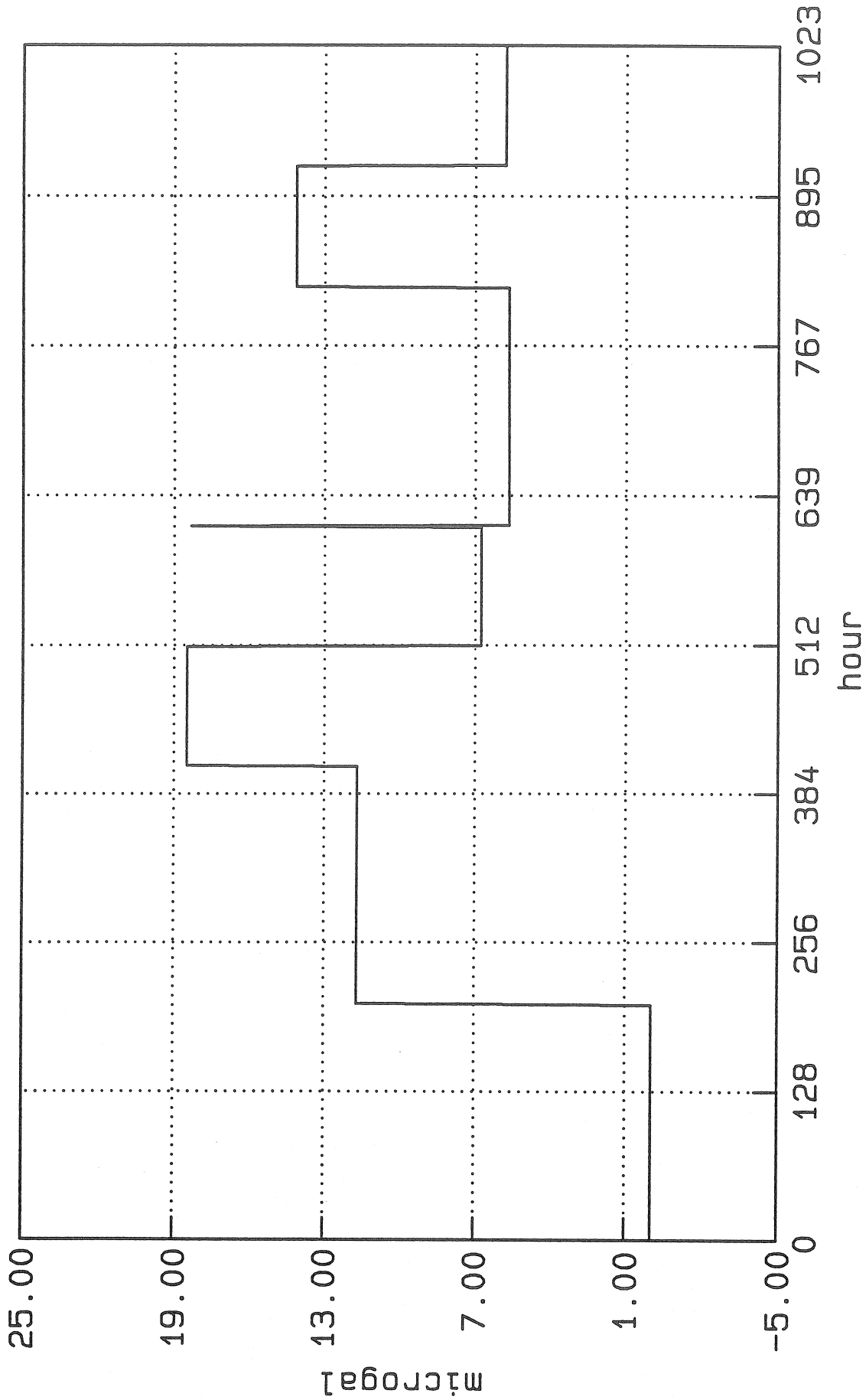


Fig 3(c) Slew function

DATA

Fig 3(d) Corrected and original noise functions

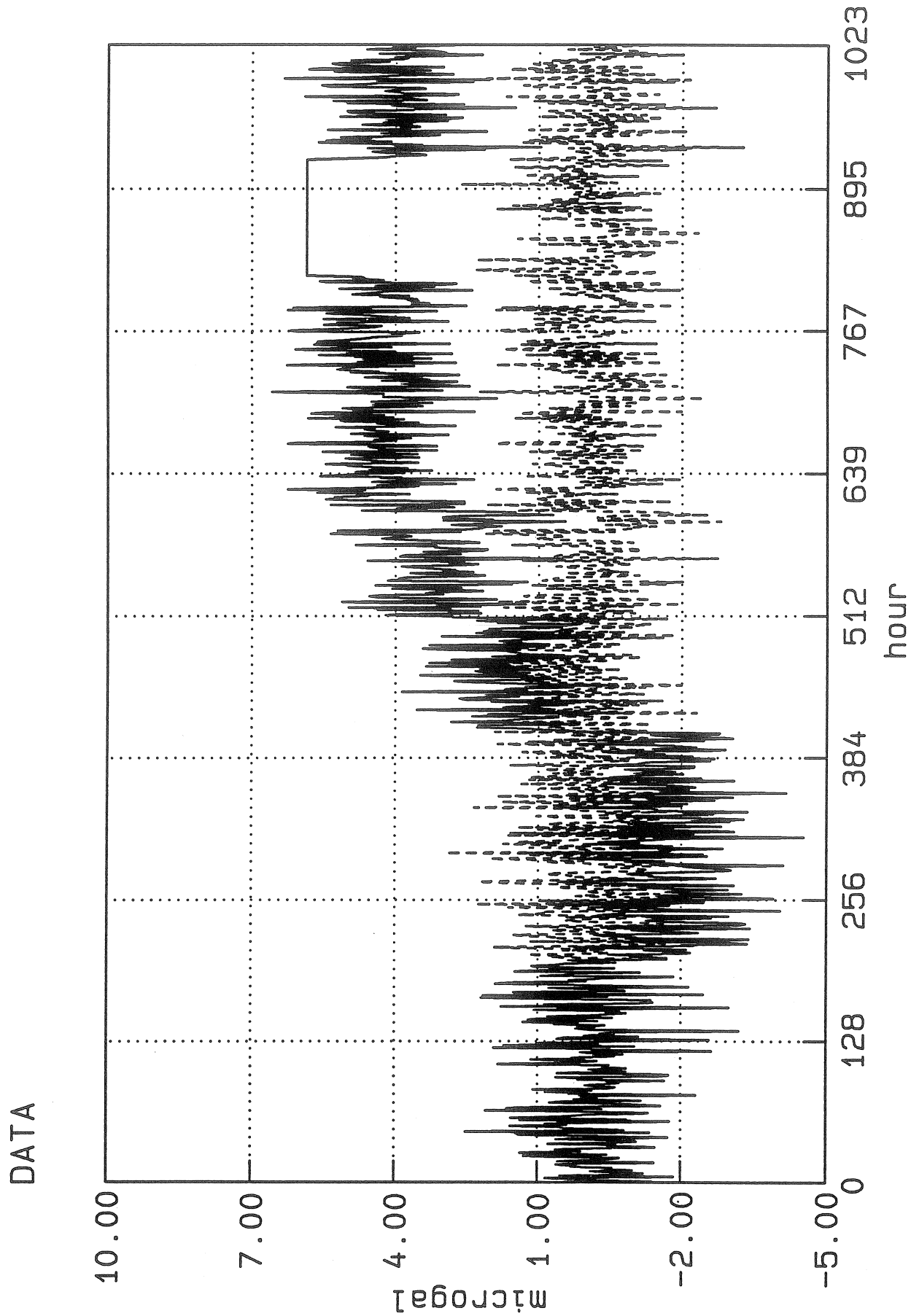

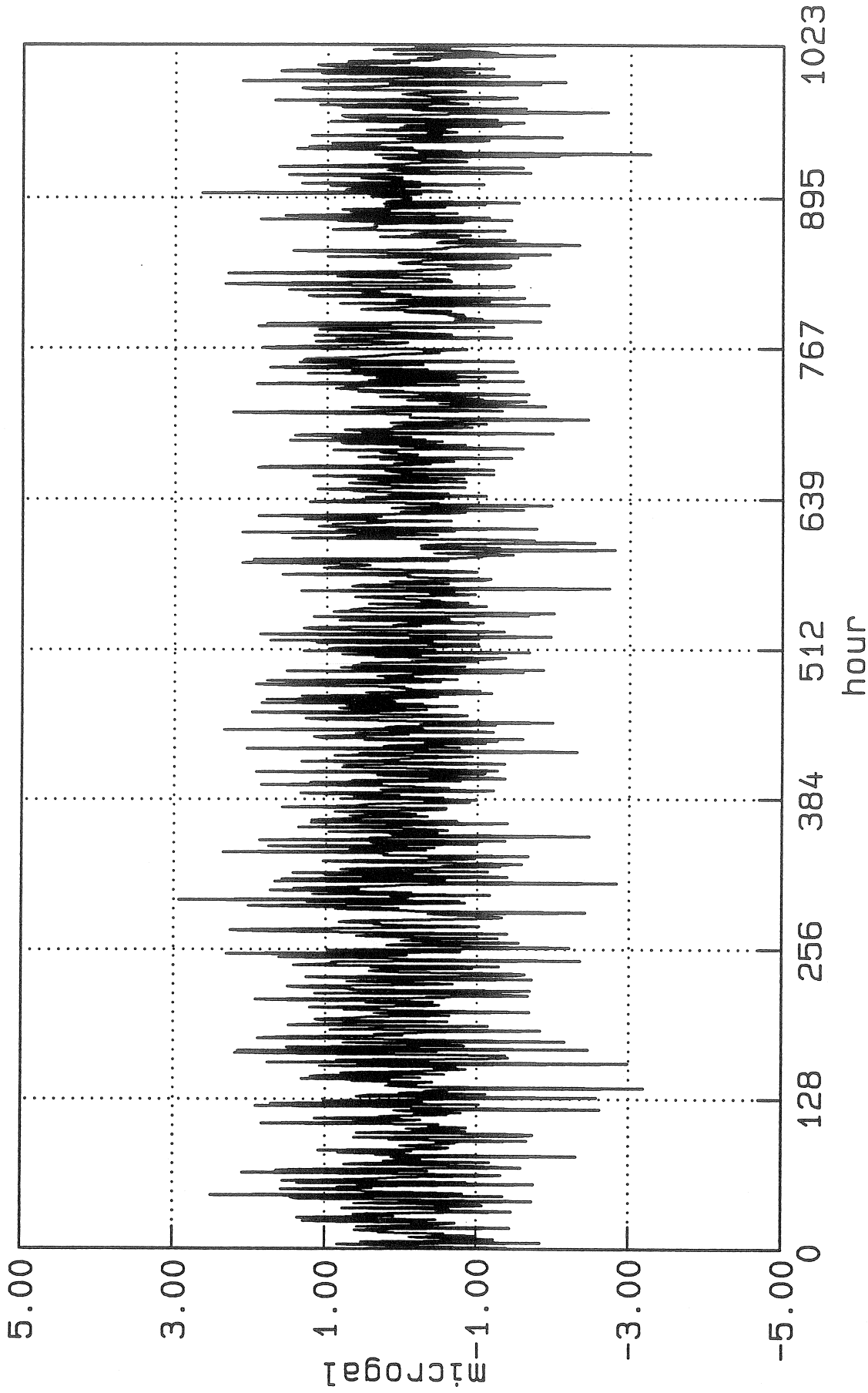


Fig 4(a) Original noise function

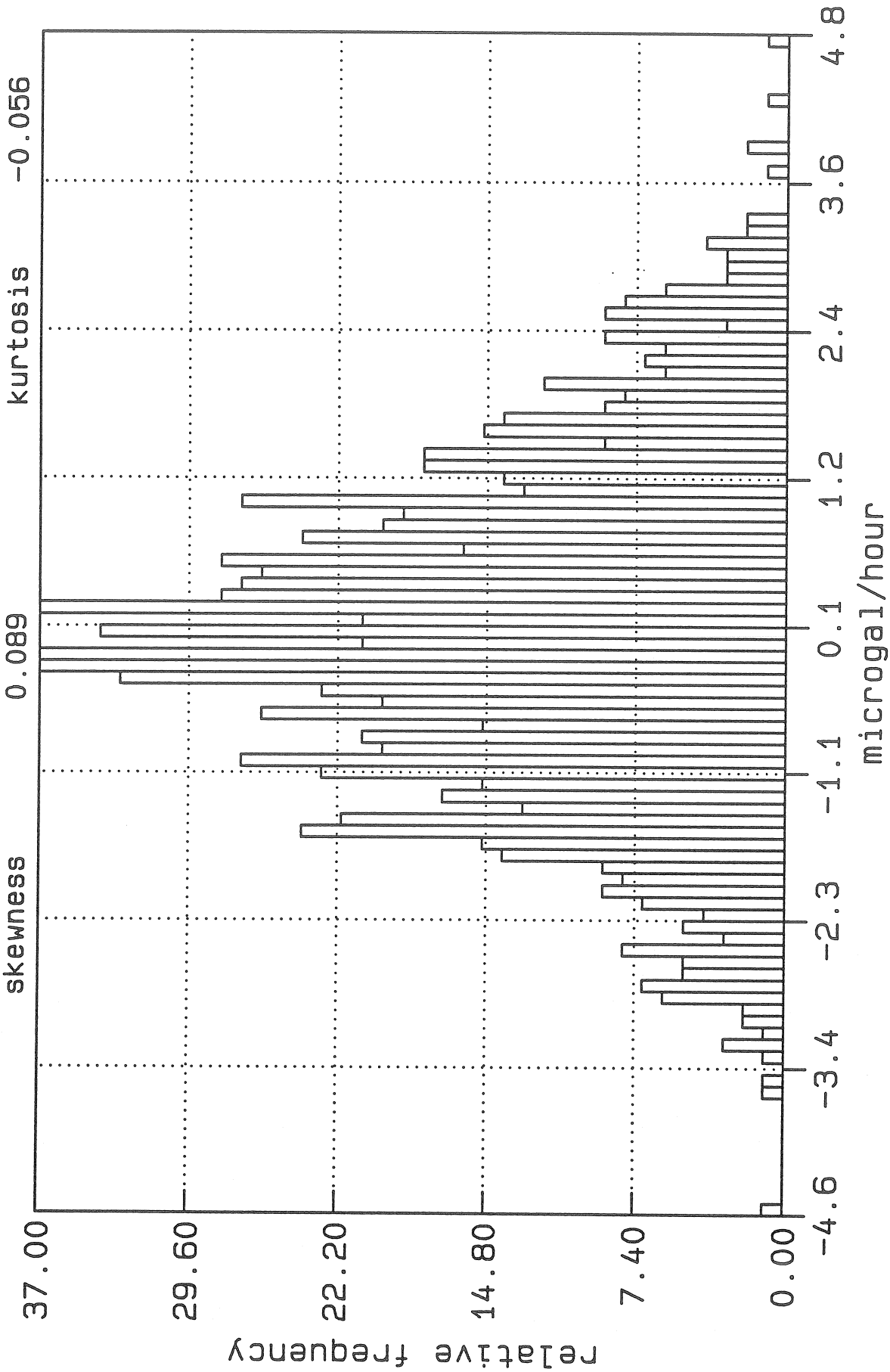


Fig 4(b) Histogram of slews

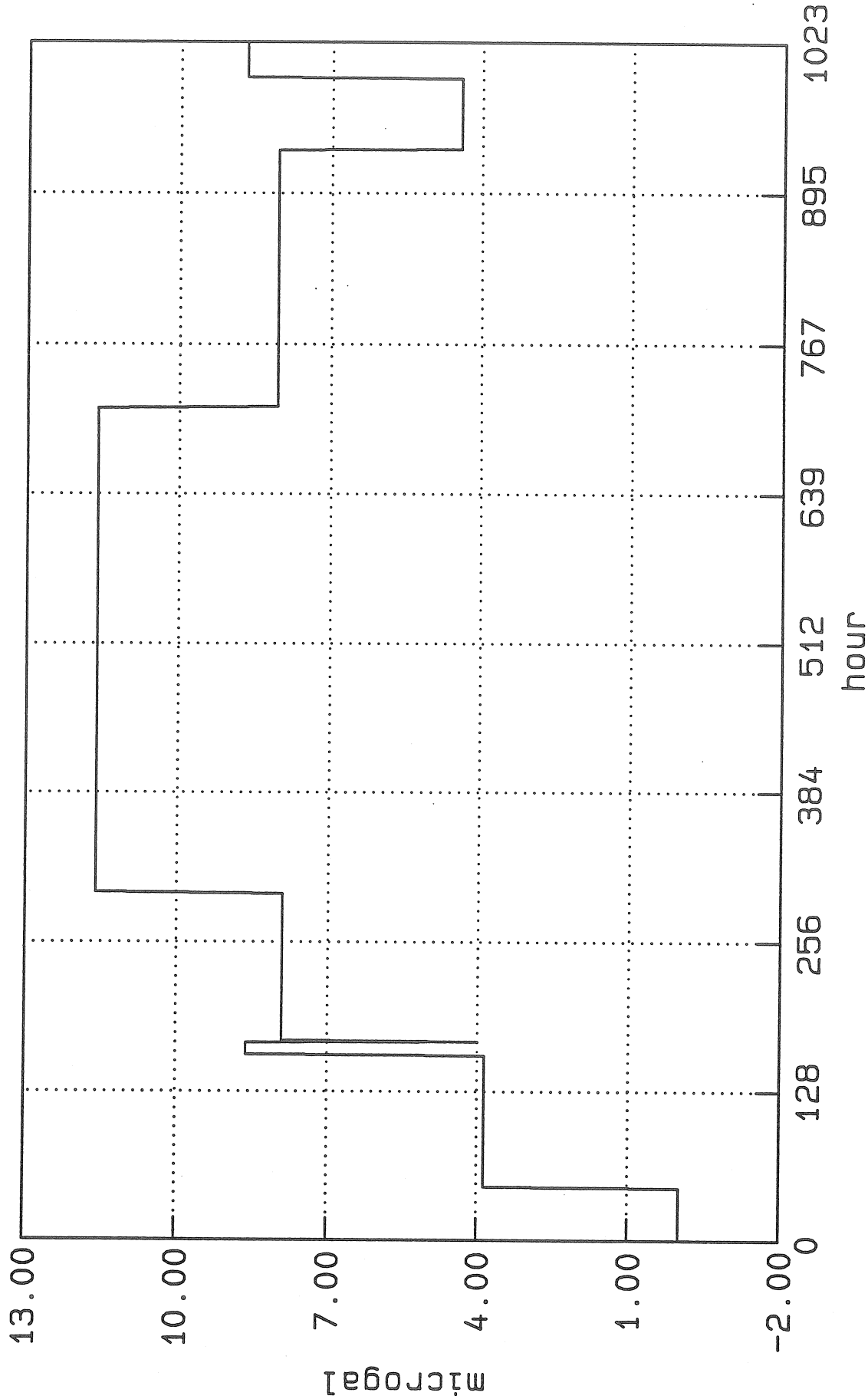


Fig 4(c) Slew function

DATA

Fig 4(d) Corrected noise function

DATA

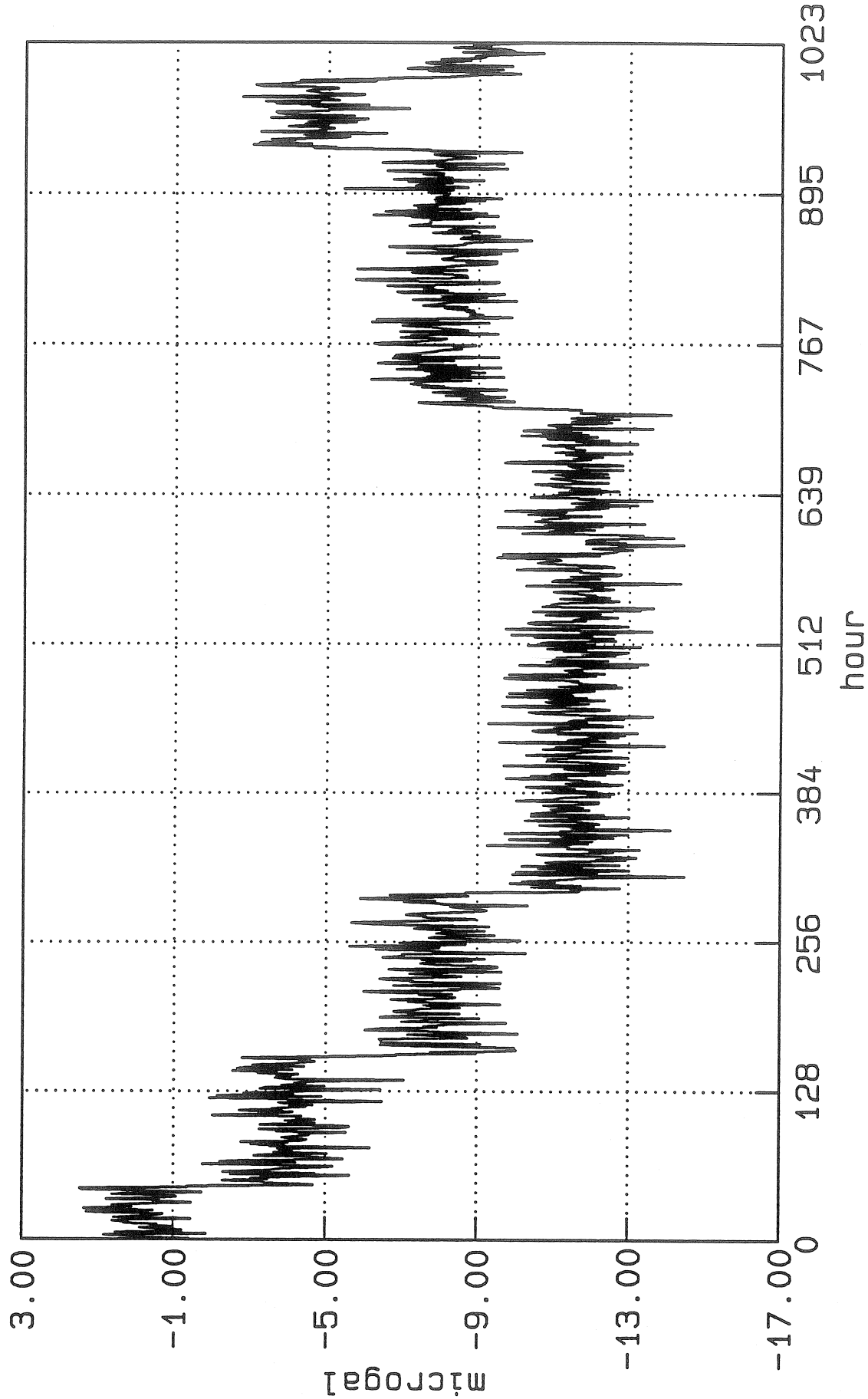

Fig 5(a) Raw gravity, 2 years CSGI

DATA

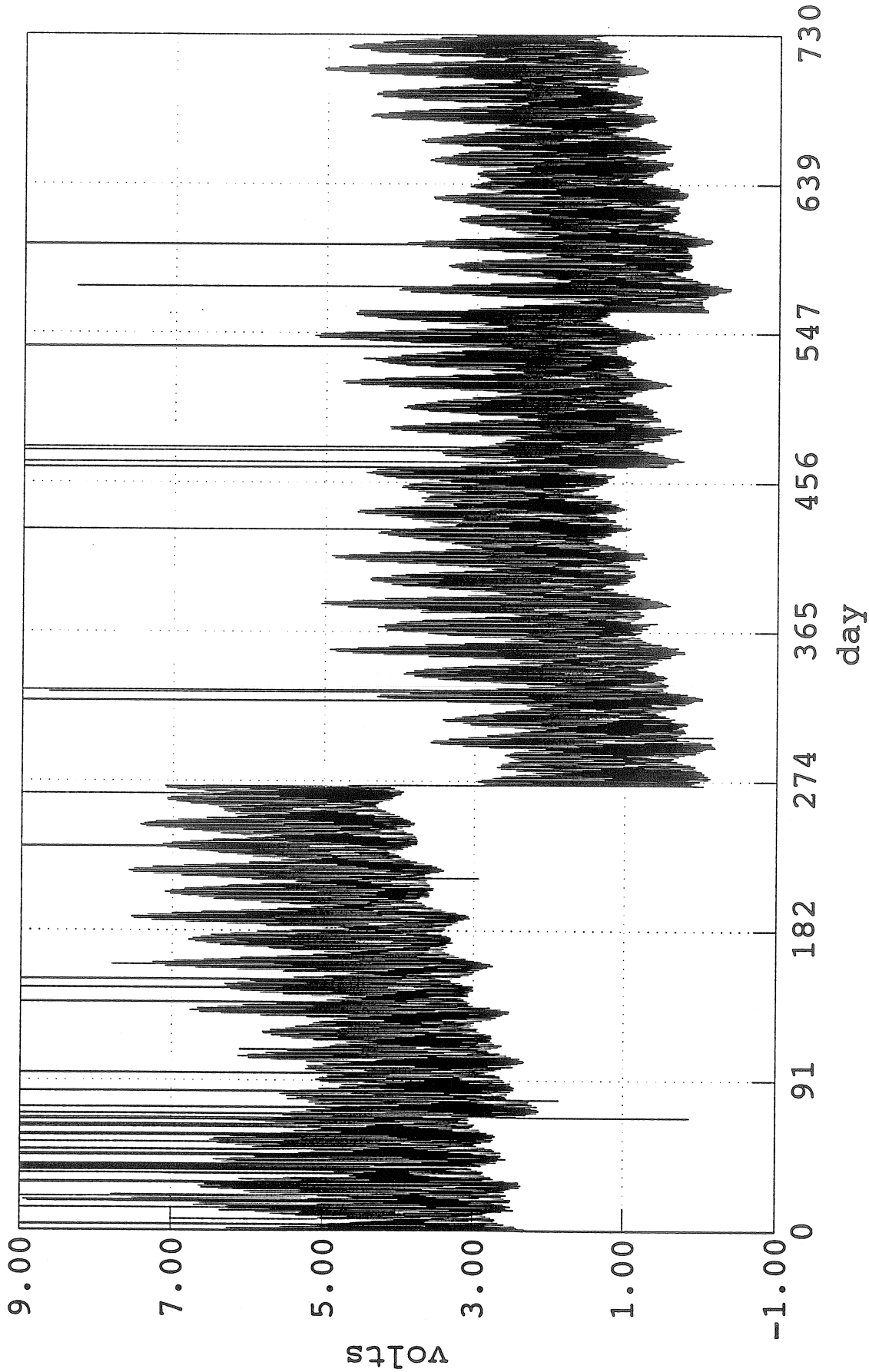

Fig 5(b) Raw gravity - synthetic tides

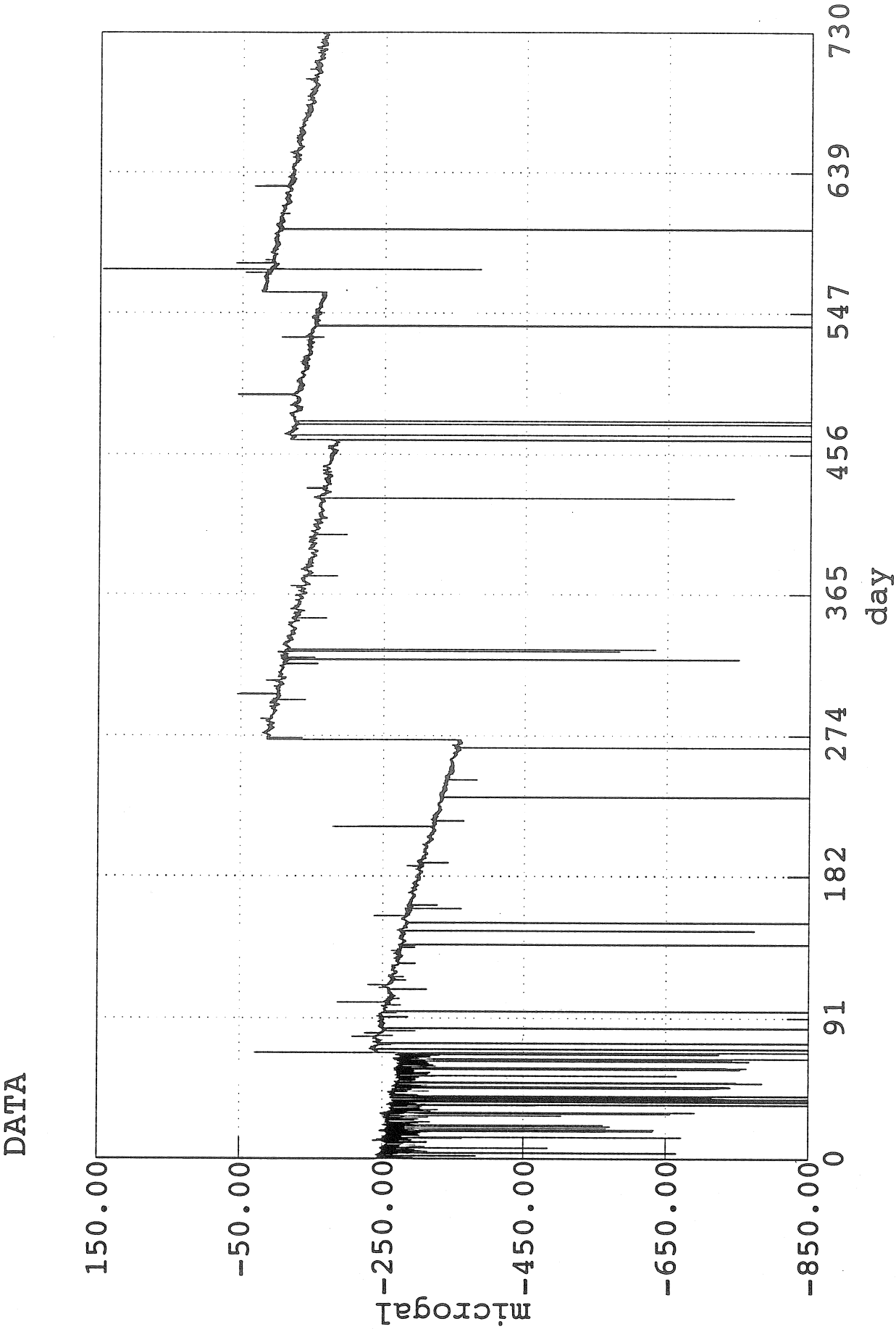

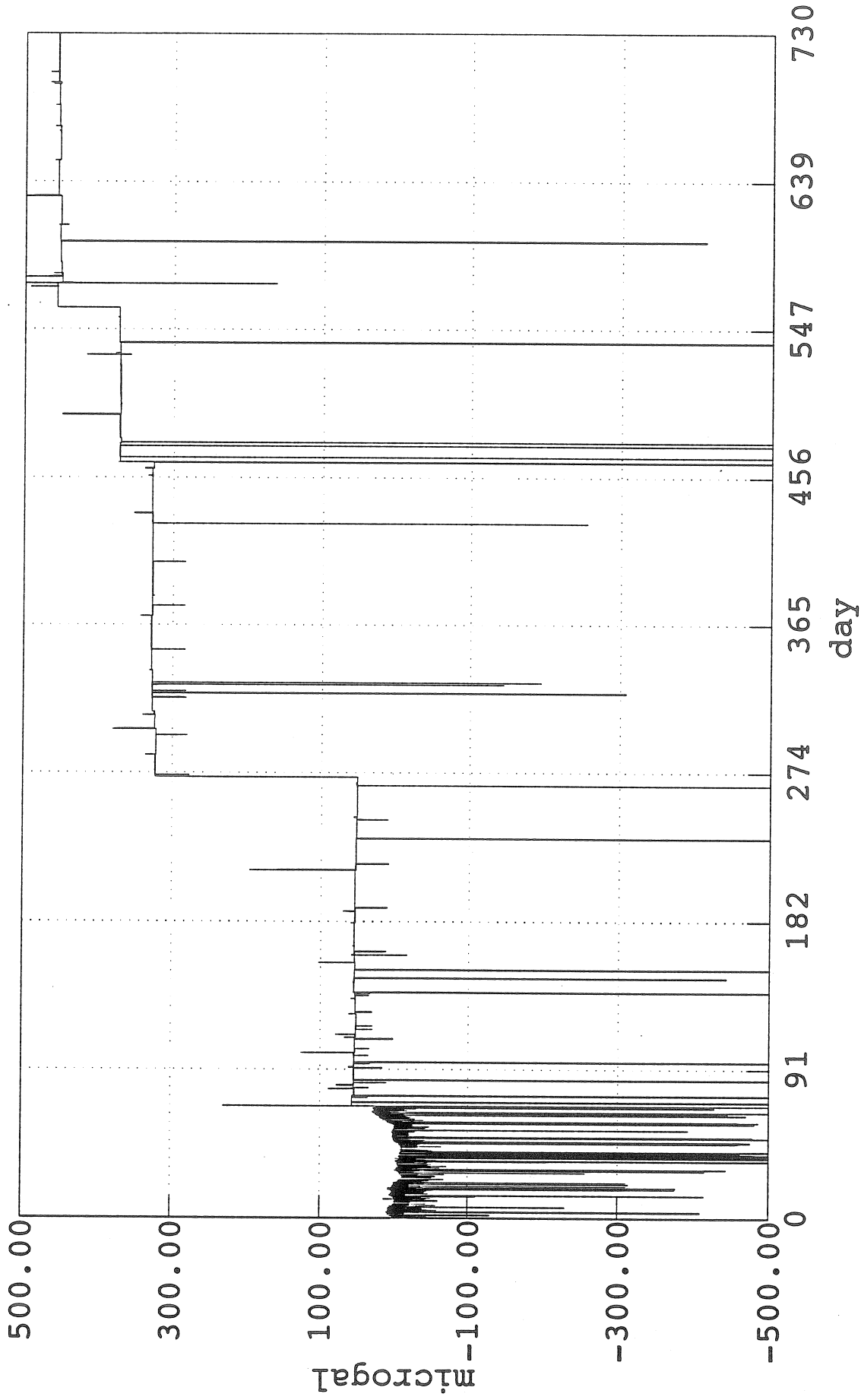


Fig 5(c) Slew function

DATA

Fig 5(d) Corrected gravity

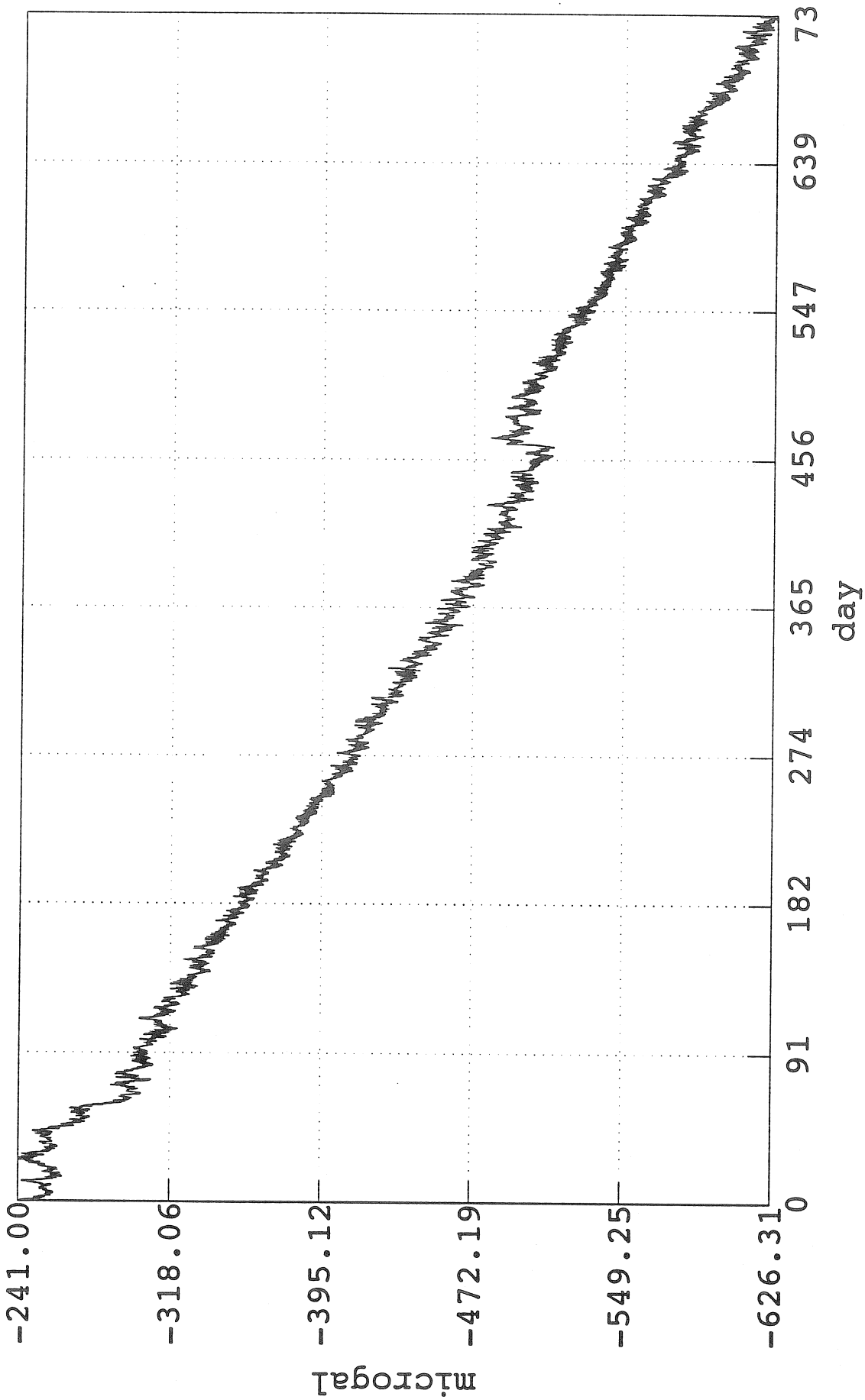

Fig 5(e) Corrected gravity - pressure

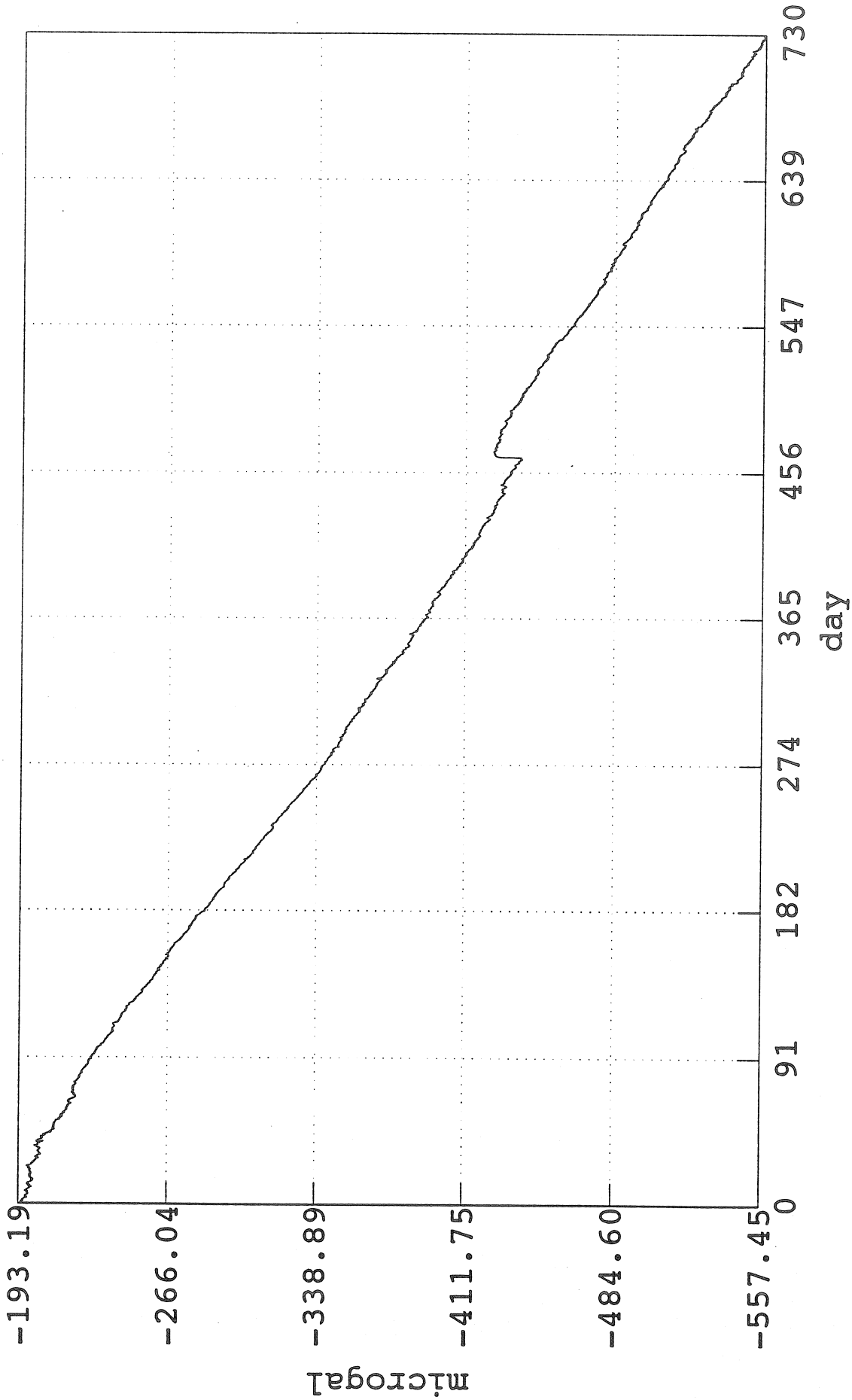

Fig 6(a) 1 hr gravity residuals (HYCON)

DATA

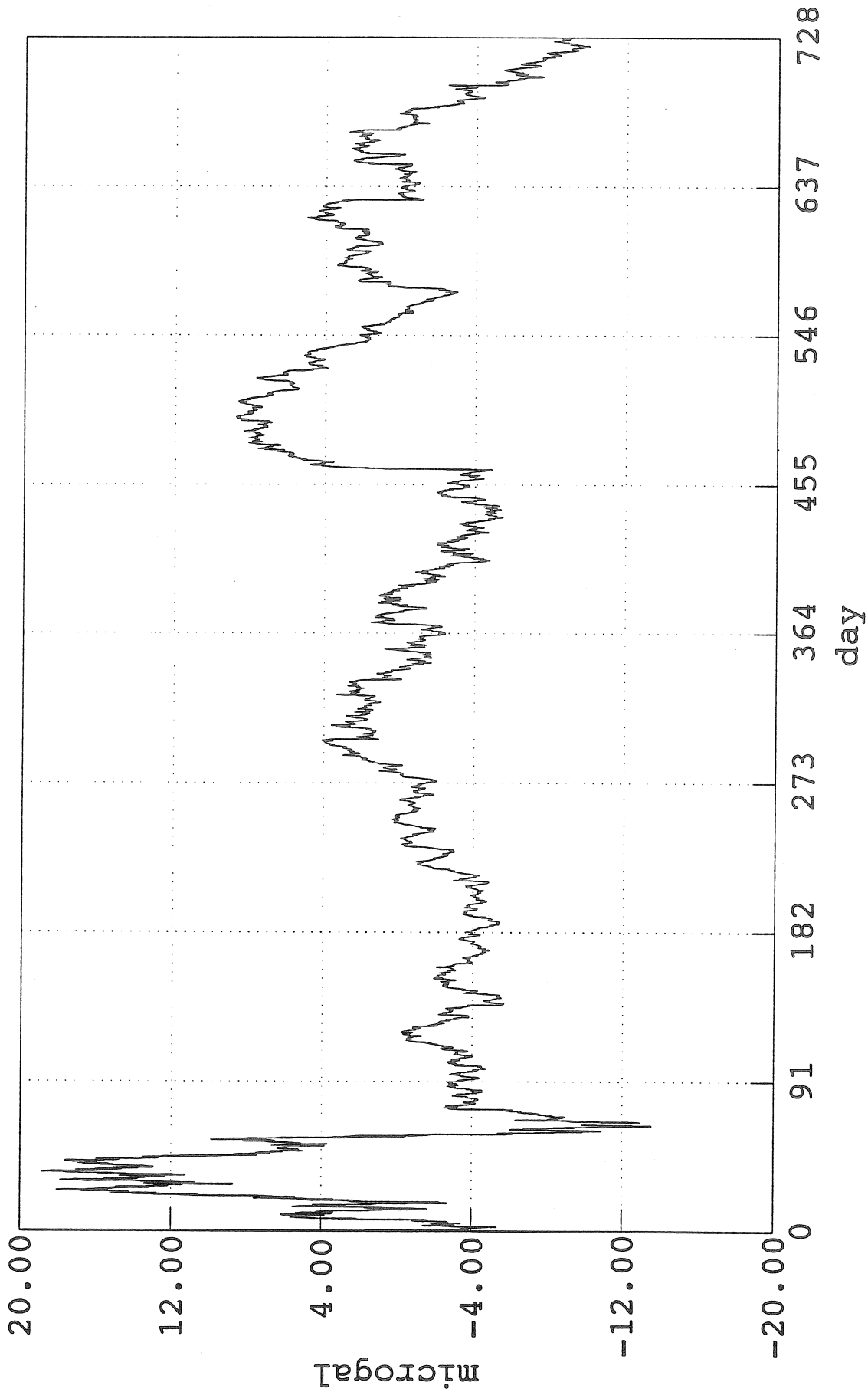

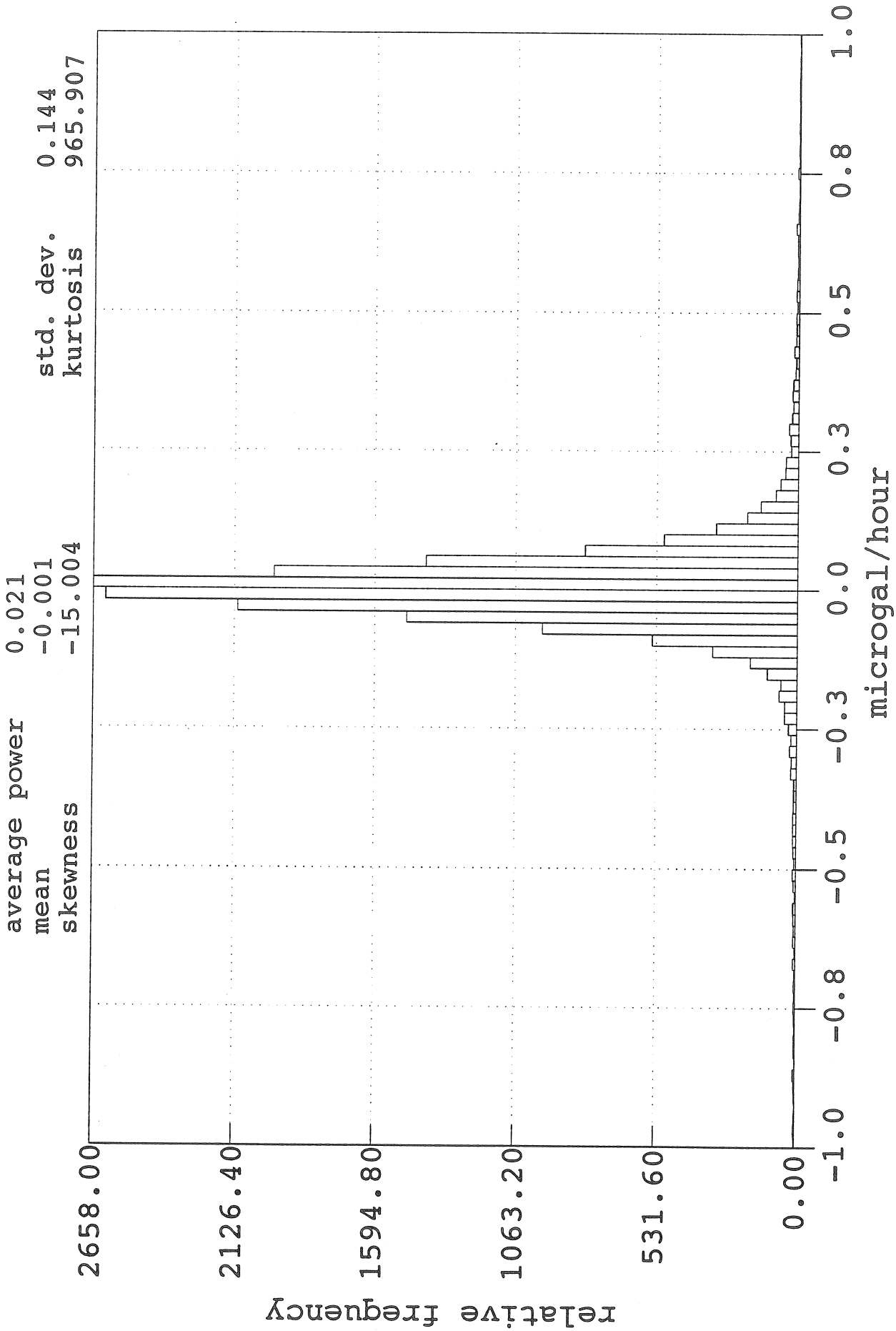


Fig 6(b) Histogram of slews

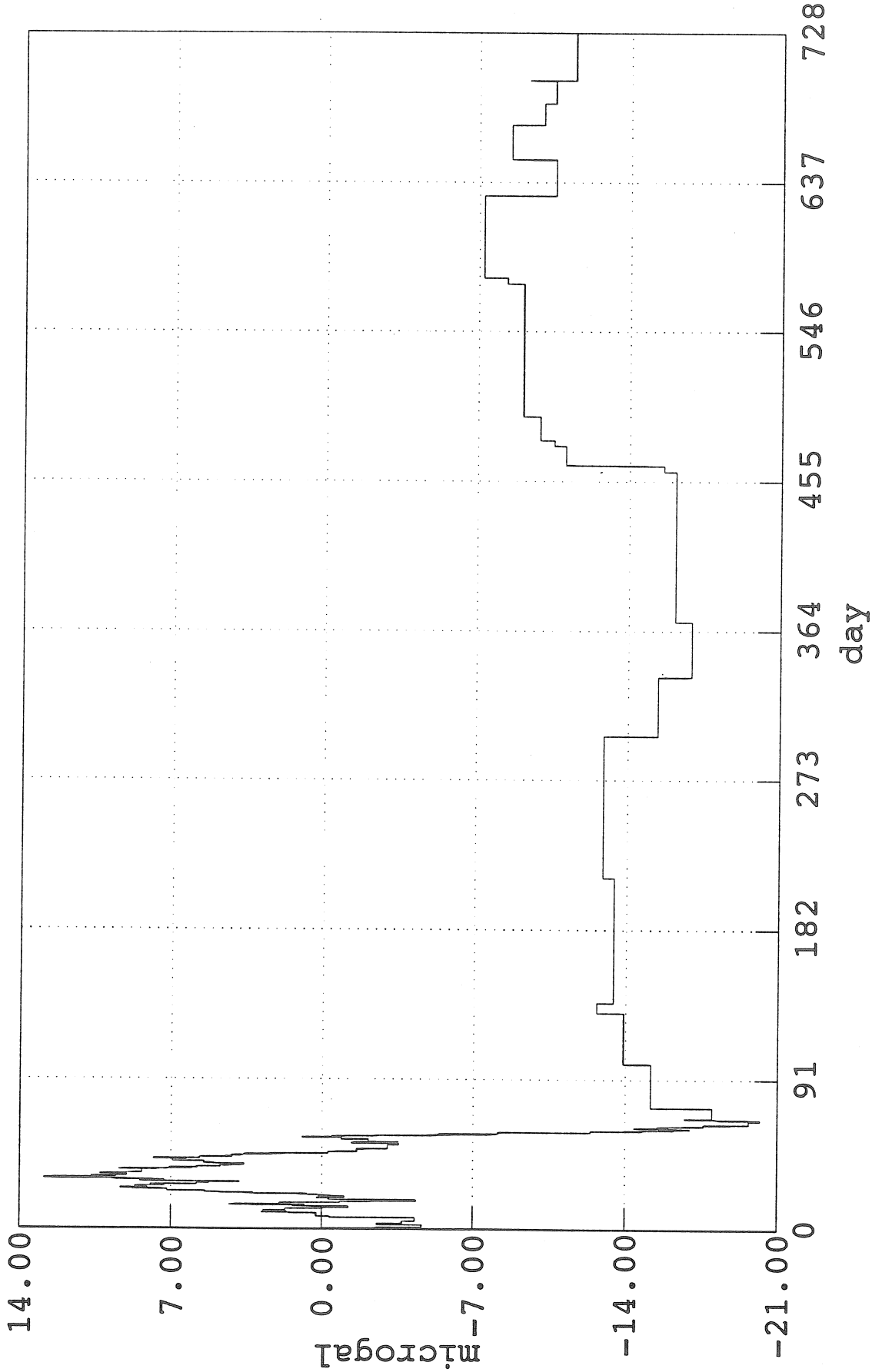


Fig 6(c) Slew function

DATA

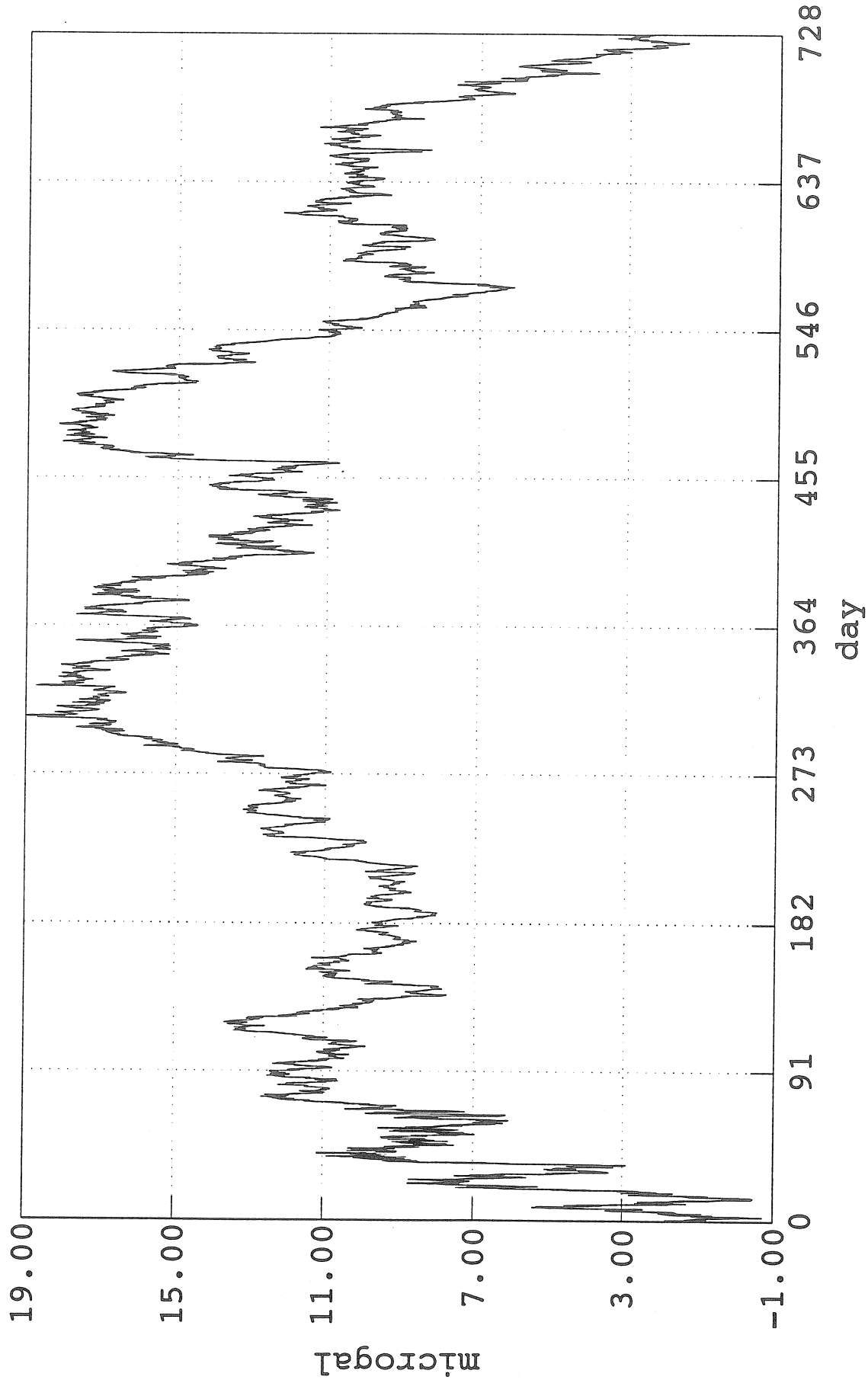


Fig 6(d) Corrected gravity

DATA

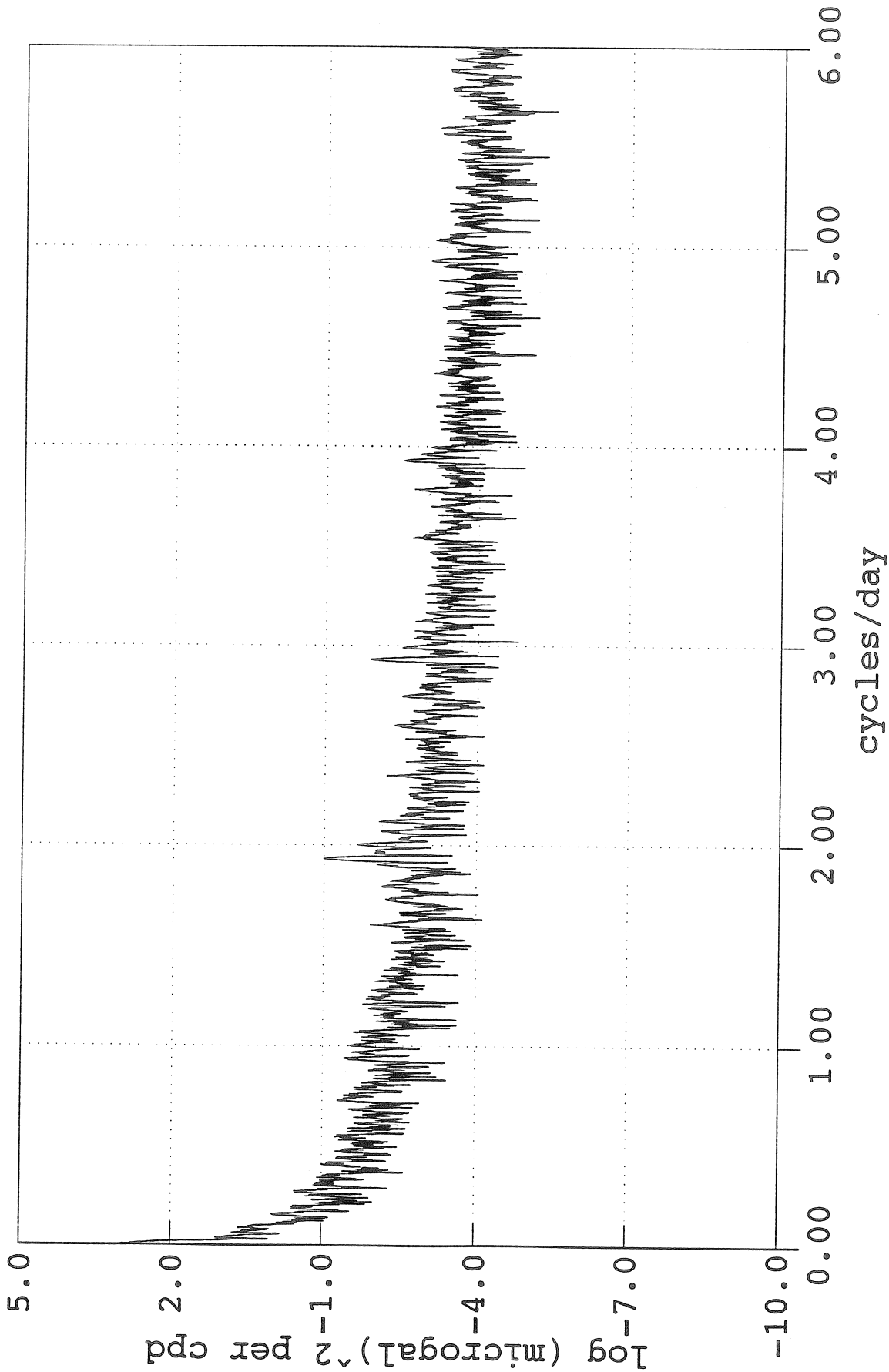


Fig 6(e) Slew function

POWER SPECTRAL DENSITY

# Preliminary Results of Gravity Tidal Observation obtained at Great Wall Station in King George Island, Antarctica.

L. Chun-Cao, Hsu Hou-Tse
Hao Xing-Hua, Ni Zhi-Hong
Institute of Geodesy and Geophysics
Academia Sinica
54 Xu Dong Road
Wuchang 430077
China

By utilizing the LCR-G 589 gravimeter, 342-day available gravity tide observation were obtained in King George island, Antarctica. Analytical results show that mean errors of tidal factor $\delta$ and phase delay $\Delta\phi$ for the main waves are less than 0.6% and 0.3° respectively. By using the Schwiderski cotidal maps to calculate oceanic tide correction, we observe that the oceanic effect on $M_2$ wave reaches 20% of the body tide magnitude, while the leading phase is 6.7°. The obtained gravity tidal factors of this station are:

$$\delta\ (O_1) = 1.2394 \pm 0.0061, \qquad \Delta\phi\ (O_1) = 0.71° \pm 0.25°$$

$$\delta\ (M_2) = 1.2350 \pm 0.0045, \qquad \Delta\phi\ (M_2) = 0.53° \pm 0.16°$$

Key-words: gravimeter calibration, tidal factor, phase delay, harmonic analysis, tide correction.

## I. Aim of Carrying out Gravity Tidal Observations in Polar Regions.

Earth tides response is closely related to latitude; for different components of earth tides Antarctic region emerges as a very exceptional case (1), as shown in Fig. 1. Polar point is a singular point, where direction has no sense. Thus the horizontal component of diurnal wave and the vertical component of long period wave are both maximum. All other components are zero at the pole. This indicates that in polar regions or high latitude region, carrying out gravity tidal observation bears a great significance (2). Earth tide observation in Antarctica can not only be applied to theoretical research of the conventional Earth models, but also to the study of the elastic character inside the continental crust in Antarctica covered with deep snow and ice. Under this condition we may explore the liquid core effect, study the interaction between long period polar tide, earth tide and loading tide. In the meantime, we can use parameters measured to provide precise tide correction for the precise gravity, astronomical and geodetic measurements. Up to now, several countries, i.e. USA (polar point), USSR (Peace station), Japan (Syowa base), Brazil (King George island, Ferraz station) and China (King George island, Great Wall station) have carried out tidal gravity observation in this area.

---

* This work is supported by National Antarctic Investigation Committee and the National Science Foundation of China.

## II. Observation.

The Earth tide station in King George island ($\phi$ = 62°13'S, $\lambda$ = 58°58'W) is built on a large bedrock about 400m northwest of the Great Wall station. The meter is placed on a cement pier. The station is 25m above sea level (Great Wall gulf height system) and 0.8 km away from the sea. The region around the station is covered with snow-ice for 8 months in a year, with an annual temperature difference of about 31°C. The observation room, with an area of 8.8m$^2$, consists of two parts and is able to resist hurricane more than force 12. Its heat preservation properties are good, room-temperature 22°C ± 0.1°C, the annual temperature variation is less than: ± 0.2°C, moisture 40%. From Feb. 15,1988 through Mar. 1, 1989 the following devices were employed to complete this observation:

LCR G589 gravimeter,
Chino 250mm 3-channel recorder, velocity 30mm/h,
SF 356 filter, quartz clock, barometer,
one set of controller for keeping a constant temperature and constant moisture,
one self-recorder of temperature-moisture,
an auto DC-AC supply transform-device,
There are two aspects in the calibration of the tidal recording scale:

### 1. The Tidal Recording Scale of Gravimeter

For the tidal recording scale LCR G589 gravimeter was calibrated once per week by measuring the screw displacement. Meanwhile the voltage difference before and after calibration was recorded. The average of two recorded results were taken as calibrated values. Interpolation was made between two calibrated values, the mean square error of interpolation calibration values is about ± 0.3%.

### 2. SF 356 filter and phase delay of the meter

The influence of large wind and seawave in Antarctica makes the recording curve of gravimeter thicker, and decreases reading accuracy, as shown in Fig. 2a. To remove this effect an SF 356 filter was connected between LCR G589 and the recording system (see Fig. 2b). Before and after doing earth tide observation in Antarctica we made 18-day and 24-day comparison observations in Wuchang station. Connection of the gravimeter with SF 356 filter, certainly causes large phase delay in the observation result. Observations with the same instrument in Wuchang station shows that the delay of $O_1$ wave is increased by 2.9°, the delay of $M_2$ wave by 2.5°. In processing the observation data, the effect of meter and filter on phase delay was removed. The results are show in Table 1.

## III. Analysis of Observation Results

### 1. Analysis Method and Observation Accuracy

Venedikov's harmonic analysis method is employed for the analysis (3). The program we utilized is revised by the Institute of Geodesy and Geophysics, Chinese Academy of Sciences, on the basis of the tidal analytic program of ICET (4). Before applying the harmonic analysis, interrupted data within 48h due to power cut or sensitivity adjustment must be removed, and then all data are checked by the use of Nakai data preprocessing (5), so that incorrect data and jumps are corrected.

Mean error of unit weight for diurnal, semi-diurnal and ter diurnal

waves is less than 2.5 $\mu$gal. This shows that in Antarctica, the reading error and the noise of gravimeter and environmental are rather small. Internal accuracy of the tidal factor $\delta$ depends on tidal observation accuracy and observation data length. Mean square error of $\delta$ value for the various main waves is usually less than 0.6%, and mean square error of phase delay less than 0.3°. The whole data are divided into 11 segments to calculate the variation of $\delta$ value of each segment with respect to the $\delta$ value of the whole length which is small. The maximum mutual error is 0.4% which indicates that data coincide well (6).

## 2. Rheological Model of the Instrument

The LCR-G gravimeter is a kind of astatic instrument, of which the rheological model expresses the response function in the form of multi-parameter rheological model of one Hooke's body and multi-Kelvin's bodies, i.e.

$$y(t) = L \{1 + \sum_{i=1}^{n} \tau_i (1 - e^{-t/\tau})\}, \tag{1}$$

where L is the output value of the meter, $\epsilon_i$ is attenuation factor, $\tau_i$, is the time delay.

As a matter of fact, we can take two-parameter rheological models with one Hooke's body and one longer time-delay Kelvin's body.

$$y(t) = L (1 - \epsilon e^{t/\tau}) \tag{2}$$

the phase delay is

$$\tan \phi = - \frac{\epsilon \omega . \tau}{1 + \omega^2 \tau^2 + \epsilon} \tag{3}$$

if $\tan \phi$ ($M_2$) (of the meter) = b, $\tan \phi$ ($O_1$) = a, then according to

$$\omega (M_2) = 8.43113 \times 10^{-3} / \text{min}$$

$$\omega (O_1) = 4.05218 \times 10^{-3} / \text{min}$$

where $\omega$ ($M_2$) is the angular velocity of the $M_2$ wave, $\omega$ ($O_1$) is the angular velocity of $O_1$ wave.

By substituting the observed values $\phi$ ($M_2$) and $\phi$ ($O_1$), we get $\tau$ and $\epsilon$, and the corresponding reduction ratio R of amplitude is

Using the tidal factor and observation data (through harmonic analysis) in Wuchang station, we obtain the phase delay of the diurnal waves and semi-diurnal waves (Table 2). We use Eqs (3) and (4) to seek the normalized factor f ($O_1$)

$$f (O_1) = 0.981576 \tag{5}$$

With Eq. (5), we derive the normalized factor f' ($M_2$) of the semi-diurnal wave as follows:

$$f' (M_2) = 0.985543 \tag{6}$$

The normalized factor f' ($M_2$) actually measured in Wuchang station is

$$f (M_2) = 0.986974, \tag{7}$$

$$f'(M_2) - f (M_2) \langle 0.2\%.$$

This demonstrates that through the use of this normalized factor the Antarctic observation results reduced to Wuchang tidal data station is reliable.

Standard tidal factors and observation results after connection of the G589 gravimeter with the SF 356 filter at Wuchang station are listed in Table 2.

## IV. Results and discussions

### 1. Venedikov Harmonic Analysis

Gravity tide results obtained at Great Wall station in King George island, Antarctica, by using Venedikov analytic method are listed in Table 3.

In Table 4, the final observed values of the main waves after correction by the rheological model are given.

### 2. Indirect Effects of Oceanic Loading and Final Results

The main factors affecting the observation of earth tides are oceanic tides and meteorological disturbances. Due to the limited space, this paper only deals with the indirect influence of oceanic tides; the effect of meteorological disturbances on earth tides will be discussed in another paper.

Earth tides and oceanic tides are both caused by the tide generating forces of the Moon and Sun. They have the same period, and it is impossible to separate them with a simple analytic method. Longman first quoted the concept of loading Love numbers (8). Using gravity Green functions and tide height to do convolution integral, he got oceanic tide correction in gravity observations. Thus this problem was solved theoretically. Then, Farrel studied the problem of high-speed convergence (9) and derived all practical formulas and coefficients. Therefore the calculation of oceanic tides was realized. Afterwards, Pertsev computed it by developing the global oceanic tide map into spherical harmonic functions (10), and adopted the separatory spherical blocks to do numerical integration. Oceanic tidal correction results used in this paper are obtained by making use of the advantage of both methods mentioned (12), i.e. numerical integral for near region and spherical function to seek solution for far region.

Taking oceanic tide as a single layer load with surface density

$$\sigma(\theta, \lambda) = \mu H (\theta, \lambda)$$

in which $\mu = 1.03$ denotes sea water density; H, the tide height of instantaneous velocity; r, $\theta$, $\lambda$, the spherical coordinates.

Then the gravitational potential of the single layer load at any point on the ground is

$$U(\theta, \lambda) = G \int \frac{\sigma(\theta', \lambda)}{\rho} dS', \tag{8}$$

where

$$\rho = 2R \sin \frac{\Psi}{2} - \cos \Psi$$

$$\cos \Psi = \cos \theta \cos \theta + \sin \theta \sin \theta' \cos (\lambda' - \lambda), \tag{9}$$

G is the gravitational constant; $\rho$ is the distance from the computed place $(\theta, \lambda)$ to the surface element $dS'$ $(\theta', \lambda)$; $\sigma(\theta', \lambda)$ is the single layer density at differential surface element $dS'$; $\sigma$ is the spherical harmonic function.

From the earth model, a set of dimension less load Love numbers $h_n'$, $k_n'$, $l'_n$ are derived.
With these Love numbers, we can calculate the gravity variation produced by loading, gravitation and deformation.

Oceanic load gravity correction values at Great Wall station, in King George island, Antarctica are shown in Table 5.

For the results after oceanic load correction of gravity tidal observation of main waves at Great Wall station in King George island, Antarctica see Table 6.

We put the gravity tidal observation results of Great Wall station in King George island, Antarctica into the following equations (10) and (11), to obtain the differences between the gravity tide observation values and the theoretical values of Molodensky's earth model (see Table 7).

$$B_i = A_T \sqrt{(\delta_i \cos \kappa_i - \delta_T)^2 + (\delta_i \sin \kappa_i)^2} \tag{10}$$

$$B_i = \tan^{-1} \frac{\delta_i \sin \kappa_i}{\delta_i \cos \kappa_i - \delta_r} \tag{11}$$

where $A_T$ is the theoretical amplitude value of the rigid earth; $\delta_T$ is the theoretical value of the corresponding elastic earth model.

## 3. Discussion

It can be seen from the observation analysis and results, after ocean tide correction, that the effect of oceanic loading on gravity tidal parameter of wave $M_2$ reaches 20% of body tide magnitude, and the phase-lead 6.7°. The phase-lead is due to interaction of oceanic load acting on crust and near-sea of our station, which is similar to the results observed by Melchior at Bordeaux station in the Gulf of Gascoigne (13). After oceanic tide correction, tidal factors of main waves, except wave $S_2$, tend towards the value of the theoretical model. Meteorological perturbations mainly come from atmospheric influence. Effect of atmospheric pressure variation on earth surface load is based on various regions. One millibar atmospheric pressure variation corresponds to $0.28 \approx 0.43$ $\mu$gal (14). Atmospheric pressure variation in King George island region is rather large, for example, in the period of our observations daily difference reaches 37 millibar, weakly difference 63 millibar, annual variation 75 millibar, and the magnitude of affected diurnal wave up to more than 10 $\mu$gal. This can't be neglected. The model of oceanic loading correction

only considers the radial heterogeneities but does not take lateral heterogeneities into account, thus the model of oceanic tide correction is not perfect. On the other hand, Schwiderski cotidal maps give no complete informations about Antarctic coast. Therefore, it is impossible to remove the near-sea influence perfectly.

We are indebted to Prof. J. Fang, Jia Genzheng et al. of the Fourth Antarctic Investigation Team for their support and help in the establishement of the Observation Station.
Authors are very grateful to Prof. P. Melchior for checking the oceanic load correction for Southern Hemisphere and revising the paper.

## Reference

[1] 方俊，<<固体潮>>，科学出版社，(1984).
[2] Melchior, P., Geophysical Surveys, Vol. 1 (1974), 3: 275-303.
[3] Venedikov, A.P., Observatoire Royal de Belgique, Série Géophysique, (1966), 76: 827-845.
[4] Ducarme, B., Bulletin d'Informations des Marées Terrestres (1975), 72: 4156-4181.
[5] Nakai, S., BIM, (1979), 81: 4955.
[6]
[7] Ducarme, B., Physics of the Earth and Planetary Interiors, Vol. 11, (1975), 122-125.
[8] Longman, I.M. J. Geophys. Res., Vol. 67, (1962), 845-850.
[9] Farrell, W.E., Rev. Geophys. Space., Vol. 10, (1972), 761-797.
[10] Pertsev, B.P., Sixième Symp. Intern. sur les Marées Terrestres (1969), 113-115.
[11] Pertsev, B.P. Akademiai Kiado Budapest (1976), 459-502.
[12]
[13] Melchior, P., Physics of the Earth and Planetary Interiors, Vol. 13, (1976), 184-196.
[14] Melchior, P., The Tides of the Planet Earth, 2nd edition, Pergamon Press, Oxford, England, (1983), 373.
[15] 郑剑东，地质论评，Vol.5, (1985), 479—484.

TABLE 1

Phase Delay of the Meter in Wuchang Station
and Antarctic Station

| Station / Phase delay | $\Delta\phi O_1$ | $\Delta\phi K_1$ | $\Delta\phi M_2$ | $\Delta\phi S_2$ |
|---|---|---|---|---|
| Wuchang (standard) | -0.44° | -0.58° | -0.42° | -0.22° |
| Wuchang (G 589 Ob.) | -3.30° | -2.64° | -2.97° | -2.78° |
| Antarctica (G 589 Ob.) | -1.36° | -3.39° | -4.19° | -7.06° |
| Antarctica (removing the effects of meter and filter) | 1.50° | -1.33° | -6.74° | -4.50° |

TABLE 2

A comparison of Standard Tidal Parameter
with Observation Results at Wuchang
after Connection of G 589 with SF 356 filter.

| Sort / Wave group | $O_1$ | | $K_1$ | | $M_2$ | | $S_2$ | |
|---|---|---|---|---|---|---|---|---|
| | $\delta$ | $\phi$ | $\delta$ | $\phi$ | $\delta$ | $\phi$ | $\delta$ | $\phi$ |
| Standard factors | 1.1777 | 0.44 | 1.1530 | -0.58 | 1.1744 | -0.42 | 1.1740 | -0.22 |
| Observed factors | 1.1995 | -3.30 | 1.1775 | -2.64 | 1.1899 | -2.97 | 1.1892 | -2.78 |

TABLE 3

Gravity Tide Results Obtained at Great Wall Station
in King George Island, Antarctica,
using Venedikov Analytic Method.

| Wave name | Wave sequence number | Wave group | Amplitude factor and m.s.e | Phase delay and m.s.e. | Observed amplitude |
|---|---|---|---|---|---|
| Diurnal waves | 01-62 | $Q_1$ | 1.3939 ± 0.0316 | -0.41 ± 1.30 | 8.11 |
| | 63-88 | $O_1$ | 1.3956 ± 0.0061 | -1.36 ± 0.25 | 42.97 |
| | 89-110 | $M_1$ | 1.3142 ± 0.0588 | -4.06 ± 2.56 | 3.98 |
| | 111-120 | $P_1$ | 1.3186 ± 0.0151 | -3.79 ± 0.66 | 15.68 |
| | 121-123 | $S_1$ | 1.8854 ± 0.9280 | 37.14 ± 28.20 | 0.36 |
| | 124-143 | $K_1$ | 1.3171 ± 0.0045 | -3.39 ± 0.19 | 52.88 |
| | 144-165 | $J_1$ | 1.3079 ± 0.0733 | -2.50 ± 3.21 | 3.18 |
| | 166-197 | $OO_1$ | 1.2245 ± 0.0856 | -5.69 ± 4.00 | 2.57 |
| | Unit weight mean error $\sigma$ = 6.66 | | | | |
| Semi-diurnal waves | 198-236 | $2N_2$ | 1.1182 ± 0.1173 | 4.03 ± 6.01 | 0.64 |
| | 237-260 | $N_2$ | 1.3273 ± 0.0229 | 10.38 ± 0.99 | 4.19 |
| | 261-286 | $M_2$ | 1.5813 ± 0.0045 | 4.19 ± 0.16 | 25.10 |
| | 287-300 | $L_2$ | 1.7265 ± 0.1891 | 14.57 ± 6.27 | 0.62 |
| | 301-309 | $S_2$ | 1.5467 ± 0.0059 | -7.05 ± 0.33 | 11.91 |
| | 310-347 | $K_2$ | 1.5876 ± 0.0253 | -7.12 ± 0.91 | 4.29 |
| | Unit weight mean error $\sigma$ = 2.59 | | | | |
| Ter-diurnal waves | 348-363 | $M_3$ | 1.1169 ± 0.2212 | 2.89 ± 11.35 | 0.16 |
| | Unit weight mean error $\sigma$ = 1.15 | | | | |

TABLE 4

Final Observed Values of Main Waves after Correction by Rheological Model.

| Tidal wave | Tidal factor ($\delta$) | Phase delay ($\Delta\phi$) |
|---|---|---|
| $O_1$ | 1.3501 | 1.50 |
| $K_1$ | 1.2742 | -1.33 |
| $M_2$ | 1.5297 | 6.74 |
| $S_2$ | 1.4963 | -4.15 |

TABLE 5

Oceanic Load Gravity Correction at Great Wall Station in King George Island.

| $\delta$ | $\phi$ | $O_1$ | | $K_1$ | | $M_2$ | | $S_2$ | |
|---|---|---|---|---|---|---|---|---|---|
| | | Ampl. | Phase | Ampl. | Phase | Ampl. | Phase | Ampl. | Phase |
| 58°58′W | 62°13′S | 3.45 | -169.84 | 3.21 | 164.14 | 5.43 | 33.91 | 1.46 | -20.29 |

Unit amplitude ($\mu$gal), phase (degree)

TABLE 6

Gravity Tide Results at Great Wall Station in King George Island, Antarctica After Oceanic Load Correction.

| $\delta(O_1)$ | $\Delta\phi(O_1)$ | $\delta(K_1)$ | $\Delta\phi(K_1)$ | $\delta(M_2)$ | $\Delta\phi(M_2)$ | $\delta(S_2)$ | $\Delta\phi(S_2)$ |
|---|---|---|---|---|---|---|---|
| 1.2394 | 0.71° | 1.1982 | -0.37° | 1.2350 | -0.53° | 1.3119 | -1.85° |
| ± 0.0061 | ± 0.25° | ± 0.0045 | ± 0.19° | ± 0.0045 | ± 0.16° | ± 0.0059 | ± 0.33° |

TABLE 7

Difference between Gravity Earth Tide Observation Values and Theoretical Values of Molodensky's Earth Model

| Method \| Factor | $O_1$ | | $K_1$ | | $M_2$ | | $S_2$ | |
|---|---|---|---|---|---|---|---|---|
| | B | $\beta$ | B | $\beta$ | B | $\beta$ | B | $\beta$ |
| Before ocean tide correction | 5.80 | 10.60 | 4.72 | -14.6 | 6.37 | 26.6 | 2.69 | -18.0 |
| | X | $\chi$ | X | $\chi$ | X | $\chi$ | X | $\chi$ |
| After ocean tide | 2.50 | 11.4 | 2.45 | -57.0 | 0.97 | -10.6 | 1.25 | -18.4 |

Fig. 1 Gravity tide main wave component varying with latitude

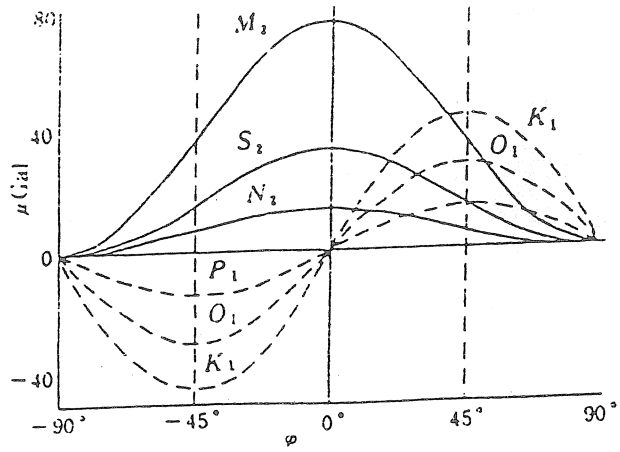


Fig. 2a Antarctic gravity tide records influenced by heavy stormy waves

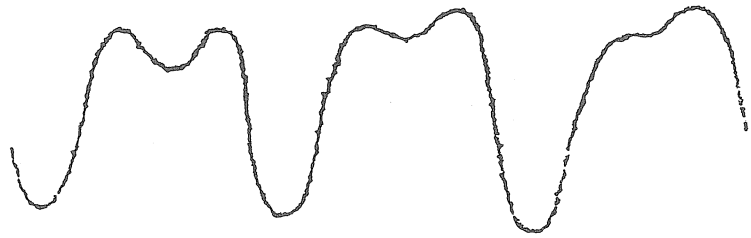

(a)

(b)

Fig. 2b Antarctic gravity tide records after using the SF356 filter

# Recommandations of the WG on "Theoretical Tidal Model".

V. Dehant
Royal Observatory of Belgium
3, avenue Circulaire
B-1180 Brussels
Belgium
Tel: 32-2-3730266
Fax: 32-2-3749822
e-mail: veroniq@astro.oma.be

August 1993

1. Considering the definitions used for tidal analysis,

   we define the *tidal gravimetric factor* ($\delta$) on the ellipsoid as the Earth's transfer function (a coefficient in the frequency domain) between the body tide signal measured at the station by a gravimeter and the amplitude of the vertical component of the gradient of the external tidal potential at the station position;

   we define the *Love number h* on the ellipsoid as the Earth's transfer function (a coefficient in the frequency domain) between the tidal displacement along the normal to the ellipsoid and the geoid tide (potential divided by gravity);

   we define the *Love number k* on the ellipsoid as the Earth's transfer function (a coefficient in the frequency domain) between the potential associated with the mass redistribution due to the tides and the external tidal potential;

   we define the *tidal tilt* on the ellipsoid as the deflection of the instantaneous vertical with respect to the mean gravity vector defined as normal gravity at the station, in east-west direction and in north-south direction.

   For the first three parameters, the local vertical is taken as the normal to the ellipsoid.

   The ellipsoid in use is corresponding to the equilibrium state of a hydrostatically pre-stressed Earth. Any other Earth's reference ellipsoid would not change the results.

   The effect of the elevation of the station which is not considered here is less than 0.01% for an elevation of 4000 $m$ and is thus negligible.

   For more details, we refer to Dehant (PEPI 49, pp 87-116) and to the reports of the Working Group on "Theoretical Tidal Model" presented at the 10th and 11th International Symposia on Earth Tides (1989 and 1993, respectively, Proceedings).

2. Considering the preliminary reference Earth model PREM (Dziewonski & Anderson, 1981, PEPI 25, pp 297-356), accepted by the seismologists,

   considering that it is necessary to include the ellipticity, the rotation and a precise internal structure of the Earth,

   and considering that it is too early to agree on an inelastic mantle model,